Solutions toward high-speed colourless optical network units

Duijn, R.L.

Award date:
2007

Eindhoven University of Technology
Faculty of Electrical Engineering
Division of Telecommunication Technology and Electromagnetics
Electro-Optical Communications Group

SOLUTIONS TOWARD HIGH-SPEED COLOURLESS OPTICAL NETWORK UNITS

R.L. Duijn

Master of Science Thesis Report
carried out from July 2006 to August 2007
Student ID: 0494515

Supervisors:
Dr. ir. H. de Waardt

Graduation professor:
Prof. ir. A.M.J. Koonen

Preface

This report describes the Master's Thesis project done as a part of my master-period at the Electro-Optical Communications group for the study Electrical Engineering at the Electrical Engineering department of the Eindhoven University of Technology in the Netherlands.

The Master's Thesis project was performed at the Eindhoven University of Technology between July, 2006 and August, 2007. The project is a part of the BB Photonic Access project, "BBPhotonics: Dynamically Reconfigurable Broadband Photonic Access Networks", which is funded by Freeband Communication. Freeband Communication is a Dutch national research program aiming to create a leading knowledge position for the Netherlands in the area of ambient, intelligent communication.

I wish to thank Prof. A.M.J. Koonen for giving me the possibility to do my Master Thesis projet at the ECO-group. I also wish to thank my supervisor Dr. Ir. H. de Waardt for his guidance and advice. Finally I wish to thank Hyun-Do Jung, Kun Wang, and Patryk Urban for the many discussions and their advice.

Abstract

A reconfigurable WDM-TDM access network can react to timely different demands for different areas like business area, domestic areas and city centres. The network reconfiguration can be established by flexible wavelength routing. To enable this, a wavelength independent (colourless) reflective modulator has to be in the optical network unit (ONU) to modulate the upstream signal. This report gives an overview of the different architectures to achieve this. A configuration with a circulator, semiconductor optical amplifier (SOA) and electro-absorption modulator (EAM) was used as a reflective modulator at 10-Gbit/s for transmission experiments. Backscattering was found to be the limiting factor for the bidirectional single-fibre architecture. An optimum gain of the ONU was found at which both the carrier- and the signal-backscattering are limited.

Abbreviations

ASE	Amplified Spontaneous Emission
AWG	Arrayed-Waveguide Grating
BER	Bit Error Rate
BPSK	Binary Phase Shift Keying
C-BS	Carrier Backscattering
CO	Central Office
DPSK	Differential Phase Shift Keying
FBG	Fibre Bragg Grating
FP-LD	Fabry-Perot Laser Diode
FSK	Frequency-Shift Keying
FTTH	Fibre-to-the-Home
IRZ	Inverse-return-to-zero
MZI	Mach-Zehnder Interferometer
MZM	Mach-Zehnder Modulator
NRZ	Non-return-to-zero
OFSK	Optical Frequency-Shift Keying
ONU	Optical Network Unit
OSA	Optical Spectrum Analyser
OSNR	Optical Signal-to-Noise Ratio
PON	Passive Optical Network
PRBS	Pseudorandom Binary Sequence
PSK	Phase-Shift Keying
RBS	Rayleigh Backscattering

RSOA	Reflective Semiconductor Optical Amplifier
RZ	Return-to-zero
S-BS	Signal Backscattering
SBR	Signal-to-Backscatter Ratio
SBS	Stimulated Brillouin Scattering
SCM	Sub-Carrier Multiplexing
SOA	Semiconductor Optical Amplifier
SSR	Sideband Suppression Ratio
TDM	Time Division Multiplexing
WDM	Wavelength Division Multiplexing

Abbreviations used in Setup Figures

BPF	Band Pass Filter
CW	Continuous Wave
EAM	Electro-Absorption Modulator
EDFA	Erbium Doped Fibre Amplifier
ONU	Optical Network Unit
PC	Polarisation Controller
PM	Power Meter
SOA	Semiconductor Optical Amplifier
VOA	Variable Optical Attenuator

Table of Contents

1. Introduction

This report describes the Master's Thesis project performed at the Eindhoven University of Technology for the Electro-optical Communications (ECO) chair which is part of the Telecommunication Technology and Electromagnetics (TTE) division. The Master's Thesis project is a part of the BB Photonic Access project, "BBPhotonics: Dynamically Reconfigurable Broadband Photonic Access Networks" [1], which is funded by Freeband Communication. Freeband Communication is a Dutch national research program aiming to create a leading knowledge position for the Netherlands in the area of ambient, intelligent communication. The scope of the project and the proposed network architecture are described first, followed by the assignment description.

1.1. BB Photonics Project

Presently fibre is used in the feeder part of the network, but in the last drop to the residential user there is a variety of media, such as twisted pair, coaxial cable, and increasingly wireless drops. Communication speeds per user residence are foreseen to rise beyond Gigabit Ethernet and even 10 Gigabit Ethernet. The trends observable in the market that drive this thirst for information are a.o. the personalisation of services, peer-to-peer communication, fast file transfer (e.g. for storage area networks), increasing high-Q video content and roaming with broadband services. As the capacity demand by the subscriber grows, also the capacity in the access network has to keep up with it. The BB Photonic Access project aims to develop and validate a novel system concept, which will enable congestion-free access to users with traffic demands fluctuating in time and in place.

The most simple way to provide the capacity for the subscribers is by brute force methods, making fixed high speed lines between the backbone and the subscribers. This results in excessive infrastructure costs. If the network costs can be shared by a large number of users this reduces the costs. A method which can be used to share the costs is to insert intelligence in the access network which enables network reconfiguration. Depending on the timely different demands for different areas like business area, domestic areas and city centres, the network is dynamically reconfigured.

Besides the capacity advantages, the reconfigurable network has also some operational advantages. It is possible to circumvent failures and congestions in the network, which increases the availability and the throughput of the network. Repair and maintenance can be done without affecting the network since parts of the network can be taken out of service. A reconfigurable network also allows the possibility for upgrading network capacity as the user demand grows. With the distributing capacity it is possible to provide hot spots with high capacity. Individual routing of different service streams enables to host several operators and service providers independently in a single network infrastructure.

Very important for the network are a well designed efficient fibre access network architecture and cost-efficient optical devices, due to the cost-critical nature of access networks. Integrated devices are required, resulting in more compact and more reliable components which are less power consuming.

1.2. Proposed Network Architecture

The reconfigurable access network that was proposed in the BB Photonics project is shown in Figure 1.1. The ring topology provides high network availability, due to the available routing redundancy. A wavelength router is used to direct the wavelength channels to the intended users; the device is controlled by a control wavelength which is separated from the data signals by a coarse wavelength splitter. For broadcasting to all the users, the routing device has to be bypassed.

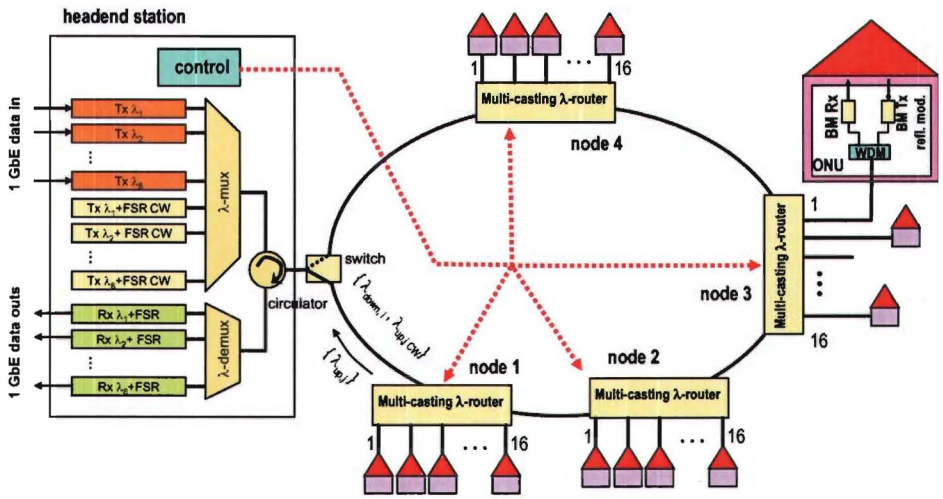

Figure 1.1.: Access network architecture: a reconfigurable WDM-PON

The wavelength router used in the project is a ringresonator based router. The principle of the resonator is shown in Figure 1.2. The signal enters from one side and each of the ringresonators can be adjusted to drop the desired wavelengths. The other wavelengths are passed through the other ringresonators, to the next network segment. The ringresonators are also capable to drop a wavelength partially, so that the remainder can be directed to another ONU. One wavelength can be used by multiple users, while the data for the designated users is split in time domain (TDM).

A single bidirectional fibre connects the central office with the remote nodes, and the remote nodes with the ONU. The downstream signal is sent at a different wavelength as the upstream signal. Two different wavelength allocation schemes have been proposed. The first scheme consists of ten pairs of interspersed downstream and upstream wavelengths with a 200 GHz channel spacing. The second scheme divides the whole band into one guard band (150 GHz) and two sub-bands (400 GHz) as is shown in Figure 1.3. The guard band

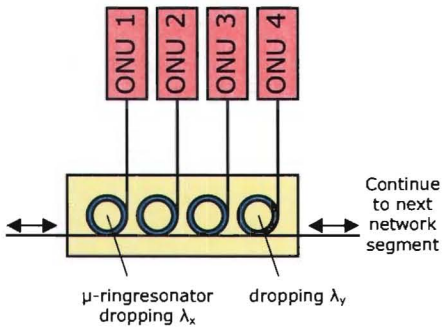

Figure 1.2.: Design of the ringresonator

is located between the two sub-bands, which are composed of the 8 downstream channels and 8 upstream channels. Within the sub-band, the channel is spaced 50 GHz, and the space between the downstream and upstream wavelength is 500 GHz. The second scheme appears to be more favourable since the downstream and upstream band can easily be filtered by a coarse optical filter.

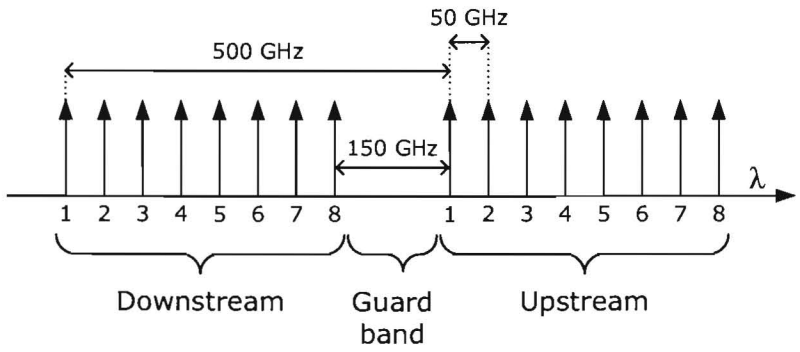

Figure 1.3.: Proposed wavelength allocation scheme

In the project two types of Mach-Zehnder wavelength duplexer structures were considered [2] to split the downstream and upstream wavelengths in the ONU. These duplexer structures require fine-tuning whenever the network is reconfigured to maximize the transmission of the wavelengths distributed from the local exchange. The maximum of the passband of the duplexers can be tuned by the thermal effect to match the incoming wavelength, due to the change in the refractive index of the semiconductor material with the temperature variation. The refractive index of the material can also be changed by applying an electrical field through electro-optic effect. However, this tuning is undesired in the ONU since it requires active control of the devices. Therefore in Appendix A different architectures are proposed to separate the downstream and upstream bands with devices that do not require active control.

A reflective semiconductor optical amplifier (RSOA) is proposed to be the modulator at the transceiver module, placed at the ONU. The frequency response of the RSOA is governed by

the relaxation oscillation frequency, which limits its operation to around 3-Gbit/s.

1.3. Assignment of the Master's Thesis Project

The assignment of the project was to find solutions toward high-speed (up to 10-Gbit/s) colourless optical network units (ONU). The assignment was split into two parts, the first part considers the devices that can be used as reflective modulators in the ONU and the second part considers the modulation formats that can be used for a reconfigurable network.

In the BB Photonic Access project an RSOA is proposed to be the modulator at the ONU, however, this device is not capable of modulating at data rates up to 10-Gbit/s. Therefore other reflective modulators have to be considered. Chapter 2 gives an overview of the reflective modulators that can be used in the ONU. Chapter 3 gives a brief overview of the combinations of modulation formats that can be used for an access network, which were found during literature research. The characterisation of the components that were used for the transmission measurements are described in Chapter 4. Chapter 5 describes the transmission measurements with the proposed reflective modulator and modulation format. Chapter 6 assesses the findings of the project and gives recommendations for future research.

2. Reflective Modulators

The reconfigurable network requires non-wavelength-specific (colourless) modulators that can work on the wavelengths assigned by the central office without active control. This eliminates the possibilities of using spectrally sliced LEDs or tunable light sources at the ONU. Several source-free colourless ONU using reflective modulators for the upstream signal have been proposed. The use of a reflective modulator with one optical port leads to simple and cost-effective packaging technology. The low-speed modulators like the mechanical modulator [3, 4] are not considered in this report. The following types of reflective modulators which are also shown in Figure 2.1 are considered in this report:

- Intensity modulators (directional couplers, interferometric modulators and electroabsorption modulators), either made reflective using a circulator or integrated
- Reflective Semiconductor Optical Amplifier (RSOA)
- Injection-locked Fabry-Perot laser diode (FP-LD)

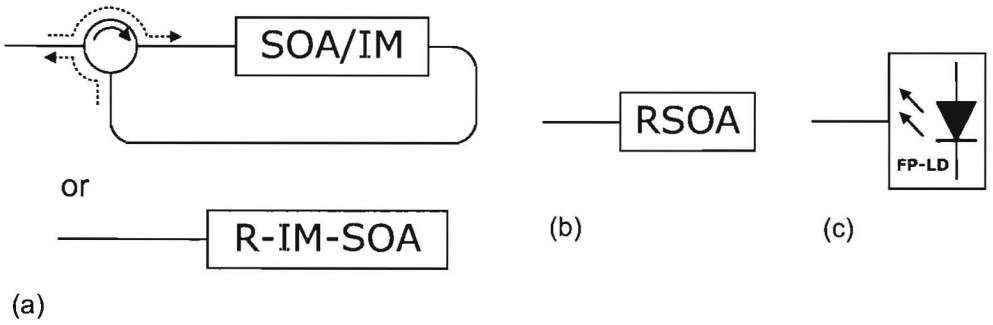

Figure 2.1.: Different possibilities for the reflective modulator in the ONU: (a) An intensity modulator in combination with an SOA (made "reflective" by a circulator or integrated); (b) RSOA; (c) injection-locked FP-LD

2.1. Reflective Modulation Using Electro-Optic Modulators

This section describes the electro-optic devices that can be used as a reflective modulator. Electro-optic devices control light by using an electric field to induce changes in the refractive index and/or absorption of the material. Three types of devices are considered, in the first subsection the directional couplers and the interferometric modulators are considered and in the second subsection the electroabsorption modulator.

Devices using III-V compound semiconductors have a smaller electro-optic effect than lithium-niobate ($LiNbO_3$), so their performance was greatly inferior to that of lithium-niobate waveguide devices until the 1980s. Advances in the fabrication technique enabled to employ phenomena such as QCSE, the Franz-Keldysh effect, and band filling, due to which the performance is equal to the lithium-niobate devices nowadays. The large advantage of compound semiconductor devices is that they can be integrated with lasers, photodetectors, optical amplifiers, and drive circuits.

An intensity modulator in combination with a circulator and an amplifier can act as an reflective modulator. However, it is more interesting to look at devices that can be integrated as a reflective modulator, what will result in smaller and cheaper solutions. Therefore, in this section we will not consider the option of an external intensity modulator in combination with circulators.

2.1.1. Directional Couplers and Interferometric Modulators

Intensity modulators have been made using a variety of waveguide structures. While space does not permit a survey of all of them, we briefly describe some directional couples and interferometric modulators.

A directional coupler is composed of two single-mode channel waveguides that are placed in close proximity to each other so that the evanescent tails of the modes overlap. The structure that is mostly used is shown in Figure 2.2(a). An external voltage can be applied to change the propagation constants of the waveguides resulting in a phase difference, which determines the direction of the optical power. Thus, depending on the voltage the light can be directed to one or the other output as a modulator.

When one of the outputs of the directional coupler is reflecting, as in Figure 2.2(b), the device becomes a reflective modulator [5]. An interesting device structure based on a directional coupler is proposed by [6], and is shown in Figure 2.2(c). The reflective modulator described enables both wavelength splitting and (re)modulation with the same device. The one-half directional coupler is basically a standard coupler folded symmetrically along its length. It is designed in such a way that the desired number of coupling lengths are achieved by traversing across, reflecting and then propagating back through the coupler. The wavelength sensitive filter reflects the modulated upstream wavelength and transmits the downstream wavelength. The downstream wavelengths are collected after the filter by a multimode fibre, and are detected by a photodiode.

The Mach-Zehnder type modulator (MZM) is the most widely used type of interferometric modulator. It is comprised of two phase modulators and two Y branches as can be seen in Figure 2.3(a). Light launched into a single-mode input waveguide splits equally between the arms of a symmetric input Y junction. The two beams are phase-modulated by the field between the planar electrodes and reach the second Y branch. When the phases of the two light beams are the same at this point, the light propagates to the single-mode waveguide output. When the phases are opposite, the light goes out of the waveguide.

A reflective interferometric modulator can be created when we terminate half a Mach-Zehnder modulator by a reflective surface as in Figure 2.3(b). The incident light splits equally into the two branches of the interferometer at the Y junction. Both signals travel through

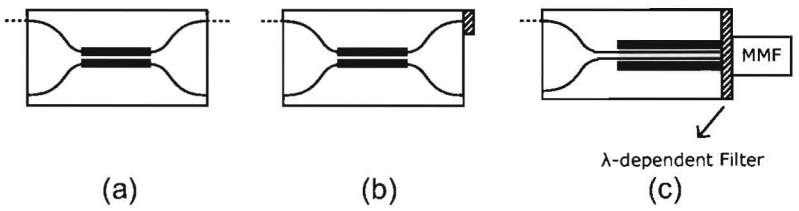

Figure 2.2.: Basic structure of directional coupler (a) and different structures resulting in reflective modulators using directional couplers in (b) and (c)

the waveguides to the mirror and are reflected back to the junction to get recombined. By applying a differential voltage to the electrodes deposited on top of the two waveguides, a difference of refractive index in the two branches is created similar as in the case of the MZM. This causes a phase difference between the two reflected light signals and, consequently, intensity modulation is realised.

An interesting structure described in [7, 8], and shown in Figure 2.3(c) acts as a power splitter and modulator using a partly reflective mirror. The device splits the light power emitted into the waveguide into two beams at the Y branch. Part of the power is reflected and modulated as described in the previous device, but the other part is detected by the photodetector after the partly reflective mirror. This allows simultaneous upstream and downstream transmission when the downstream signal is re-used for modulation, e.g. using techniques described in Section 3.2.

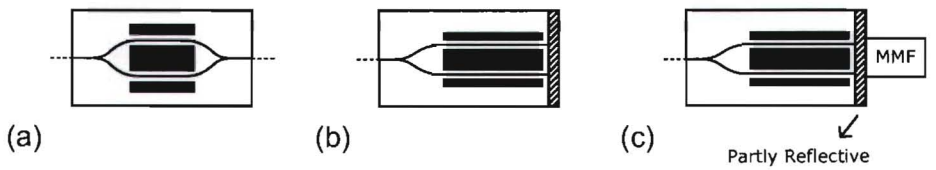

Figure 2.3.: Structure of: (a) a Mach-Zehnder interferometer; (b) a reflective interferometric modulator; and (c) interesting structure based on a reflective interferometric modulator

The techniques with the wavelength dependent filter and the partly reflective mirror mentioned before were realised with lithium niobite technology and no research has been found that surveyed these options with III-V semiconductor technology. Therefore, if two different wavelengths are used for the downstream and the upstream signal, I suggest a reflective modulator, based on the directional coupler or MZM structure, made with III-V semiconductor technology, with a coarse wavelength sensitive filter. The filter has to be a coarse filter with is transmissive for the downstream wavelength band and reflective for the upstream wavelength band (if a wavelength allocation scheme like in Figure 1.3 is used). The signals transmitted through the filter are detected by a photodetector, and the reflected signals are modulated. This structure reduces the need for an additional wavelength splitter. If the same wavelength is used for the downstream and the upstream signal, a similar reflective modulator can be used. The only difference is that in stead of the wavelength

sensitive filter, a partly reflective mirror can be used. This reduces the need for an additional power splitter.

2.1.2. Electro-absorption Modulator (EAM)

In contrast to the modulators described above, the electro-absorption modulator (EAM) operates through a voltage-controlled change in light absorption. The semiconductor EAMs are based on III-V semiconductor technology and operate through either the Franz-Keldysh effect in bulk semiconductor layers, or the quantum-confined Stark effect in multiple quantum well (MQW) layers. The optical propagation loss in the EAM is quire large, therefore the device has to be combined with an optical amplifier to overcome the losses. The adoption of an all semiconductor/integrated approach enhances the prospects for low-cost manufacture of the ONU at high volume, which is necessary for an access application. The modulator described in [9] is based on a semiconductor EAM monolithically integrated with a semiconductor optical amplifier (SOA). The integrated SOA-EAM is capable of modulating signals at 10-Gbit/s [10]. Recently also single-port monolithically integrated amplified reflective EAMs have been proposed [11, 12]. These devices can work at 10-Gbit/s and over a large spectral width up to 40nm.

Besides the very high modulation ability and the best compromise between driving voltage and high extinction ratio, it is also possible to use the EAM as a photodetector. If such a device is used in the ONU combined with the scheme where the same wavelength is used for downstream and upstream transmission, it is not necessary to split the downstream signal. Therefore, all the optical power can be used for upstream transmission. Furthermore no additional photodiode is required. An architecture was demonstrated in [13] which uses the EAM as both modulator and photodetector over a bidirectional fibre. The downstream signal is interspersed with a continuous-wave signal in a TDM architecture. The downstream signal is detected with the EAM and the same device modulates and reflects the continuous-wave signal with upstream data (half-duplex). In [14] a modulator is described that enables simultaneous detection and upstream modulation (full-duplex) using electrical sub-carriers.

2.2. Reflective Semiconductor Optical Amplifier (RSOA)

Another device that combines modulation, gain and a single-port geometry is the reflective semiconductor optical amplifier (RSOA), which is a special type of SOA. An SOA has the same structure as a laser without feedback. The gain is realised by electrical pumping. When the device is driven by an electrical current, the active region in the device amplifies an input signal, via stimulated emission. Spontaneous emission is also present in the amplification process, therefore the output signal is accompanied by additive noise, known as amplified spontaneous emission (ASE). When one of the faces is coated with a high reflectivity, the SOA becomes reflective, called an reflective SOA (RSOA). The light enters inside the cavity after which it is reflected in the opposite direction. The internal gain of the amplifier compensates for splitting and coupling losses. However, the frequency response is governed by the relaxation oscillation frequency, which limits its operation to around 3-Gbit/s.

The first RSOAs designed as reflective modulators for access networks were called

semiconductor laser amplifier-reflectors and are described in [15, 16]. The RSOA has a large optical bandwidth and can also be used as a detector. This implies that a single chip with a single-port can achieve emission (by modulation and reflection) and reception functions. The incoming light is modulated by the RSOA injection current carrying the upstream data, and the RSOA acts as a photodetector by sensing the voltage variation of the electrode. Therefore it is a very attractive solution for reducing the cost of the subscriber module for half duplex transmission since detection takes place alternately with modulation. An electro-optic transceiver at the ONU based on a single RSOA performed both operations, modulation and detection, at a bit rate of 1.25-Gbit/s in [17]. Full duplex transmission is also possible, using electrical sub-carriers to distinguish between the upstream and the downstream signal.

Having similar functionality to the RSOA, but encapsulated in a vertical cavity is the vertical-cavity semiconductor optical amplifier (VCSOA) [18, 19]. The technology allows fabricating 2-D arrays on wafer and on-wafer testing. The VCSOA can, like the RSOA, be used simultaneously as an amplifier and detector using the junction voltage modulation by an amplified optical signal. In a vertical-cavity structure, the optical mode passes perpendicularly through the different material layers. Consequently, the electrical field is always parallel to the plane of the active layers, which makes it a polarisation insensitive device. The shorter active region of the VCSOA makes the single-pass gain much smaller, on the order of a few percent. To compensate for this, the VCSOA uses feedback, which is provided by a resonance cavity created by the two mirrors. The resonance cavity results in an optical bandwidth that is limited to the linewidth of the Fabry-Perot mode. The optical bandwidth is, hence, significantly smaller than that of an RSOA. The small optical bandwidth makes the device less interesting for colourless modulator. Tunable VCSOA by varying the temperature or the cavity by MEMS have been proposed [20, 21], but are not attractive since they require external control.

2.3. Injection Locked Fabry-Perot Laser Diode

Another device that can be used as a reflective modulator in the ONU is the injection-locked Fabry-Perot laser diode (FP-LD). The FP-LD can be converted into a single-mode laser by injection locking with a single-mode coherent light source [22, 23]. An FP-LD injection-locked by a broadband ASE source was demonstrated in [24] for the first time for access networks. With direct modulation the FP-LD is capable of transmitting at bitrates up to 10-Gbit/s [25], but the highest bitrate found in an access network using an injection locked FP-LD in the ONU is 2.5-Gbit/s [26, 27].

The FP-LD needs a relatively high injection power to have a good locking performance (around -15dBm). With an injection-locked FP-LD a number of discrete channels are available to be used for upstream transmission. The discrete channels have to overlap with the other wavelengths dependent components, like the wavelength router, to prevent channel mismatching resulting in a power penalty.

2.4. Comparison of the Reflective Modulators

In this section the reflective modulators are compared. For the comparison we consider the following properties: electrical bandwidth, optical bandwidth, integratability, the required input power and the cost. An overview of the properties for the different reflective modulators is given in Table 2.1. The components described in Section 2.1 are considered to be combined with an additional optical amplifier to provide gain.

The intensity modulators like the EAM or the MZM have the largest electrical bandwidth and reach 10-Gbit/s easily. The directly modulated FP-LD is capable of data modulation at 10-Gbit/s, but this is near the electrical bandwidth limit of the device. The electrical bandwidth of the RSOA is limited to around 3-Gbit/s.

The optical bandwidth of the RSOA is the largest, but the optical bandwidth of the EAM is also large enough to cover the whole C-band. The FP-LD also has a large bandwidth, but unlike the other devices it has a large number of discrete wavelengths on which it locks. Therefore, there are some requirements on the feeder signal and the wavelength specific devices in the network.

The RSOA and the reflective intensity modulators are capable of being integrated with a photodiode and the EAM and the RSOA are also both capable of detecting signals. The FP-LD can also be integrated with a photodiode, but is not able to use as a detector itself.

The required input power into the FP-LD to assure wavelength locking is larger than the required input power for the RSOA. If the intensity modulator is integrated with an optical amplifier the required input power is also low.

The fabrication cost of both an RSOA and an FP-LD can be low when they are produced in mass-production. The cost of an EAM however, is higher due to its complex semiconductor structure.

Table 2.1.: Comparison of the reflective modulators

Property	**IM (e.g. EAM)**	**RSOA**	**FP-LD**
Electrical bandwidth (10-Gbit/s)	++	−	+
Optical bandwidth (colourless)	+	++	o
Integratability with PD	+	+	o
Required input power	+	+	−
Fabrication costs	−	+	+

The RSOA is not able to modulate at 10-Gbit/s and no high-speed FP-LD was present in the lab environment. Therefore an EAM was used as the modulator for the transmission measurements that were performed and that are described in this report. The EAM was used in combination with an SOA to overcome the high insertion loss.

3. Modulation Formats

The size of the outside plant is critical when deploying an access network. The number of kilometre of fibre that is deployed and the number of optical fusions needed to connect the ONUs to the central office (CO) depends on the network topology. The strategy using double unidirectional fibre with one wavelength for upstream and one for downstream, as in Figure 3.1(a), has the least problems with backscattering and crosstalk, but it also requires the most number of components, since it requires more fibre and a light source for the continuous-wave (CW) feeder signal. If the downstream signal is re-used to feed the upstream signal as in Figure 3.1(b), no additional light source is required. Bidirectional transmission using a single bidirectional fibre, as in Figures 3.1(c) and (d), reduces optical component ports and fibre length by 50 percent in comparison to a network using separate fibre for downstream and upstream transmission, but the backscattering and crosstalk are increased. Some methods to reduce the backscattering are described in Appendix B.

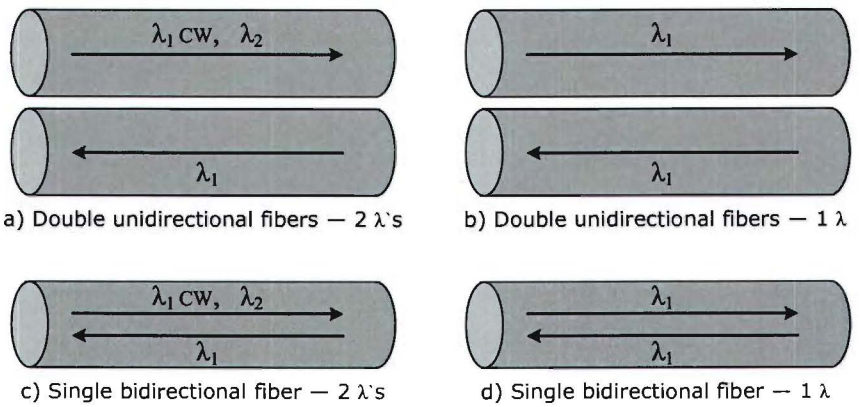

Figure 3.1.: Wavelength transportation schemes

In this chapter we consider the possible modulation formats that are suited for an architecture with a single bidirectional fibre. A considerable amount of literature has been published on the use of different modulation formats for the downstream and the upstream signals. The most simple manner is to use a continuous-wave signal for the upstream signal and a different wavelength for the downstream signal as is described in Section 3.1.

The other modulation formats that are described in this chapter re-use the downstream wavelength for upstream transmission. Section 3.2 given an overview of the techniques that enable the transmission of an intensity modulated signal for both the downstream and the upstream signal. Section 3.3 describes the use of frequency- and phase keying modulation formats for the downstream signal and intensity modulation for the upstream signal. The

use of sub-carrier multiplexing to differentiate between the downstream and the upstream signal is discussed in Section 3.4. Section 3.5 describes the use of coherence modulation to be able to transmit the downstream and the upstream simultaneously on the same wavelength. The final section in this chapter, Section 3.6, gives a comparison of the techniques and explains the technique used for the transmission experiments. No papers have been found that use polarisation modulation for access networks. Therefore this technique will not be considered in this report.

3.1. Continuous-wave Feeded Upstream Transmission

The easiest and most straightforward manner to feed the ONU is with a continuous-wave signal. The light source in the central office can be shared by a large number of users at a relatively short distance from the central office (access network). The BB Photonics project and the experiments described in Chapter 5 use this technique.

The first architecture found that proposed an architecture for an access network with a centralised light source was reported by [28] in 1985. The proposed architecture consists of two unidirectional fibres, one to carry the feeder signal to the user and one for the upstream signal. In [29], a transmission experiment using the same architecture is described using an Mach-Zehnder modulator at the ONU. Recently with a single fibre architecture 10-Gbit/s was achieved with a modulator based on an EAM monolithically integrated with SOAs [10, 30]. Transmission experiments using a monolithically integrated reflective modulator comprising a concatenated SOA and an EAM section (R-SOA-EA) has been shown feasible at a bitrate up to 7.5-Gbit/s in [31]. Architectures using an RSOA [32, 33] or a wavelength-locked FP-LD [24, 26, 34, 35] as the reflective modulator in the ONU have also been proposed to modulate the continuous-wave signal with upstream data.

Time partitioning can be used to separate the downstream and upstream signals [36]. The modulated downstream signal from the central office is alternated with a continuous-wave optical carrier. At the ONU a portion of the light is detected by a receiver. The remainder is looped back through a modulator to the central office. The modulator uses the continuous-wave optical carrier to modulate the upstream data upon.

3.2. Intensity Modulation Downstream and Upstream

In this section we discuss the techniques that enable simultaneous downstream and upstream transmission while both signals use intensity modulation. Part of the power reaching the ONU is used for detection and the other part is remodulated. The first method discussed uses different bitrates to differentiate between the downstream and the upstream signal. The second method uses special coding formats to enable both downstream and upstream intensity modulation. The third method uses different modulation depth to distinguish between the two signals and the final method suppresses the modulated downstream signal before it is modulated with the upstream signal. Combinations of the methods are also possible.

3.2.1. Bitrate Differentiation

This methods uses two different bitrates, a high-speed bitrate for the downstream signal and a low-speed bitrate for the upstream signal. At the ONU the high-speed intensity modulated downstream signal is remodulated by the low-speed upstream signal with a (reflective) modulator. Figure 3.2(a) shows an example of the bit patterns of the signals. Because of the bitrate difference, the low-speed data can be recovered by envelope detection with a receiver that has the proper low-pass characteristic. For envelope detection to be possible it is required that the high-speed data cannot have long strings of zeroes; scrambling of the intensity modulated data is not sufficient to overcome this. Therefore this technique has to be combined with a special coding scheme as described in the following section.

3.2.2. Coding

Two types of coding are considered in this section, but different kinds of coding that eliminate the possibility of long strings of zeroes are also possible. First the inverse-return-to-zero (IRZ) is discussed, followed by the Manchester coding.

A coding that can be used as the downstream signal format to facilitate the upstream data remodulation is a special line coding, namely the inverse-return-to-zero (IRZ) format. An IRZ signal is formed by inverting the intensity level of a conventional return-to-zero signal, thus it carries optical power at both the ones and the zeroes in each bit period as is shown in Figure 3.2(b). Therefore, the downstream optical power received at the ONU can be directly remodulated by the upstream data. With this coding it is possible to maintain a high extinction ratio of the downstream data. Meanwhile, the downstream IRZ signal does not require any demodulation circuit, except an inverting post-amplifier after the photodiode. Downstream transmission at 2.5-Gbit/s IRZ signal and 2.5-Gbit/s upstream data remodulation on the downstream signal was experimentally demonstrated [37].

The IRZ scheme carrying the optical power at both the logic level '1' and '0' in each bit period gives a simple transceiver structure. However, its performance degrades owing to optical power fluctuation caused by the pulse width difference between the two levels. In [5, 38], a scheme based on a Manchester coded downstream signal in combination with bitrate differentiation is proposed to reduce the low frequency optical power fluctuation. Because the logic level '1' and '0' of the Manchester code have '10' and '01' pattern, respectively, it has less optical power fluctuation than the scheme using IRZ. A remodulation scheme using conventional receivers and an intensity modulator has been demonstrated experimentally with a downstream bitrate of 5.0-Gbit/s and an upstream bitrate of 2.5-Gbit/s [39].

3.2.3. Modulation Depth Differentiation

With the modulation depth differentiation technique a low modulation depth is used for the downstream signal. Part of the signal is used for detection at the ONU, the other part of the signal is used for the upstream signal which has full modulation ratio as is shown in Figure 3.2(c). The downstream modulation is considered as a perturbation which reduces the usable amplitude of the upstream signal [8]. In [40] a system with an RSOA in the

ONU is demonstrated experimentally that is capable of a bitrate of 1.25-Gbit/s for both the downstream and the upstream signal. This method can can also be combined with the bitrate differentiation using an RSOA [41].

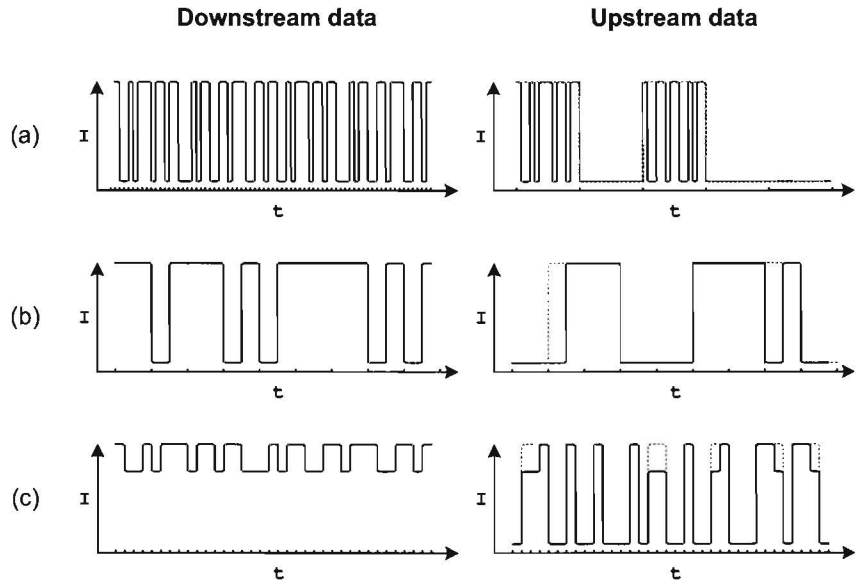

Figure 3.2.: Patterns of the downstream signals (left) and the remodulated signals (right) for; (a) bitrate differentiation; (b) coding differentiation, IRZ; and (c) modulation depth differentiation. The dashed lines represents the upstream data signal

3.2.4. Downstream Data Suppression

This method requires also a low modulation depth for the downstream signal as in the previous subsection. The downstream signal is suppressed and flattened, after which it is modulated with the upstream signal. In this section we will consider different devices that can be used for the downstream data suppression. First data suppression using intensity modulators is considered, followed by data suppression by SOAs. Finally data suppression using injection-locked FP-LDs is discussed.

Downstream Data Suppression using a Modulator

A method to suppress the downstream modulated signal using a modulator is described in [42]. At the ONU the incoming signal power is split by a coupler; part of the power is detected by a receiver. The detected electrical signal is feed-forwarded to an electro-optic modulator and synchronised with the optical signal. Data suppression of the data occurs in the second part by modulating the 'ones' down to the same level as the 'zeroes', creating a nominally flat "optical chalkboard". A second modulator modulates the lightwave to generate an upstream signal. There are several drawbacks with this method. For example, the need for two modulators will probably make the system complicated and relatively expensive. In

addition, the modulator for remodulation requires a large bandwidth that is sufficient for erasing a downstream bit pattern, which also adds to the cost.

Downstream Data Suppression using an SOA

In this section downstream data suppression using an SOA is considered. Three techniques are discussed: the first technique uses a feed-forward similar as in the previous section, the second technique uses a heavily saturated SOA, and the third technique uses a gain saturated RSOA.

The technique proposed in [43, 44] splits the incoming optical signal into two directions. One part of the incoming optical pulse is converted into an electronic signal and is inverted. This current-converted electronic signal is then feed-forwarded into the SOA through its bias current, provided that the optical signal and the inverted current signal are synchronised in relation to each other. As the pulse rises towards its high level, the current pulse moves towards its minimum. This results in a lower overall SOA gain. However, for lower optical pulse levels, the opposite effect occurs and the SOA gain rises from its average value. Therefore, higher optical signal levels will be amplified with a lower optical gain, and lower level signals with higher SOA gain. In this way, the extinction ratio of the resulting optical pulse will be close to the unit if a convenient amount of feed-forward current is injected in the SOA terminal. Therefore, data suppression or equalisation between the zero and the one logical levels could be obtained with this scheme. However, overshoot noise exists and represents the main drawback for a complete regeneration of the optical carrier. Another drawback is that very fast SOAs are required for operation at several gigabits per second.

In [43, 44] a linear SOA followed by a gain saturated SOA is used to suppress the downstream signal. The optical bit sequence of a downstream signal, designed with a relatively low extinction ratio, is amplified by the linear amplifier so that its power is in the SOA saturation region, and then input into the second SOA. As a result, the difference between the '1' and '0' levels is considerably reduced in the SOA output, which means that the downstream signal modulation pattern can almost be erased. In [45, 46] the lightwave is modulated at the same time by modulating the SOA injection current with the upstream signal. Thus, we can generate an upstream signal with the same wavelength as the downstream signal. Downstream and upstream transmission simultaneously at 2.5-Gbit/s was experimentally demonstrated using this technique.

A gain-saturated RSOA can be used to suppress the downstream signal and to modulate the upstream signal. The data rate used for the downstream signal is higher than the upstream signal, so that the unsuppressed part of downstream signal that induces upstream power penalty is filtered out by the electrical low pass filter at the upstream receiver. A bitrate of 2.5-Gbit/s downstream and for 1.25-Gbit/s upstream was experimentally demonstrated [47].

Downstream Data Suppression using an Injection Locked FP-LD

An optical injection-locked Fabry-Perot laser diode (FP-LD) can also be used to suppress the downstream signal. In [48] an FP-LD is used for the amplification and suppression of the

downstream information signal using a feed-forward technique, where the current to the FP-LD is dependent on the incoming optical signal. For low input powers the current to the FP-LD is higher and for high input powers the current is lower; this decreases the extinction ratio considerably.

It is also possible to remodulate the downstream signal with a directly-modulated FP-LD. Under the condition that both the 'ones' and 'zeroes' power levels of the injected downstream signal are above a certain threshold power, the injection-locked FP-LD will emit at the same wavelength as the downstream signal with the original data content largely suppressed. Experimental results show that the scheme can largely suppress the original 10-Gbit/s downstream data stream, allowing re-use of the optical power and simultaneous direct modulation of 1-Gbit/s upstream data [49, 50].

3.3. Frequency- and Phase Modulation Downstream and Intensity Modulation Upstream

In this section the use of frequency- and phase modulation for the downstream signal is considered. Part of the power reaching the ONU is used for detection and the other part is remodulated. An advantage of both modulation formats is that both increase the optical spectrum of the signal and subsequently reduce the Rayleigh backscattering. A disadvantage is that more complicated devices are required at both the CO and the ONU. A schematic representation of the frequency- and phase modulated signal downstream and the intensity modulated signal upstream is shown in Figure 3.3.

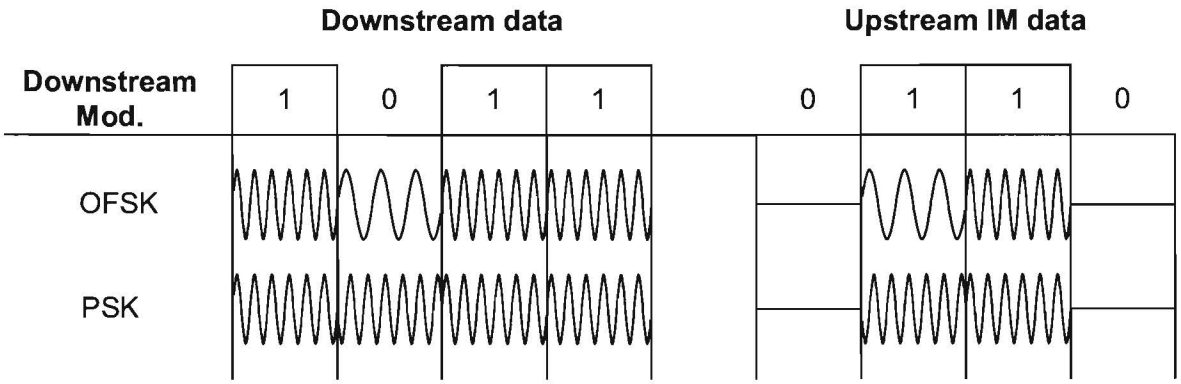

Figure 3.3.: Representation of the signals when an FSK or PSK modulated signal is used for downstream and an intensity modulated signal for upstream

3.3.1. Optical Frequency Shift Keying (OFSK)

In this section the use of optical frequency shift keying (OFSK) as the downstream modulation format is considered to facilitate upstream data remodulation. A binary OFSK signal exhibits constant light intensity with information denoted by two closely-spaced optical carriers. At

the ONU, part of the received downstream signal is tapped off and is fed into the an OFSK receiver, for downstream data detection. The other part of the received downstream signal power is fed into an optical intensity modulator for upstream intensity remodulation. The first architecture found was described by [51].

The OFSK signal can be generated by directly modulating the electrical current of a DFB laser diode. However, the drive current variation also results in a simultaneous intensity modulation of the emitted light. This intensity modulation can be suppressed when the device is integrated with an optical intensity modulator [52], which is driven by the complementary downstream data signal. The intensity modulation depth should be properly adjusted to exactly eliminate the intensity difference between the 'one' and the 'zero' levels of the output signal from the DFB laser. Another method to apply the OFSK modulation is to use a grating assisted co-directional coupler with rear sampled reflector (GCSR). A third simple method that is described in [53] employs two discrete DFB laser diodes of relatively closely-spaced wavelengths, each of which is externally modulated by a complementary electrical data signal. By appropriately adjusting the electrical tunable delay lines to synchronise the two complementary electrical data signals, the combined modulated light output will be a downstream OFSK signal, which has constant light intensity.

As the frequency spacing of the OFSK signal is much smaller than the passband of a common AWG, the downstream signal can be routed smoothly, without bringing extra crosstalk to the adjacent channels. When a narrow channel spacing is used (e.g 25 GHz), this modulation format can cause crosstalk for high data rates. Furthermore, the dispersion in the fibre has to be small to prevent walk-off which will introduce a power penalty for the upstream data. With dispersion compensation the constant intensity of the downstream signal can be preserved.

At the ONU, part of the received downstream signal is tapped off and is fed into the OFSK receiver, which can consists of an optical frequency discriminator [54] or a narrowband optical bandpass filter, followed by a photodetector, for downstream data detection. The other part of the received downstream signal power is fed into an optical intensity modulator for upstream intensity remodulation. A system with a 10-Gbit/s OFSK signal and a 2.5-Gbit/s intensity modulated signal has been demonstrated experimentally [53]. Remodulation using an RSOA at the ONU is also possible using an OFSK modulated downstream signal [55].

3.3.2. Phase Shift Keying (PSK)

In this section the use of phase shift keying (PSK) as the downstream modulation format is discussed to facilitate upstream data remodulation. A distinction is made between binary phase shift keying (BPSK) and differential phase shift keying (DPSK). At the ONU, part of the received downstream signal is tapped off and is fed into the PSK demodulator. The other part of the received downstream signal power is fed into an optical intensity modulator for upstream intensity remodulation.

For the BPSK modulation format a constant-amplitude and fixed frequency carrier signal is permitted to have two phases and these are used to represent the two digital bits '0' and '1'. Usually the two phases are chosen to differ by 180°. At the ONU a complicated coherent BPSK demodulator is needed to retract the signal. This makes this modulation format not very interesting for access networks. In [56] is proposed to use a BPSK downstream data signal to injection-lock an FP-LD. With this setup 2.5-Gbit/s downstream data and 1.25-Gbit/s upstream remodulated data was experimentally demonstrated.

In DPSK the phase does not indicate directly whether a '0' or a '1' is transmitted. Instead the data stream is conveyed by the change or no change of phase between bits. If a '0' is to be transmitted, the phase in that bit period is changed by 180° relative to that in the previous bit period. If a '1' is to be transmitted, the phase in that bit period stays unchanged. In practice, this is done by encoding the binary data stream differentially and then applying the resultant sequence to a PSK modulator. Note that a DPSK demodulator, which usually consists of a Mach-Zehnder interferometer with 1-bit delay, is needed at the ONU to facilitate direct detection.

When a constant-intensity optical DPSK signal is injected into an FP-LD for injection locking, the injection-locked signal will suffer from amplitude fluctuations due to the phase-to-intensity conversion during the injection-locking process in the FP-LD. This definitely leads to crosstalk to the upstream data when this injection-locked signal is used as the upstream optical carrier. One possible solution to suppress such crosstalk is to reduce the phase modulation depth of the downstream injection signal. However, this will inevitably impose a power penalty to the downstream signal. Another possible solution is to use a polarisation-offset modulation technique. Using the second technique 2.5-Gb/s upstream data has been experimentally demonstrated by directly modulating an FP-LD injection-locked with a 10-Gbit/s downstream optical DPSK signal [27, 57].

3.4. Sub-carrier Multiplexing

With the sub-carrier multiplexing technique the downstream and upstream signals are modulated onto a different electrical carrier. The most efficient way is to modulate one signal at baseband and the other signal onto an electrical carrier. After detection by a photodiode the downstream and the upstream signals are split by an electrical filter. The modulated signal with high frequency subcarrier is very susceptible to dispersion during fibre transmission.

Because the most important backscattering, the Rayleigh backscattering remains mainly at the optical centre frequency, also for the sub-carrier signal, it only interferes with the baseband signal and not severely with the data modulated onto the sub-carrier. This means that when the downstream signal is modulated at baseband and the upstream onto a sub-carrier as in Figure 3.4 the main part of the backscattering towards the central office can be filtered out by an electrical high-pass filter. Because the backscattering occurs at the optical centre frequency, the signal-backscattering towards the ONU does not interfere with the upstream modulation, but it does interfere with the downstream baseband signal. When the downstream signal is modulated onto an electrical carrier and the upstream signal is modulated at baseband the backscattering interferes at the ONU with the upstream modulation and at the central office with the upstream detection. The backscattering at the ONU at the detection of the downstream signal can be filtered out by an electrical high-pass filter.

Detection of a data signal modulated onto an electrical sub-carrier normally requires complex components which would be too costly for an ONU in access networks. Therefore, it is more advantageous to send the downstream signal at baseband and the upstream signal onto a sub-carrier. However, some methods have been proposed to recover the signal modulated onto the sub-carrier at baseband using either an optical or electrical technique. An optical technique is to use an optical filter like a fibre bragg grating (FBG) [58] or a delay-interferometer [59] to separate the pure optical carrier from the sub-carrier signal. Since the subcarrier is separated from the optical carrier, a baseband receiver can be used at the ONU. The filtered optical carrier can be used for upstream modulation. However, baseband components are generated from the downstream data after photodetection when the sub-carrier signal is optically filtered. This can lead to crosstalk in the upstream data from the downstream signal. Therefore it is better to split the power before detection and to remodulate the complete sub-carrier downstream signal with baseband data for upstream transmission. An electronic technique can be used where the baseband data can be detected without the optical carrier rejection filter using a high-speed photodiode, a dc block, and a full- or half-wave rectifier without any phase locked loop (PLL) for down-conversion [59]. This method requires a photodiode with a high bandwidth and may have dispersion-induced power penalties for high-frequency sub-carriers. With the delay-interferometer and an external intensity modulator 2-Gbit/s downstream and 2-Gbit/s upstream data transmission has been demonstrated experimentally.

With an RSOA at the ONU it is possible to simultaneously detect the baseband downstream signal, and to modulate the upstream signal using a sub-carrier [60, 61]. The residual baseband downstream signal does not affect the SCM upstream signal detection seriously in case an electrical filter is used after the photodiode. The RSOA has a limited bandwidth

which will limit the maximum bitrate severely. An EAM is also capable of simultaneously detecting a signal and modulating at different electrical sub-carriers [62]. Due to the large bandwidth of an EAM it is possible to transmit high bitrates in both the downstream as well as the upstream direction.

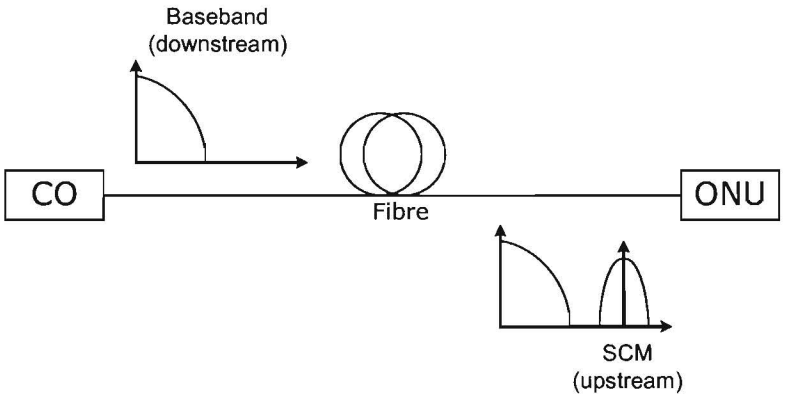

Figure 3.4.: Downstream and upstream modulation on the same wavelength using SCM

3.5. Coherence Modulation

In this section coherence modulation is considered to facilitate both downstream and upstream on the same wavelength. The key of the coherence modulation relies on the implementation of optical delays greater than the coherence length to code the signals in one direction. Broadband optical sources with a short coherence length are required. Single-mode laser diodes can be used, but require large optical delays whose implementation can introduce practical problems. This makes this technique unsuitable for WDM architectures.

In the central office, the light is launched into a Mach-Zehnder interferometer which has two path pairs of different length mismatches. The optical path length difference is chosen to be much longer than the source coherence length so that a change in the relative phase between the arms of the interferometer will not be converted into detectable intensity modulation at the output. The information imprinted on the light is the difference in the phase between the two arms of the interferometer. After the light has traveled to the ONU, phase information can be retrieved by the receiving interferometer with the same path length difference, to within a fraction of the coherence length. Thus the phase modulation is converted to amplitude modulation.

At the ONU, part of the incoming power is used for detection as described above. The other part of the power can be re-used for upstream intensity modulation [63] or for coherence modulation [64, 65]. A different optical path length is required for the upstream signal when both signals use coherence modulation.

3.6. Comparison of the Modulation Formats

In this section the modulation formats are compared. For the intensity modulation downstream and upstream only two methods are considered which are the most promising: 1) coding (in combination with bitrate differentiation) and 2) remodulation by suppressing the downstream signal. Table 3.1 gives an indication whether the properties of the different modulation formats are positive or negative.

All the techniques, except for the continuous-wave, use the same wavelength for upstream and downstream transmission and are therefore considered bandwidth efficient. The coherence modulation method cannot be combined with a WDM architecture since it requires a light source with a very broad optical spectrum and is therefore also not considered to be efficient.

An equal bitrate for the downstream and the upstream signals (on the same wavelength) is possible for all the techniques except for the continuous-wave feeded technique. The method using coding is capable of transmitting synchronous bitrates, but performs better when different bitrates are used and electrically filtered.

Because the signal is remodulated with the same modulation format the crosstalk will be the largest for the coding method. The suppression method suppresses the downstream signal, but some leftover signal can still interfere with the upstream signal. With the coherence modulation method also some crosstalk can be present. For the other modulation formats the crosstalk is limited.

For the OFSK and DPSK modulation formats additional components are required to demodulate the downstream signal. The SCM method can use an EAM or an RSOA that works simultaneously as modulator and detector, but more complex electrical components are required for the modulation and the demodulation of the signal modulated onto the sub-carrier. The modulator and demodulator for the coherence modulation technique are not very complex, but can become complex when a light source with a narrower linewidth is required.

The coherence modulation method requires, as mentioned before, a light source with a broad optical spectrum, which makes it unsuitable for WDM architectures. Both the OFSK and the DPSK method increase the optical spectrum of the signal which can cause problems if a dense WDM (DWDM) architecture is used. The other modulation formats can be used in a DWDM architecture without problems.

The increased optical spectrum has the advantage that the backscattering is reduced for the OFSK, DPSK and coherence modulation formats. Since for the SCM one signal is modulated onto a sub-carrier, and the backscattering is mainly at the frequency of the optical carrier, some backscatter components can be electrically filtered out. When a gain saturated device is used for the suppression method the signal backscattering impairments are also reduced. The backscattering is not reduced for the other modulation formats.

For the measurements described in this report the method using a continuous-wave signal downstream and intensity modulation upstream is used. This is the most simple setup to build and can be extended to one of the different methods.

Table 3.1.: Comparison of the modulation formats

Property	CW-IM	IM-IM (coding)	IM-IM (suppression)	OFSK-IM	PSK-IM	SCM	Coh. mod.
Bandwidth efficiency	–	+	+	+	+	+	–
Synchronous bitrate	–	o	+	+	+	+	+
Crosstalk between DS on US	+	–	o	+	+	+	o
Complex components	+	+	+	–	–	–	o
Suitable for (D)WDM	+	+	+	o	o	+	–
Reduces BS impairments	–	–	o	+	+	o	–

4. Characterisation

In this chapter the characterisation of the devices is described. The characterisation consists of mainly static measurements for the two SOAs, the EAM and the EDFA that were used for the transmission measurements described in Chapter 5. The manufactures and the model numbers of the devices are given in Appendix C. The characterisation was performed for different wavelengths to determine the optical bandwidth at which the devices can be used. The wavelengths under test were 1530, 1540, 1550, 1560 and 1570nm. The output power of the laser was kept constant at +10dBm for all the measurements, and the resolution of the OSA was set at 0.01nm.

Most of the measurements carried out in this chapter were performed using Labview to control the measurement equipment. The specifications of the measurement equipment are described briefly in Appendix C.

4.1. Characterisation of the Pre-amplifier SOA

The semiconductor optical amplifier (SOA) is used to amplify the the optical signal before the EAM in the ONU. In this section the static measurements for the SOA are described. The specifications that were measured are the amplified spontaneous emission (ASE-)spectrum, the transparency current, the gain-saturation power, and the optical signal to noise ratio (OSNR).

Measurement Setup

The measurement setup, as shown in Figure 4.1, is used for the measurements. The power of the laser was kept constant at +10dBm. The VOA was used to adjust the power level into the SOA. The isolator is placed after the laser to prevent any signals to be directed into the laser. The optical signal was divided by a 50/50 coupler, one output was connected to the power meter and the other output to the SOA. The output of the SOA was monitored by the OSA for different currents, different input power levels, and different wavelengths. The current and the temperature to the SOA were controlled with a controller unit. The temperature of the SOA was kept constant at 20 degrees.

The wavelengths used for the measurements range from 1530 to 1570nm in steps of 10nm. The input powers used in this measurement range from -40 to -5dBm in steps of 5dB, measured with the power meter. The gain was measured as the difference between the peak input signal and the peak output signal of the SOA. The peak input signal was acquired by first taking a reference measurement with a fibre in stead of the SOA. The measurements were carried out for the best polarisation state which was set in the linear region (-15dBm

input power) and at a current of 250mA. The polarisation was adjusted until the highest output power was received at the OSA.

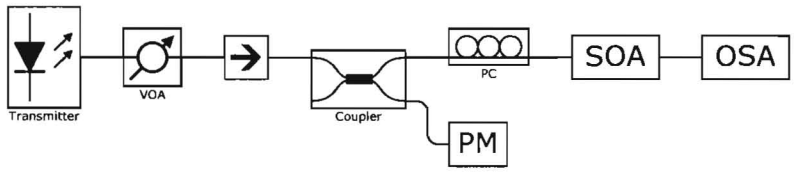

Figure 4.1.: SOA measurement setup

Results and Discussion

The ASE-spectrum of the SOA with no optical input and a driving current of 300mA is shown in Figure 4.2(a). From this figure can be seen that the peak of the ASE-spectrum is around 1525nm. The superimposed spectra for different wavelengths with an input power of -10dBm are shown in Figure 4.2(b). All the spectra show a lower ASE level than for the case with no input. For the longer wavelength the ASE level is a bit higher than for the shorter wavelengths.

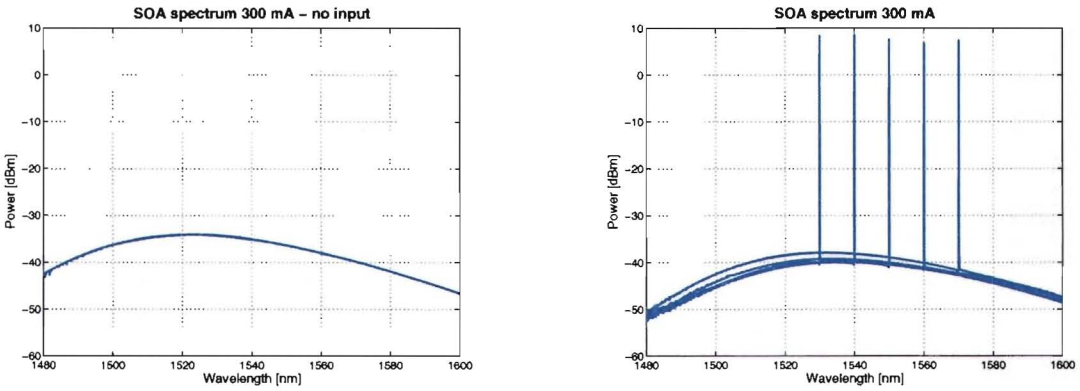

(a) (b)

Figure 4.2.: Spectrum of SOA at 300mA with no input (a) and superimposed spectra of SOA with inputs of -10dBm (b)

To determine the optimum drive current a measurement for different currents was carried out for one wavelength, 1550nm. From the resulting curve in Figure 4.3(a) can be seen that the gain region of the SOA starts around 50mA (the transparency current) and that the gain is the highest for 300mA. Figure 4.3(b) shows that the gain saturation occurs at higher input powers for lower driving currents.

The gain of the SOA for the different wavelengths at 300mA is shown in Figure 4.4(a). From this figure can be seen that the gain is lower for longer wavelengths, this is due to a lower carrier density for longer wavelengths. Between the outer wavelengths there is a gain difference of around 4dB. As the input power to the SOA is increased, the gain decreases due

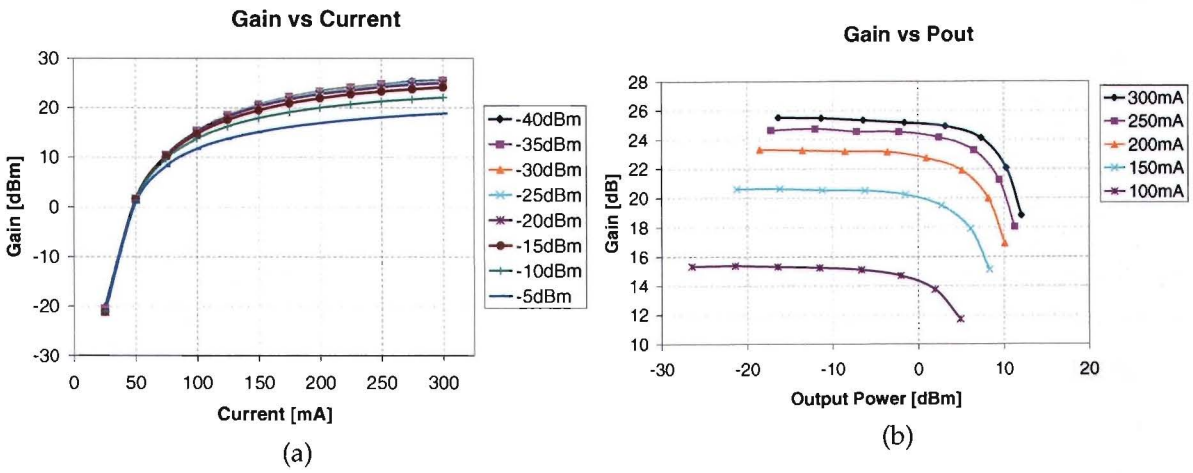

Figure 4.3.: Gain versus current (a) and versus output power (b) for 1550nm

to depletion in the carrier density of the active region of the SOA. The saturation power is defined as the optical power at which the gain drops by 3 dB from the small signal value. The saturation powers for the different wavelengths are shown in Figure 4.4(b). The graph shows that the longer wavelengths have a higher saturation output power; this is due to the larger availability of carriers with a lower energy.

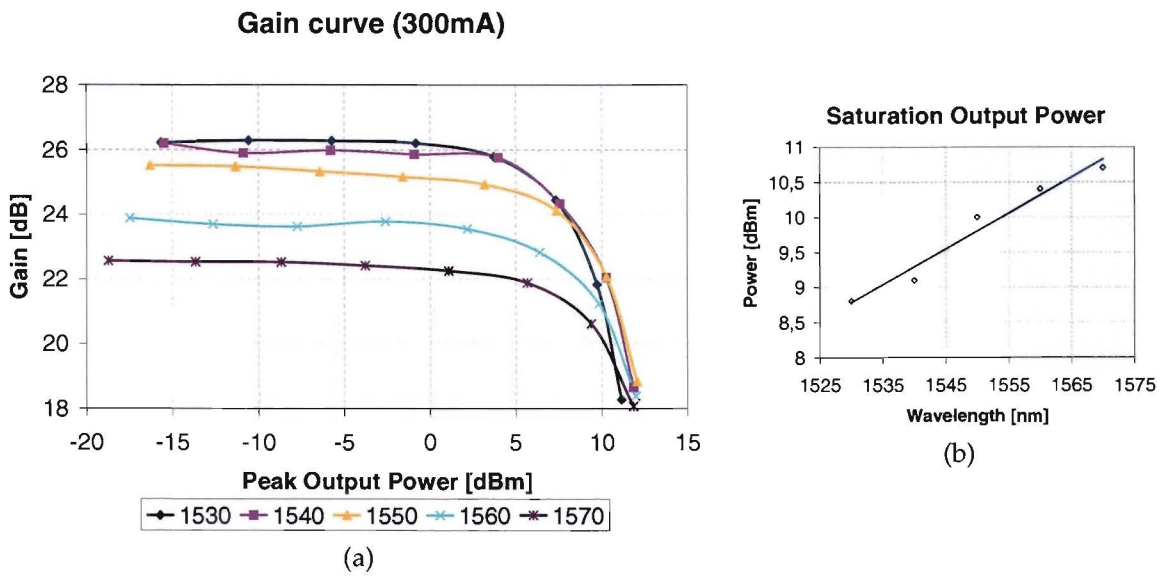

Figure 4.4.: Gain curve (a) and saturation output power curve (b) at 300mA

The noise levels and signal levels versus input power are shown for the different wavelengths in Figure 4.5(a). The noise levels and the signal levels of the shorter wavelengths are lower than for the longer wavelengths. In the gain-saturation region, the noise level is decreasing and the increase of the power level is declining. The differences of the signal levels and the noise levels for the different wavelengths are such that the OSNR curves of all the wavelengths are almost identical. At the saturation region the increase of the signal

power is decreasing at the same rate as the noise floor decreases, what causes that the OSNR stays linear as is shown in Figure 4.5(b).

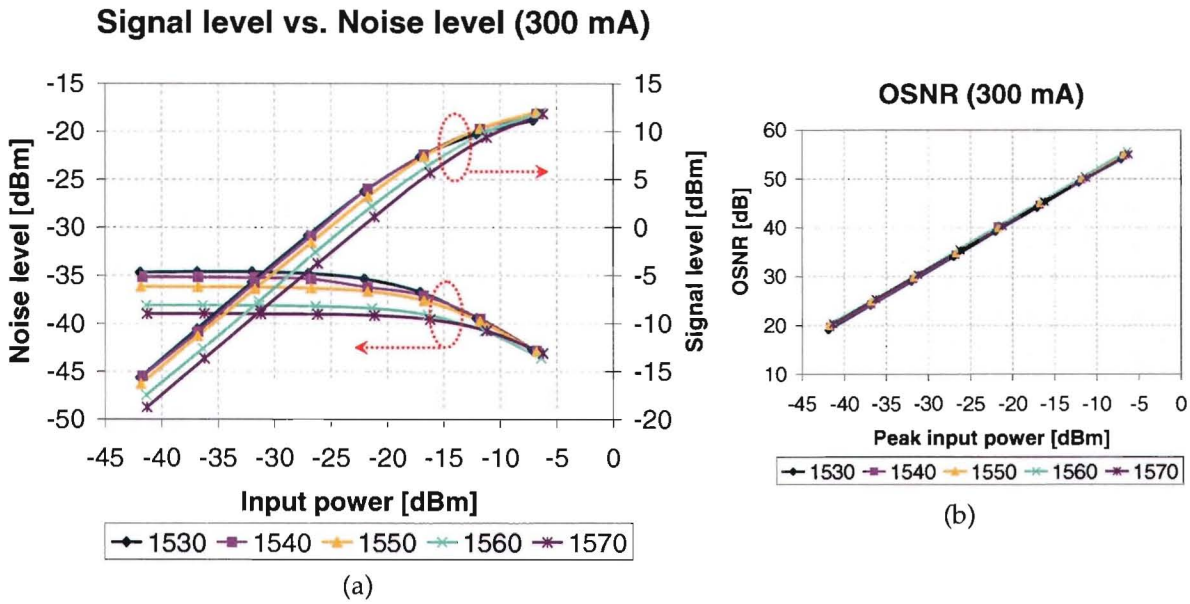

Figure 4.5.: Noise and signal levels (a) and the corresponding OSNR (b) for the SOA at 300mA

4.2. Characterisation of the Booster SOA

This SOA is placed after the EAM to boost the optical power. The characterisation is performed in a similar manner as for the SOA in the previous section. The specifications that were measured are the ASE-spectrum, the transparency current, the gain-saturation powers, and the optical signal to noise ratio (OSNR).

Measurement Setup

The same measurement setup as in Figure 4.1 is used, but a different SOA is characterised. The measurements were carried out in the same manner.

Results and Discussion

The ASE-spectrum of the SOA with a driving current of 350mA is shown in Figure 4.6(a) with no input signal and in Figure 4.6(b) for input signals of -5dBm. The peak of the spectrum is around 1500nm as can be seen in the figures. From the spectra with input signals can be seen that the ASE-spectrum is depleted more for the shorter wavelengths than for the longer wavelengths.

Figures 4.7(a) and (b) show the gain of the SOA for different currents and different input powers. The transparency current of the SOA is around 50 mA. From the second figure can

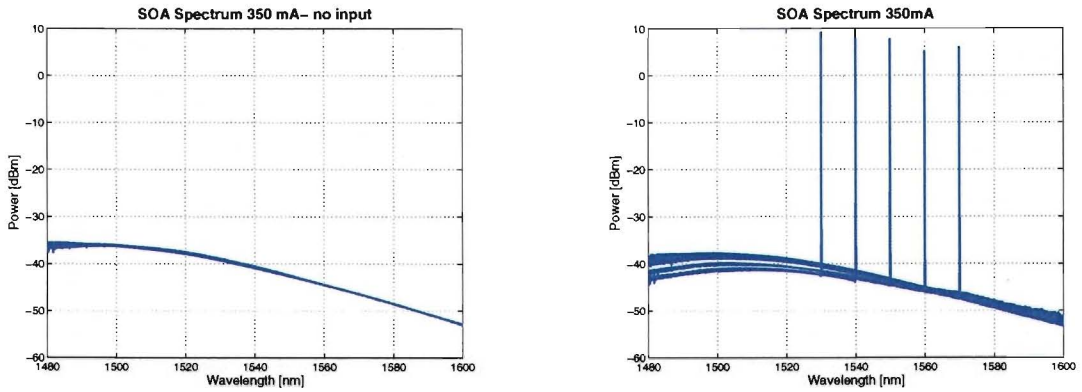

(a) (b)

Figure 4.6.: Spectrum of SOA2 with no input (a) and superimposed spectra of SOA2 with inputs of -5dBm at 350mA (b)

be seen that the saturation output power is higher for higher currents. Furthermore shows the figure that the saturation occurs at higher input powers for lower currents.

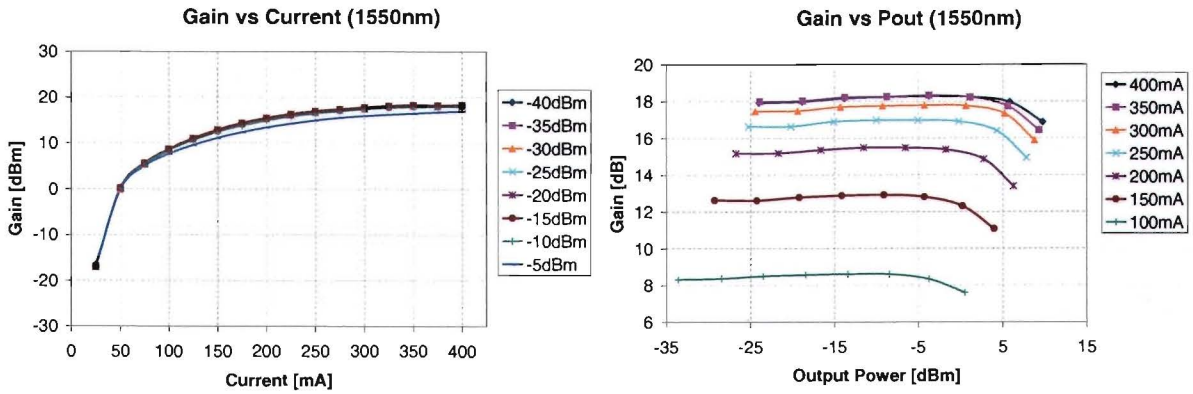

Figure 4.7.: Gain versus current (a) and versus output power (b) for 1550nm

The gain curves for the different wavelengths are shown in Figure 4.8. The input power during the measurement was too low to determine the saturation power values, but it is clearly visible that the saturation powers are higher for the shorter wavelengths. The gain difference in the linear region between the two outmost wavelengths is around 6dB.

The noise levels and signal levels versus input power are shown for the different wavelengths in Figure 4.9(a). The noise levels and the signal levels of the shorter wavelengths are lower than for the longer wavelengths. At the gain-saturation region, the noise level is decreasing and the increase of the power level is flattening. The differences of the signal levels and the noise levels for the different wavelengths are such that the OSNR curve of all the wavelengths are almost identical. At the saturation region the increase of the signal power is decreasing at the same rate as the noise floor decreases, what causes that the OSNR stays linear as is shown in Figure 4.9(b).

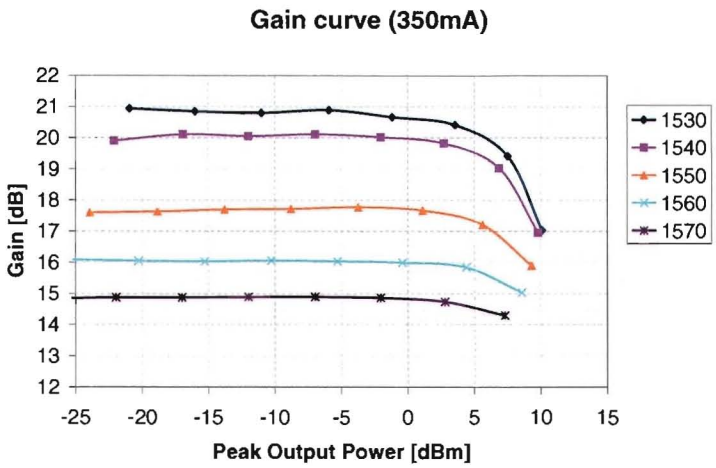

Figure 4.8.: Gain curve at 350mA

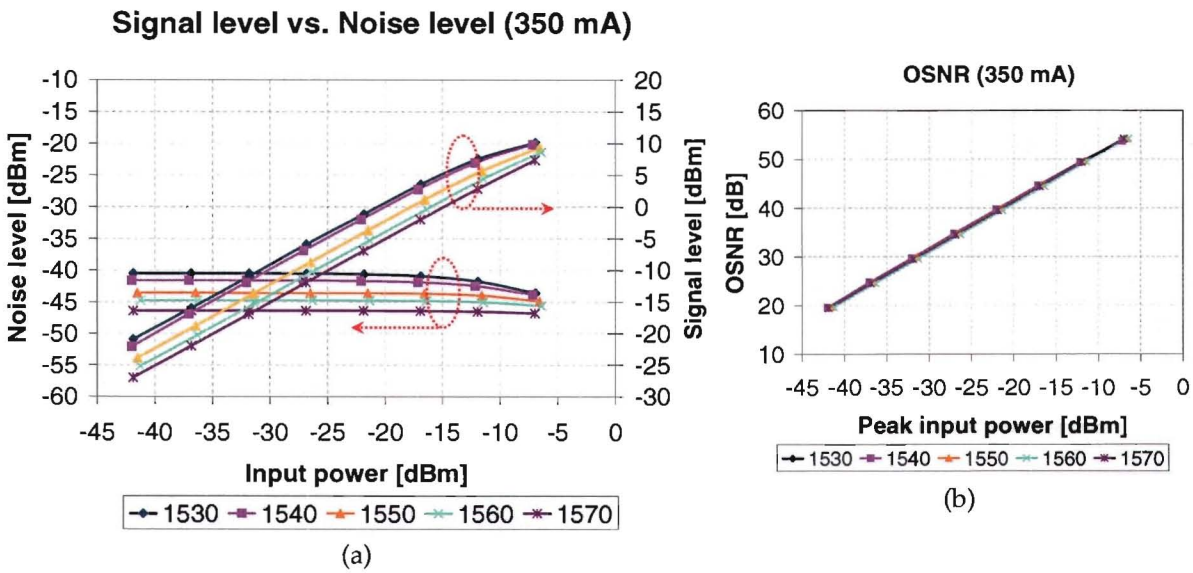

(a) (b)

Figure 4.9.: Noise and signal levels (a) and the corresponding OSNR (b) for the SOA2 at 350mA

4.3. EAM Characterisation

The electro-absorption modulator (EAM) located at the ONU is used to modulate the upstream data onto the CW-signal from the central office. The characterisation of the EAM is described in this section. The characteristics that are measured are the absorption for different reverse voltages, the extinction ratio, and the polarisation dependence.

Measurement Setup

The setup as is shown in Figure 4.10 is used for the static EAM measurements. The light of the laser was attenuated to the desired power level by the VOA. The 50/50 coupler divides one part of the signal power to the EAM and the other part of the power to the power meter to measure the input power. A polarisation controller was used to set the polarisation into the EAM. A second power meter is used after the EAM to measure the output power.

The output power of the EAM was measured for different voltages for two input powers: 0 and +10dBm. For the measurement with +10dBm input power, the light of the laser was coupled directly into the EAM. This was done to reduce the attenuation, since the maximum stable output power of the laser for the wavelength range is +10dBm.

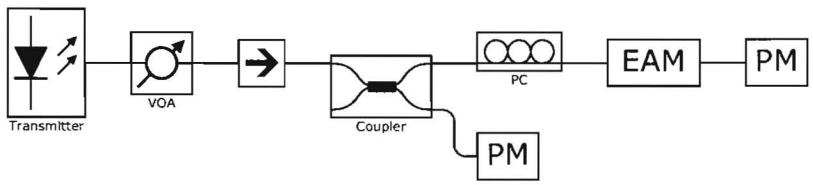

Figure 4.10.: EAM measurement setup

The temperature of the EAM was kept constant with a Newport temperature controller, with the resistance set to 10 kΩ. The reverse voltage is applied to the EAM by a voltage source. The electrical scheme can be seen in Figure 4.11.

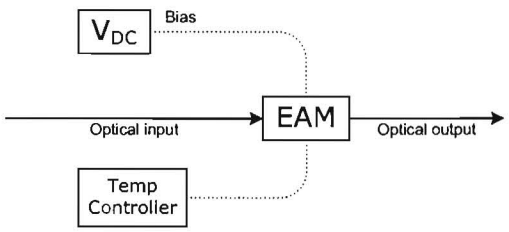

Figure 4.11.: Electrical Connection Scheme EAM

The polarisation state was once optimised with the polarisation controller for the highest attenuation at 4V reverse voltage (best polarisation (BP)) and once for the lowest attenuation at 4V reverse voltage (worst polarisation (WP)).

Results and Discussion

The attenuation curves for 0dBm input power are presented in Figure 4.12, and for +10dBm input power in Figure 4.13. The figures show the normalised ($P_{out} - P_{in}$) attenuation values. The left curves show the results for the best polarisation states which corresponds with a TE-polarisation and the right curves for the worst polarisation states, which corresponds with a TM-polarisation. The attenuation curves for the worst polarisation states show much lower attenuation than for the best polarisation state.

The figures indicate that the longer wavelengths, close to the band edge, have a relatively small absorption change, due to the relatively low density of states there. This absorption, however, for the wavelength of 1530nm at the best polarisation state is flattening at higher reverse voltages. This behaviour is normal for an MQW-EAM and is also shown in [66]. For the higher input power this flattening is stronger than for the lower input power.

The insertion loss (attenuation at $0V_{rev}$) for the shorter wavelengths is considerably higher than for the longer wavelengths, the differences are compared in Figure 4.14(a). It can be seen that the insertion loss is much lower for the worst polarisation state than for the best polarisation state. It can also be seen that the insertion loss for the input signal of 0dBm is a bit higher than for the input signal of +10dBm.

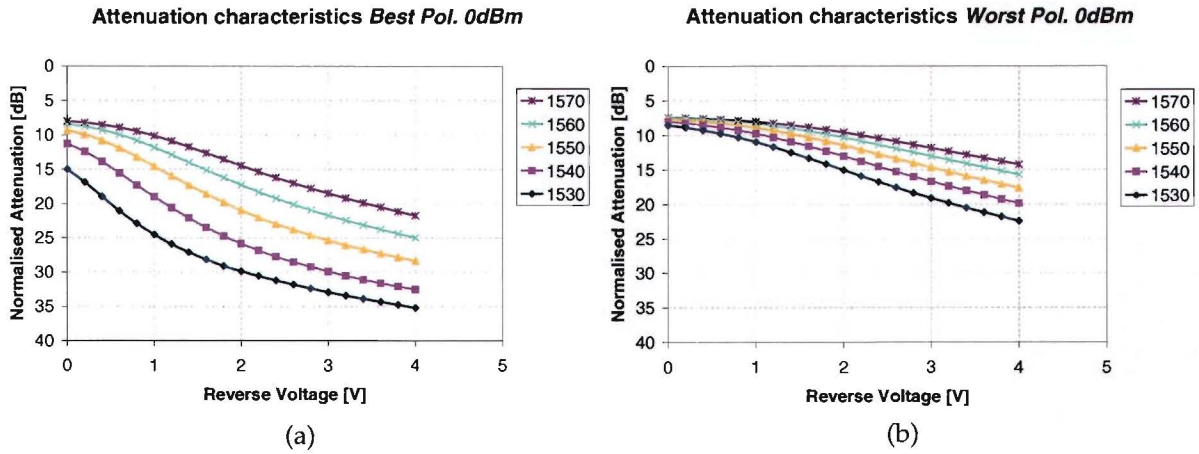

Figure 4.12.: Attenuation for the best (a) and worst (b) polarisation state for 0dBm input power

Figures 4.15 and 4.16 show the extinction ratio of the EAM. The extinction ratio is defined as the difference between the output power at $0V_{rev}$ and at the maximum reverse voltage of $4V_{rev}$. It can be seen from the curves in the figures that the extinction ratio is larger when the reverse voltage is increased. The extinction ratio at $4V_{rev}$ is larger for the case with the higher input signal as is better shown in Figure 4.14(b). From this figure and from the extinction ratio figures can be seen that the largest extinction ratio is not at the shortest wavelength but at 1540nm (of the used wavelengths). At lower reverse voltages until 2V the extinction ratio is still the largest for 1530nm, but for higher voltages the extinction ratio of 1540nm becomes the largest. This difference is larger for the measurement with the higher input signal.

It is not clear why the measurement with a higher optical input power shows different behaviour. It can be a measurement error or it is due to the behaviour of the device. No

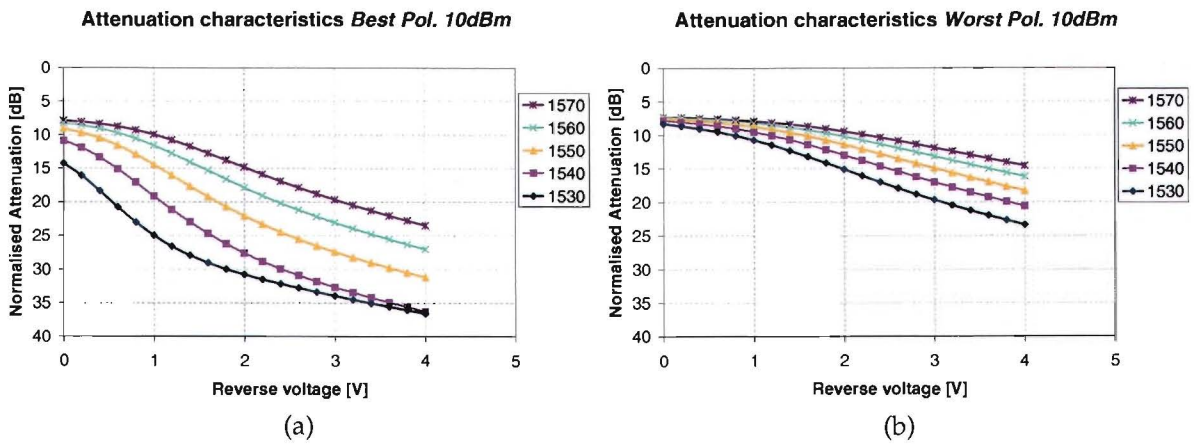

Figure 4.13.: Attenuation for the best (a) and worst (b) polarisation state for +10dBm input power

publications were found that describe a similar behaviour. Maybe there is some insertion loss difference, due to the different setups used, but these differences are absolute and not relative, so the normalised loss and extinction ratio should not be influenced by that. Another option is that the polarisation is not set correctly or that there is some polarisation changing for high input powers in the EAM.

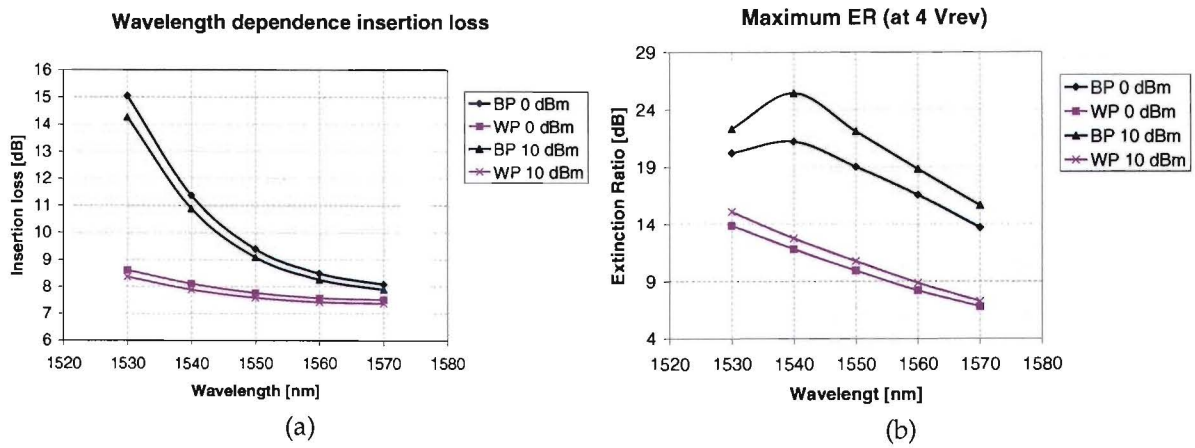

Figure 4.14.: Insertion loss (a) and the ER difference (b)

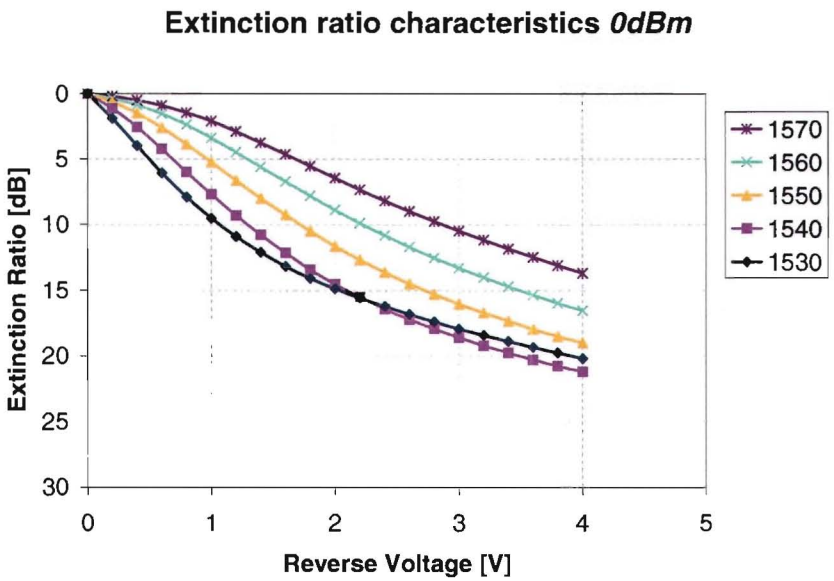

Figure 4.15.: Best ER for 0dBm input power

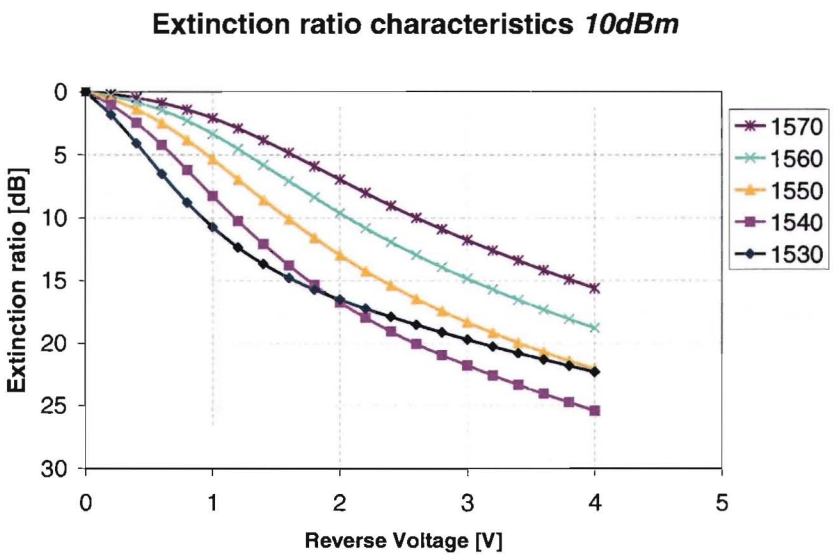

Figure 4.16.: Best ER for +10dBm input power

4.4. EDFA Characterisation

The erbium doped fibre amplifier (EDFA) is used at the receiver site in the central office as an optical pre-amplifier to increase the receiver sensitivity. The specifications that were measured are the ASE-spectrum, the gain-saturation power, and the optical signal to noise ratio (OSNR).

Measurement Setup

The characterisation of the EDFA was performed with the setup shown in Figure 4.17. The power of the laser was kept constant at +10dBm and the desired power into the EDFA was achieved by adjusting the VOA. The 50/50 coupler divides the light to the EDFA and the power meter, so that the power meter indicates the input power of the EDFA. The output of the EDFA was monitored by an OSA.

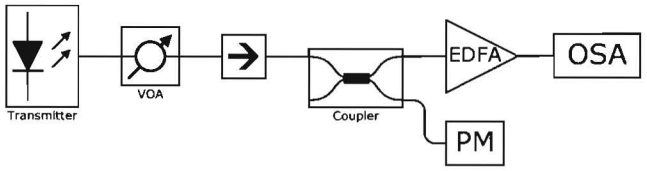

Figure 4.17.: EAM Measurement Setup

The EDFA unit is driven by a voltage of 15 V. In the unit, this voltage is converted to a fixed drive current. For different input powers the spectrum was measured and analysed. The gain was measured as the difference between the peak input signal and the peak output signal of the EDFA. The peak input signal was acquired by first taking a reference measurement with a fibre in stead of the EDFA. The OSNR was measured in the same way as for the SOA measurements.

Results and Discussion

Figure 4.18 shows three output spectra of the EDFA: (a) shows the output spectrum with no input signal, (b) shows the superimposed spectra for all the wavelengths with an input signal of -40dBm, and (c) shows the superimposed spectra for all the wavelengths with an input signal of -20dBm. The ASE-spectrum of the EDFA with no input, has a peak around 1530nm and an almost flat region between 1540 and 1560nm. Before 1530 and after 1560 the values are decreasing rapidly. For the low input powers ASE-spectrum stays the same for all the wavelengths. When the input power becomes higher and the EDFA becomes into saturation, the ASE-spectrum gets depleted. For the shorter wavelengths it depletes more than for the longer wavelengths due to the larger carrier availability.

The gain for 1530nm in the linear region is with 45dB around 10dB larger than the gain for 1540, 1550 and 1560nm, which are within 1dB difference as can be seen in Figure 4.19(a). The gain for 1570nm is the lowest and is around 23dB. The shape of these gain values correspond

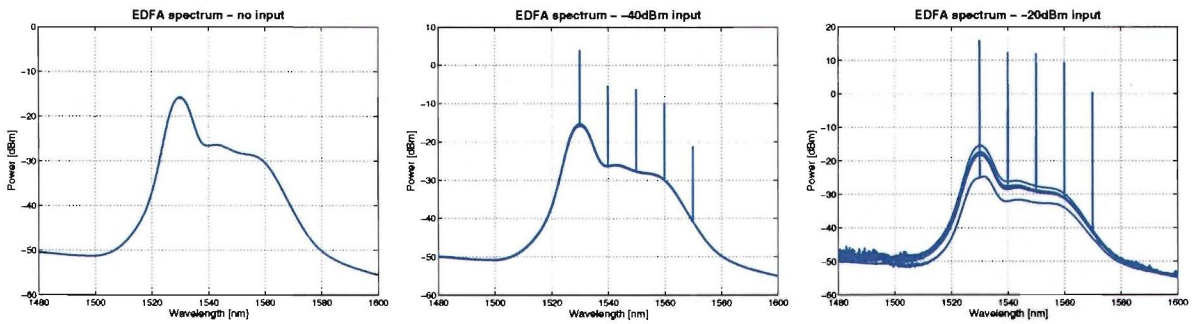

Figure 4.18.: Output spectrum of EDFA for: (a) no input signal, (b) -40dBm input, and (c) and -20dBm input

to the shape of the ASE-spectrum of the EDFA. The saturation output power curve in Figure 4.19(b) shows that the saturation output powers are higher for longer wavelengths.

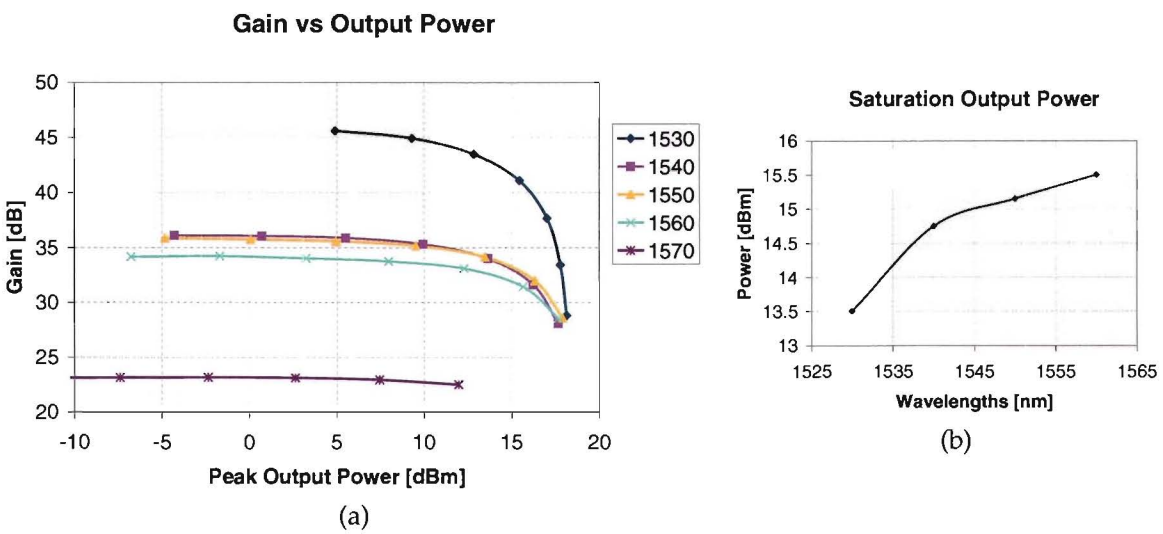

Figure 4.19.: Gain curve (a) and saturation output power curve (b) for the EDFA

Figure 4.20(a) shows the noise and power levels at the output of the EDFA for different input powers. The signal power is the highest at 1530nm, but also the noise power is the highest. The noise level of the EDFA when a low input power at 1530nm is inserted is even higher than the signal level with an input at 1570nm with the same power. When the input power is increasing and the EDFA is getting into saturation, the increase in signal level is flattening and the noise level is decreasing due to depletion of the ASE power. The difference between the signal and the noise level is the OSNR, and is shown in Figure 4.20(b). The effect at the signal and noise levels in the saturation region balance out and the OSNR stays linear with the input power for the whole measured range.

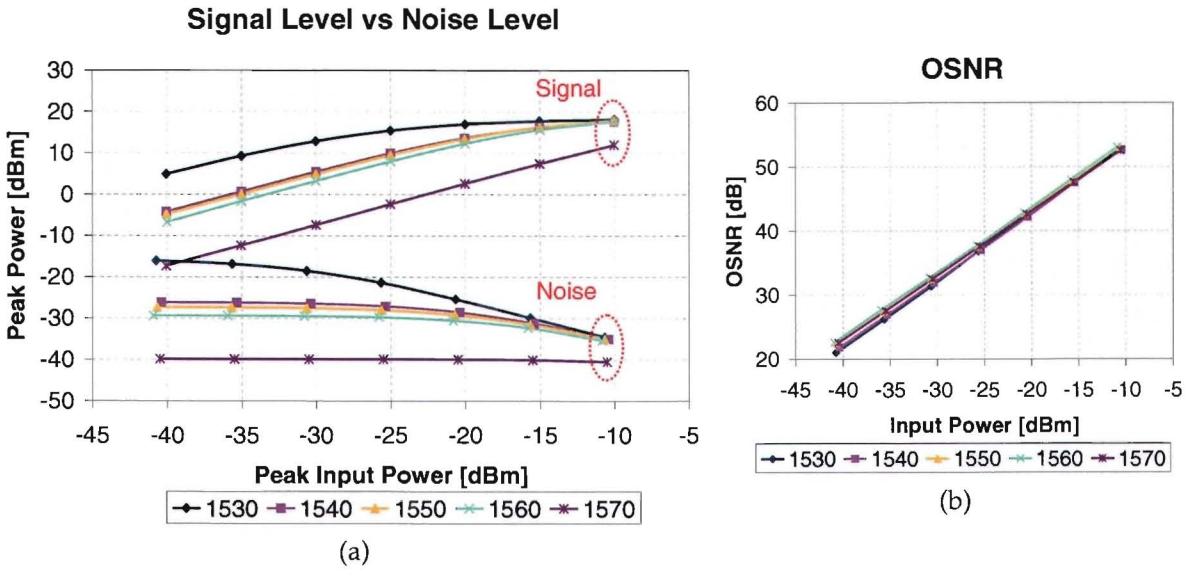

Figure 4.20.: Noise and signal levels (a) and the corresponding OSNR (b) for the EDFA

4.5. Receiver Characterisation

The EDFA, together with a few other passive components is used as the receiver which will stay in the same setup during the transmission measurements. Because we will consider this as one unit and because different wavelengths are used in the transmission measurements this section characterises the gain of the complete receiver for the channels used for the transmission experiments.

Measurement Setup

Since the EDFA suffers from high transient effects when the electrical current is turned on, an optical delay line is inserted which can be used to block the optical signal by inserting a paper card in the light path. The insertion loss of the delay line is around 2dB. After the delay line a filter is placed to filter out the ASE-noise generated by the EDFA, a fixed AWG was used as the filter. The channels are according to the ITU-grid and have a channel spacing of 100GHz and a passband of 0,8nm. The insertion losses and the wavelengths of the channels are shown in Table 4.1. An in-line attenuator/power meter is finally placed after the filter to keep the power going into the receiver constant, so that the receiver is shot noise limited and not limited by the thermic noise. The total measurement setup is shown in Figure 4.21.

The gain of the receiver is measured as the previous measurement by changing the input power and measuring the output power with an OSA.

Results and Discussion

The gain curve can be seen in Figure 4.22. All the four wavelengths are on the reasonable flat part of the ASE-spectrum. The gain increases about 2dB each time when the channel moves

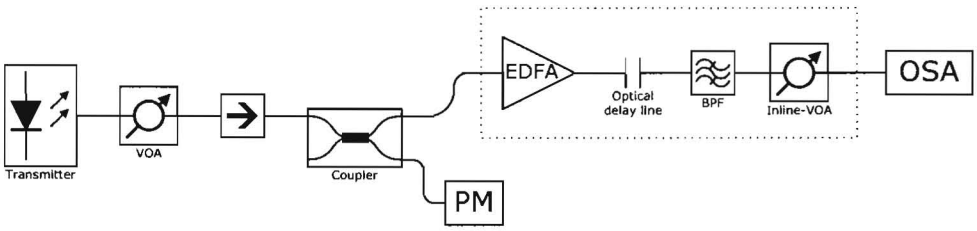

Figure 4.21.: Receiver measurement setup

Table 4.1.: Insertion los AWG

Channel number	Wavelength [nm]	Insertion Loss AWG [dB]
C19	1562.23	0.94
C30	1553.33	2.34
C40	1545.32	1.41
C50	1537.40	1.38

to a shorter wavelength. This is due to the different gain of the EDFA and due to the different insertion losses for the channels as are given in Table 4.1. The insertion losses of the optical delay line and the in-line VOA introduce a loss which is constant for all the channels.

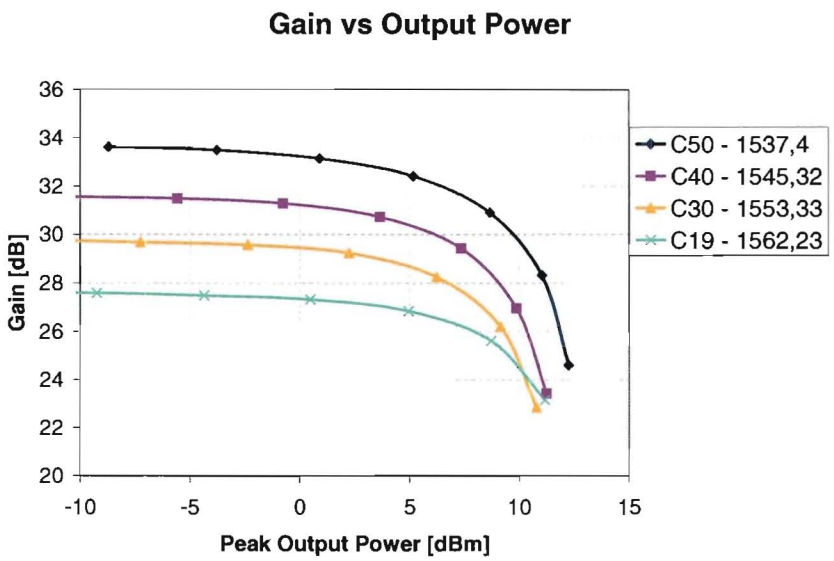

Figure 4.22.: Gain cure for receiver

4.6. Backscattering Measurements

Since a single fibre network architecture is used it is important to know how much power is scattered back in the fibre. The light is reflected at discontinuities and is scattered mainly in the elastic process of Rayleigh backscattering (RBS), which is caused by the microscopic fluctuations of the refractive index in the fibre. Besides the elastic Rayleigh backscattering, the inelastic processes of Raman and Brillouin scattering occur in optical fibres. Raman scattering is caused by the molecular vibrations, while Brillouin scattering results from reflection at thermally activated acoustical phonons. The Raman scattering occurs only at very high input powers and will not be considered in this section, the Rayleigh scattering and the Brillouin scattering are considered.

Measurement Setup

The measurement setup that was used to measure the backscattering is shown in Figure 4.23. The laser signal is attenuated and the power is split by a 90/10 coupler to determine the power into the fibre. The circulator directs the backscattered signals to a 50/50 coupler which divides the power equally among a power meter and an OSA. The OSA measured the peak values of the Rayleigh, and the two Brillouin backscattering peaks. The laser was operated in a condition without coherence control which corresponds to a linewidth of <0.2MHz, and with coherence control which corresponds to a linewidth of around 200MHz. For four wavelength channels the reflections are measured for different input powers.

Because the laser has a maximum stable output of +10dBm, and because of the insertion losses of the VOA, the 90/10 coupler and the circulator, the maximum power coupled into the fibre is limited to around +5dBm. To reach higher input powers, some points were measured with only an inline attenuator/power meter in stead of the step VOA and the coupler. Because of the lower insertion loss of the inline attenuator/power meter a maximum power of around +7.5dBm could be coupled into the fibre with this setup.

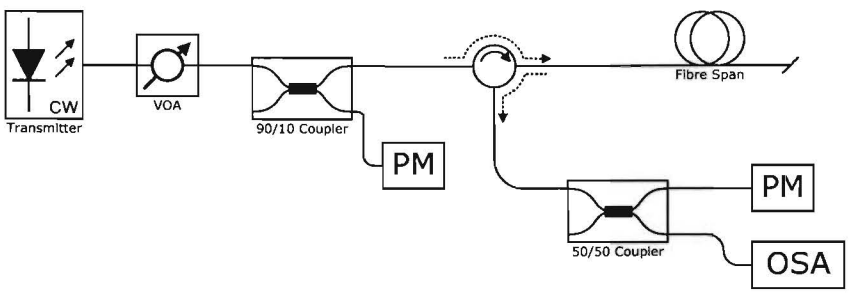

Figure 4.23.: Setup to measure the backscattered signals

Results and Discussion

The spectrum of the backscattered signal is shown in Figure 4.24 for different input powers. The spectrum for channel C30 with an input power of -1.5dBm into the fibre (a) shows that the Rayleigh backscattering (RBS) forms the main backscatter mechanism and it shows that Brillouin backscattering is present at both sides of the Rayleigh backscattering. The difference in wavelength between the Rayleigh and the Brillouin backscattering is around 10.9GHz for both sides. When the input power is increased to +5.5dBm (b) we can see that the Brillouin scattering at the longer wavelength is increasing while the Brillouin scattering at the shorter wavelength is still small. When the input power is increased even more to +7.5dBm (c) we can see that the Brillouin scattering at the longer wavelength shift is the main backscattering, while the Brillouin scattering at the shorter wavelength shift is still small.

The wavelength shift of the Brillouin scattering is caused by the fact that the light reflected at the thermally activated acoustical phonons experiences a Doppler shift of -10.9GHz or +10.9GHz, depending on the direction of propagation of the phonons. As the phonons have no preferred direction of propagation along the fibre, the powers from Brillouin scattering are the same [67]. An asymmetry occurs for higher powers, then the Brillouin process introduces gain at the 10.9GHz longer wavelength, while the same process introduces depletion (attenuation) at the 10.9GHz shorter wavelength.

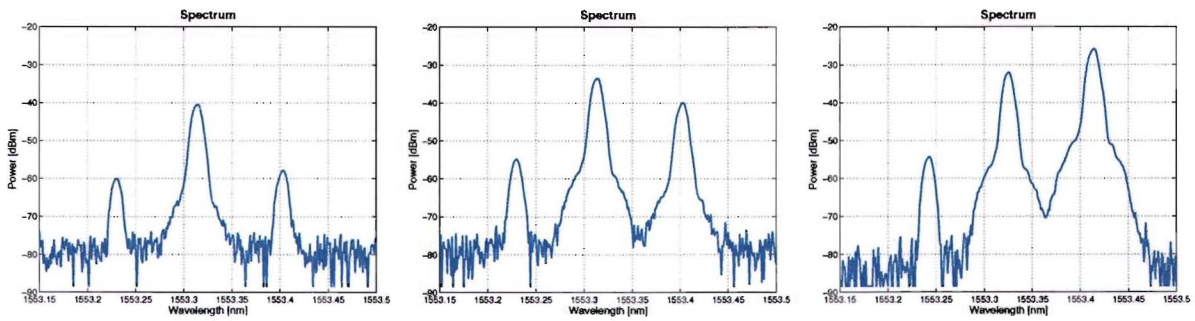

Figure 4.24.: Spectrum of the backscattered signals for channel C30 input powers of: (a) -1.5dbm, (b) +5.5dBm, and (c) +7.5dBm

Figures 4.25 and 4.26 show the measured backscattering for 25km and for 50km. For both figures (a) is without the coherence control option and (b) is with the coherence control. The figures show that the backscattering is independent of the wavelength. It can be seen that with the narrower linewidth condition the Brillouin scattering at the longer and shorter wavelengths are equal until a threshold power. If this threshold power is exceeded, the Brillouin scattering grows exponentially at the longer wavelength range and become stimulated Brillouin scattering (SBS). When the laser is operated at the broader linewidth condition this threshold cannot be observed. The input power into the fibre where the SBS becomes larger than the RBS without coherence control is for the shorter length of fibre at a bit higher than for the longer length.

Figure 4.27(a) shows the absolute and normalised (P_{BS}-P_{in}) total backscatter powers for channel C30 measured with the power meter. The normalised backscattered powers are

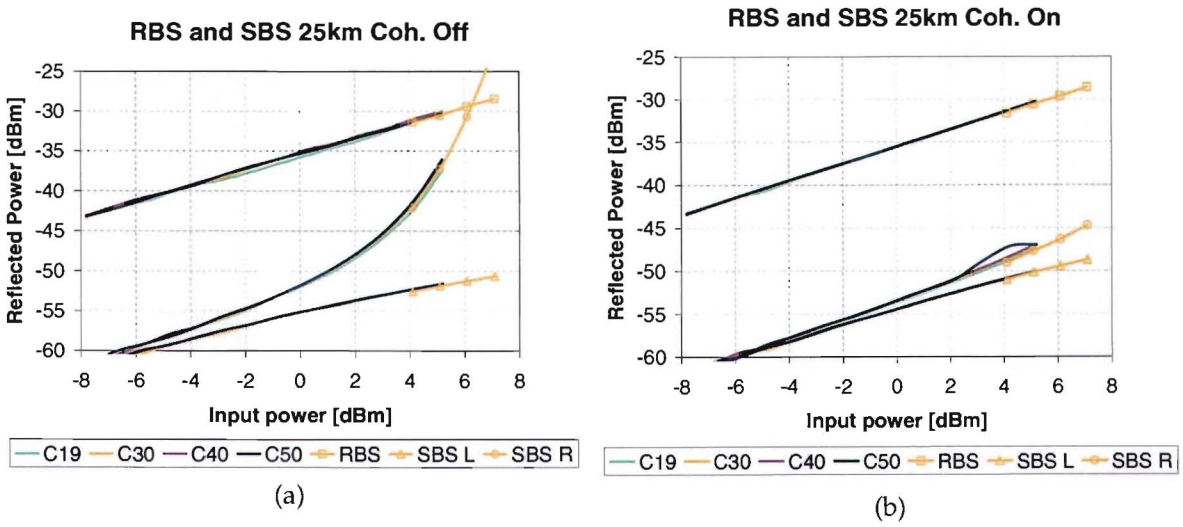

Figure 4.25.: Backscattering of 25km fibre without (a) and with (b) coherence control

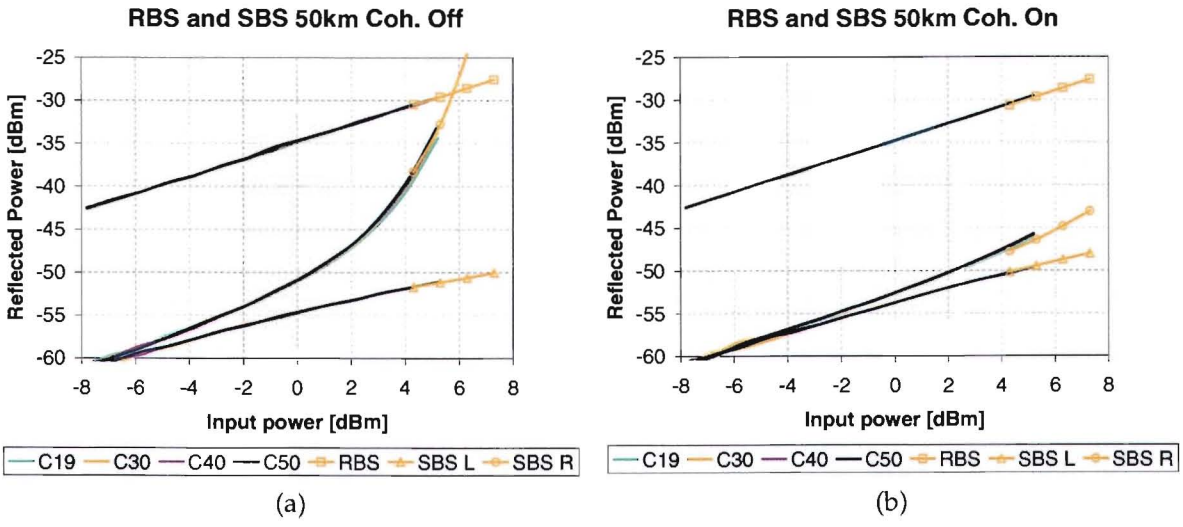

Figure 4.26.: Backscattering of 50km fibre without (a) and with (b) coherence control

constant except for the last value of +5dBm, this is due to SBS as was seen in the previous figures. The power values of the backscattered signals are around 1dB larger as was seen in Figures 4.25 and 4.26. This can be cause by some insertion loss of the input of the OSA. Figure 4.27(b) shows the normalised backscattered powers for different lengths. The normalised powers were taken as an average of the points between -7 and 0dBm. It can be seen that the RBS increases with the length of the fibre, but the increase is getting smaller and converges. The values found are similar to the values described in Appendix B

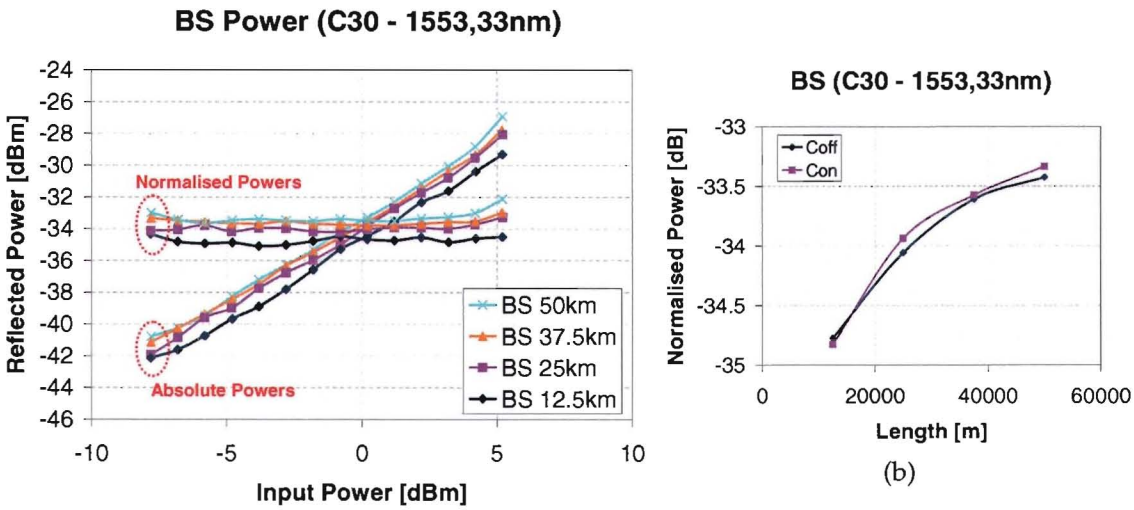

Figure 4.27.: Backscattering measured with the power meter (a), and the backscattering versus fibre length for the coherence control of the laser on (*Con*) and off (*Coff*)(b)

5. Transmission Experiments

For the transmission measurements an electro-absorption modulator (EAM) was used in the ONU to modulate the upstream signal. Because of the high insertion loss of this modulator the signal was pre-amplified by an SOA. First some experiments were carried out with the SOA-EAM combination, but for the later experiments another SOA was added as booster after the EAM to increase the gain of the ONU. The higher gain is expected to be required to overcome the high losses in the network proposed in the BB Photonics project. The ONU is feeded by a CW feeder signal from the central office. This is the most simple setup for measurements and can be extended with methods that are described in Chapter 4.

The devices that are used for the transmission measurements were characterised in Chapter 4 and the specification of the measurement equipment can be found in Appendix C. The input power into the receivers for the BER, the eye diagram and the optical spectrum was kept constant at -10dBm. The measurements, except stated otherwise, were performed with a PRBS of 2^{31}-1 at a bitrate of 10-Gbit/s (9.953.280 kHz).

The first section of this chapter, Section 5.1, describes the dynamic back-to-back measurements that were carried out for an ONU with only the EAM, and for an ONU with the SOA-EAM combination. The measurements in Section 5.2 determine the impairments of both carrier- and signal backscattering. Section 5.3 describes the measurements that were carried out for transmission over 25km with both the SOA-EAM combination and the SOA-EAM-SOA combination in the ONU. Finally in Section 5.4 the conclusions of the measurements are given.

5.1. Back-to-back Measurements

Section 5.1.1 describes the back-to-back measurements that were carried out with only the EAM, to determine the sensitivity of the receiver, and Section 5.1.2 with the SOA-EAM combination, to determine the minimum required input power into the ONU.

5.1.1. Back-to-back Measurement with EAM

This section describes the measurements with only the EAM as modulator, which were done to obtain reference values for the receiver sensitivity. The measurements were done for the four wavelengths channels C19, C30, C40, and C50, which correspond to the wavelengths: 1562.23, 1553.33, 1545.32, and 1537.40nm.

Measurement Setup

The measurement setup for the back-to-back measurement is shown in Figure 5.1. The inline attenuator after the laser is used to set the power level into the EAM. The power into the EAM is indicated by the in-line power meter placed before the EAM. After the signal is modulated and directed back to the central office, the signal is attenuated to set the received optical power to the receiver. The 50/50 coupler divides the power to a power meter, to determine the received optical power, and to the optical pre-amplifier (described in Section 4.5). After the optical pre-amplifier the signal is detected with the 10-Gbit/s receiver for the BER measurements and with the lightwave converter in combination with the oscilloscope for the eye diagrams.

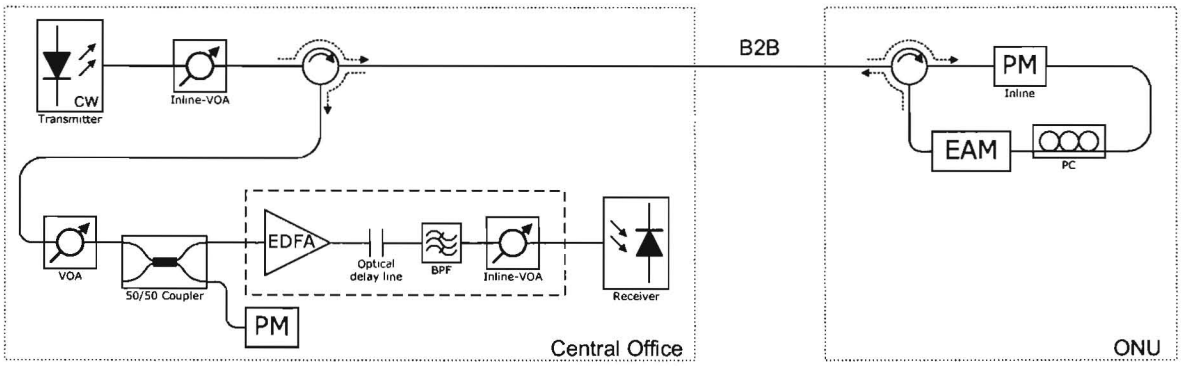

Figure 5.1.: Back-to-back setup for the reference measurements

The electrical scheme to drive the EAM is shown in Figure 5.2(a). The DC is set at a stable reverse voltage. The maximum data signal voltage of the pattern generator is $2V_{pp}$ and is thus not high enough to attain a large enough voltage swing for the EAM, which requires around $4V_{pp}$ for the largest extinction ratio. Therefore an electrical amplifier is used to amplify the data signal. The SHF 315P amplifier that was used is actually an RZ/NRZ converter, but it works well as an amplifier for this purpose. The maximum output voltage of the amplifier is 5V. An attenuator of 12dB is placed between the pattern generator and the amplifier to limit the input signal into the amplifier and a 3dB attenuator is placed between the amplifier and the bias-t to limit the maximum voltage to prevent damage on the EAM. The optimum value for the data voltage of the pattern generator was found to be $1.75V_{pp}$, at which the output of the electrical amplifier was around $3.5V_{pp}$. The optimum bias voltage was $1.9V_{rev}$. The electrical eye diagram of this signal at 10-Gbit/s (9.953.280kHz) can be seen in Figure 5.2(b).

The BER was measured for various received optical powers and for the wavelengths channels C19, C30, C40, C50. C19 and C50 are the shortest and the longest wavelength available for the AWG used. The power into the EAM was also varied: one BER curve with 0dBm input power, and one BER curve with +8dBm input power was made for each wavelength. The power after the optical pre-amplifier was kept constant at -10dBm for all to measurements to make sure that the 10-Gbit/s receiver unit was limited by shot noise and not by thermal noise. However, because of the EDFA in the optical pre-amplifier, the receiver was limited by the signal-ASE beatnoise.

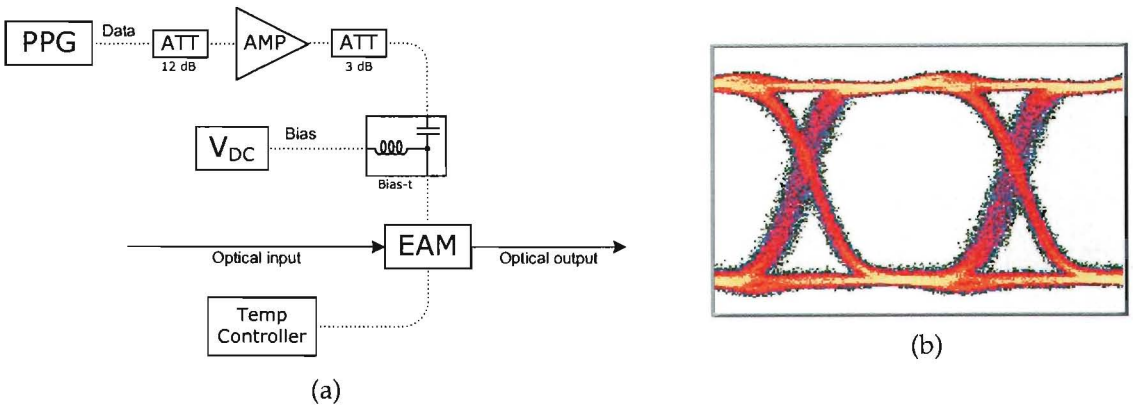

Figure 5.2.: Connection scheme of the EAM (a) and the output of electrical amplifier at 10-Gbit/s with PPG 1.75V, V_{pp} = 3.5V (b)

Results and Discussion

The resulting BER curves are shown in Figure 5.3(a). The eye diagram shown in Figure 5.3(b) was taken directly after the EAM for the 0dBm input power. Figures 5.3(c) to (f) show the eye diagrams of the signal after the optical pre-amplifier for C19 to C50 at a BER of 10^{-9} and at an input power of 0dBm into the EAM. The power values below the eye diagrams show at which received power the eye diagram was taken.

From the BER curves can be seen that the receiver sensitivity at a BER of 10^{-9} is almost the same for the channels C19, C30, and C40 and that the results are equal for both the 0dBm as well as the +8dBm input power. Channel C50 has a power penalty of around 1dB, which is probably caused by the higher noise factor of the optical pre-amplifier for that channel. From the eye diagrams can clearly be seen that the EDFA adds some noise at the '1' level compared to the eye diagram directly after the EAM. This noise is larger for the shorter wavelengths, which is due to the larger ASE noise of the EDFA. Furthermore can be seen that the intersections of the eye diagrams are shifted from the centre for the eye diagram after the EAM, to somewhat below the centre for the pre-amplified signals.

5.1.2. Back-to-back Measurement with SOA-EAM Combination

The back-to-back measurements with the SOA-EAM combination are described in this section. The measurements were carried out for different input powers into the SOA to determine the minimum required optical power into the ONU. With lower input powers the BER curves are expected to have an increasing power penalty until an error floor is reached, due to the ASE-noise of the SOA.

Measurement Setup

The setup that was used to measure the BER curves for different input powers is shown in Figure 5.4. The central office is the same as in the previous measurement. The SOA is added at the ONU to provide more gain the overcome the high insertion losses of the EAM. An

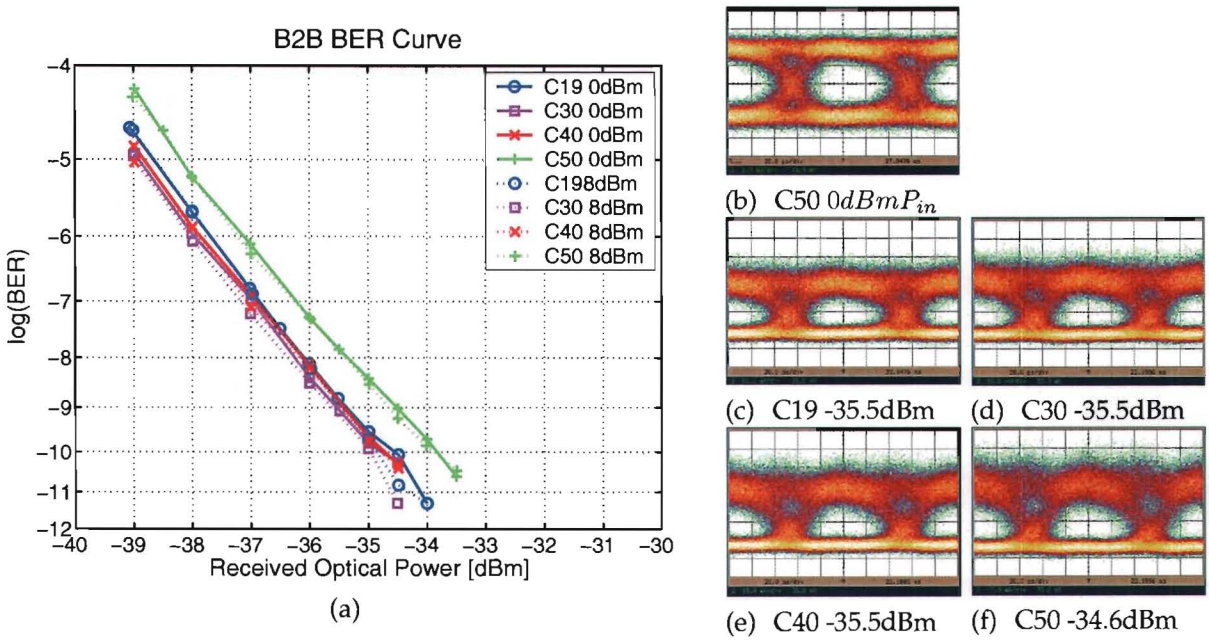

Figure 5.3.: BER curves of the B2B measurements with only the EAM in the ONU (a), and the eye diagram at the EAM-output with 0dBm input power (b), and after the optical pre-amplifier for: (c) C19, (d) C30, (e) C40, and (f) C50

isolator is inserted after the SOA to reduce the reflections caused by the PC-connectors of the EAM. A filter is present in the ONU to simulate a WDM network structure. In the proposed network this filter is a ring-resonator and will be located in the remote node. The filter also filters out nearly all ASE-noise coming from the ONU, so it is not amplified by the EDFA. The insertion losses of the filter for the different channels used are shown in Table 5.1.

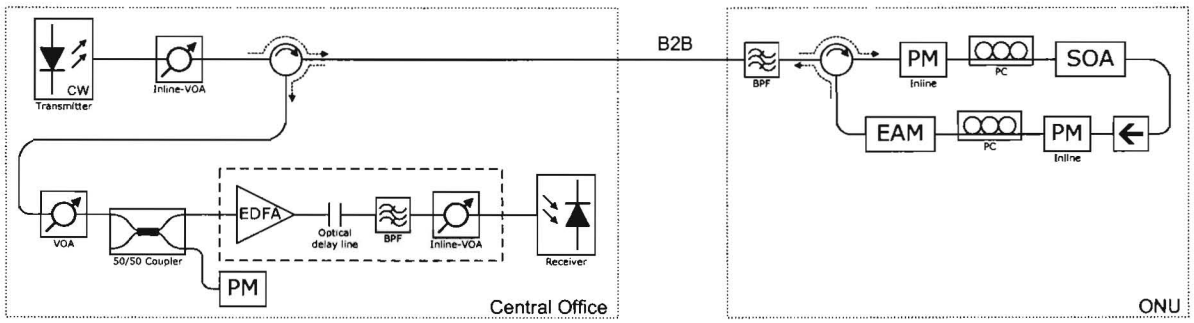

Figure 5.4.: Back-to-back measurement setup for the SOA-EAM combination

Results and Discussion

The results of the back-to-back BER measurements of the setup with the SOA-EAM combination can be seen in Figure 5.5 for channel C19 and C30 and in Figure 5.6 for channel C40 and

C50. The reference lines are the lines from the back-to-back measurements with 0dBm input power in the EAM, from Section 5.1.1. The eye diagrams that were taken at a BER of 10^{-9} (for the curves without error floor) are shown in Figure 5.7. The values under the eye diagrams show the received optical power at which the eye diagram is measured.

The BER curves show that when a high input power is applied to the ONU no visible degradation occurs, but when the input power is decreased the power penalty increases until an error floor is reached. For all the channels -20dBm input power gives no power penalty compared to back-to-back measurement with only the EAM; for an input of -25dBm the power penalty is around 0.9dB for all the channels. For the measurements with an input of -30dBm not enough power was received at the receiver to reach a BER of 10^{-9} due to the limited gain of the ONU and the fact that an error floor is present. The eye diagrams show almost the same result as was achieved in Section 5.1.1, but there is a bit more noise visible. The same trend that more ASE-noise is present for the shorter wavelengths is visible. Furthermore can be seen that when the input power into the SOA is lower, the noise is higher. This is expected because less ASE-noise of the SOA is depleted for low input powers.

The gain of the whole ONU (indicated by the dashed ONU area in Figure 5.4) was determined using the recorded power levels. The filter has a high insertion loss for channel C30 and the lowest insertion loss is for channel C19, the gain of the SOA is larger for the shorter wavelengths, but also the insertion loss of the EAM is larger for the shorter wavelengths as was seen in Section 4.1 and 4.3. The resulting gain values that were measured are shown in Table 5.1.

Table 5.1.: The insertion losses of the AWG and the gain/loss of the ONU

Channel	**Insertion Loss AWG [dB]**	**$Gain_{onu}$ [dB]:**		
		-20dBm	***-25dBm***	***-30dBm***
C19	0.94	+1.9	+2.2	+2.2
C30	2.34	-0.3	0	+0.4
C40	1.41	+2.3	+3	+3.3
C50	1.38	+1	+1.6	+2.2

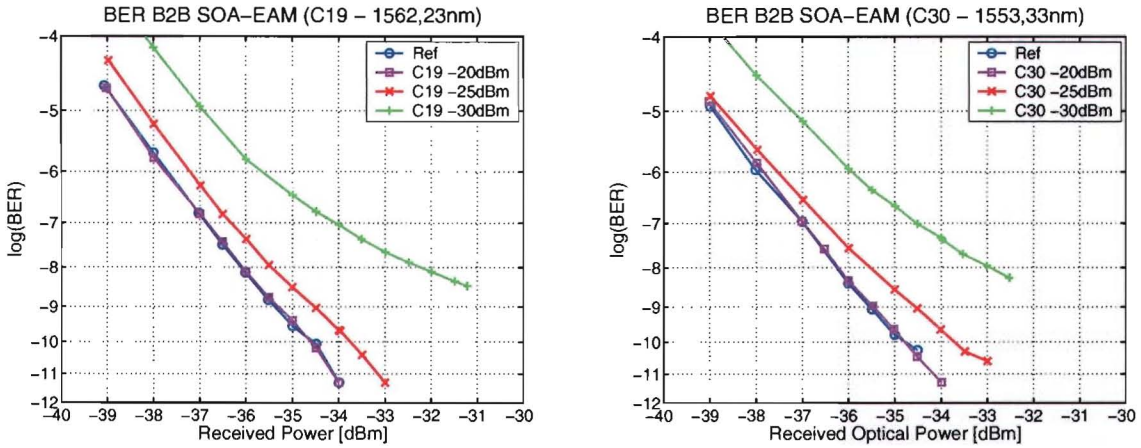

Figure 5.5.: BER curves for C19 (a) and C30 (b)

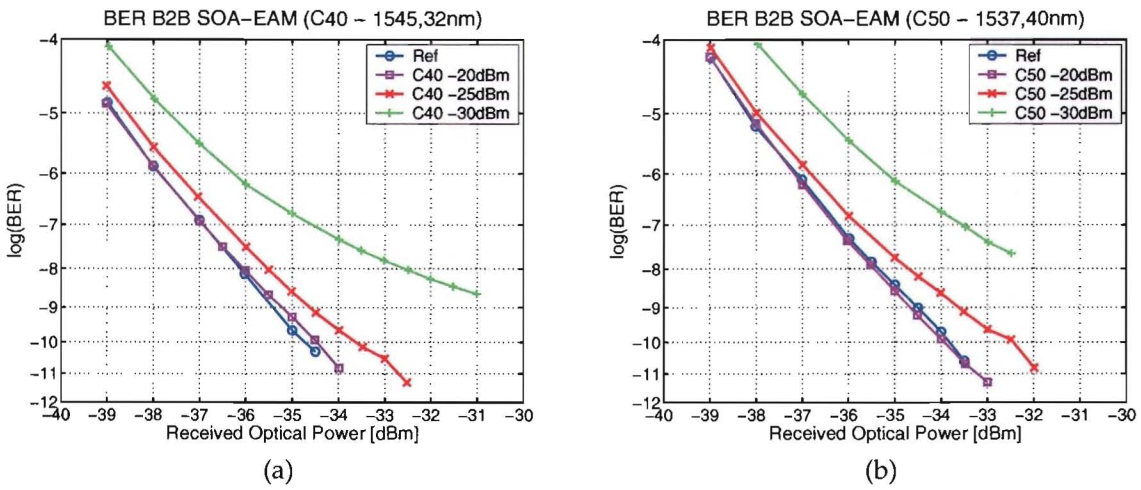

Figure 5.6.: BER curves for C40 (a) and C50 (b)

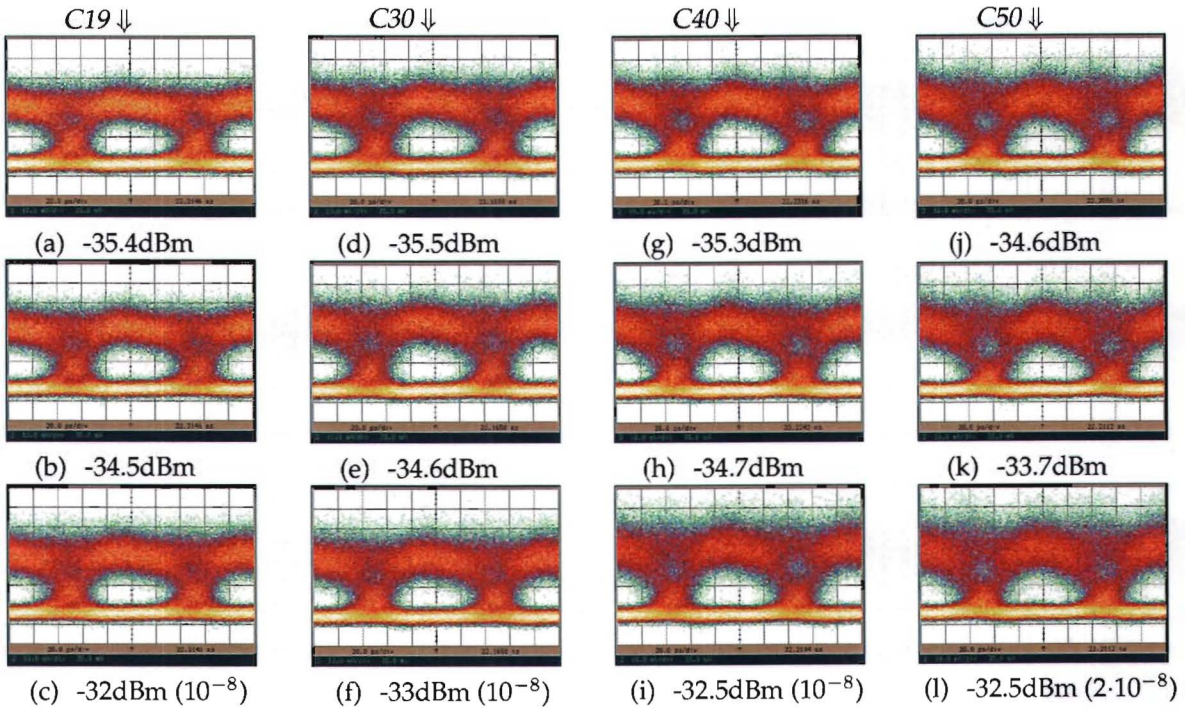

Figure 5.7.: Eye diagrams of: (a) C19 -20dBm; (b) C19 -25dBm; (c) C19 -30dBm; (d) C30 -20dBm; (e) C30 -25dBm; (f) C30 -30dBm; (g) C40 -20dBm; (h) C40 -25dBm; (i) C40 -30dBm; (j) C50 -20dBm; (k) C50 -25dBm; and (l) C50 -30dBm

5.2. Backscattering Measurements

This section considers the impairments that occur due to backscattering. The backscattering into the two directions is considered: in Section 5.2.1 the backscattering into the direction of the central office is considered, and in Section 5.2.2 the backscattering into the direction of the ONU. Figure 5.8 shows the schematic representation of the backscattering. The power levels of the signals in the figure are written down in Equation 5.1. We consider the power of the backscattered signal a fixed value lower than the power of the signal itself, this value we call the backscatter factor (BS-factor). Furthermore we consider the gain of the ONU (Gain_{onu}) the gain of all the components at the ONU site including the filter. The BS-factor is taken as 35dB for the calculations. This value is equal to the average of the normalised backscattered power (for 25km), measured with the OSA (±-36) and the power meter (± 34) in Section 4.6. The attenuation for 25km fibre is taken as 5dB (0.2 dB/km).

We consider the signal-to-backscatter-ratio (SBR) as an indicator of the ratio between the backscattered power and the power level of the desired signal. We distinguish between the SBR at the CO site SBR_{co} and the SBR at the ONU site SBR_{onu}. The SBR_{co} is, according to Equation 5.2, equal to the gain of the ONU unit plus the BS-factor minus two times the attenuation of the fibre if we use the definitions in Equation 5.1. In the same way the SBR_{onu} results in the BS-factor minus the gain of the ONU according to Equation 5.3.

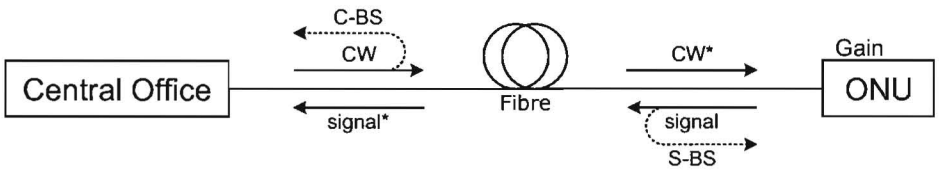

Figure 5.8.: Backscattering

$$\begin{aligned}
\text{C-BS} &= \text{CW} - \text{BS-factor} \\
\text{S-BS} &= \text{signal} - \text{BS-factor} \\
\text{CW*} &= \text{CW} - \text{att}_{fibre} \\
\text{signal} &= \text{CW*} + \text{Gain}_{onu} \\
\text{signal*} &= \text{signal} - \text{att}_{fibre}
\end{aligned} \tag{5.1}$$

$$\begin{aligned}
\text{SBR}_{co} &= \text{signal*} - \text{C-BS} \\
&= (\text{CW} - 2 \cdot \text{att}_{fibre} + \text{Gain}_{onu}) - (\text{CW} - \text{BS-factor}) \\
&= \text{Gain}_{onu} + \text{BS-factor} - 2 \cdot \text{att}_{fibre} \qquad (5.2) \\
\text{SBR}_{onu} &= \text{CW*} - \text{S-BS} \\
&= (\text{CW} - \text{att}_{fibre}) - (\text{CW} - \text{att}_{fibre} + \text{Gain}_{onu} - \text{BS-factor}) \\
&= \text{BS-factor} - \text{Gain}_{onu} \qquad (5.3)
\end{aligned}$$

5.2.1. Impairments of Carrier Backscattering

The measurements in this section were carried out to determine the impairments of the backscattering into the central office, the carrier-backscattering. Backscattering was added to the back-to-back system to achieve this. The measurements were performed for several SBR_{co} values. A second SOA was inserted into the ONU to increase the gain; the ASE-noise will be increased due to the SOA and some pattern effects might occur. The measurements were done for one wavelength channel C30 and are assumed to be representative for the other channels.

Measurement Setup

The measurement setup is shown in Figure 5.9. The power from the central office is split by a 3-dB coupler. One output is connected directly to the ONU, the other output is connected to 25km of fibre; the 25km of fibre is terminated with an angled connector. The active components of the ONU are the SOA, EAM and SOA. The power into the first SOA was -20dBm for the measurements. The first SOA is driven with a current of 300mA and the second SOA with a current of 100mA for the measurements in this section. An inline power meter/attenuator is used before the first SOA to set the input power. Another attenuator is used at the end of the ONU to set the output power of the ONU. By keeping the power from the central office constant and varying the power from the ONU the power penalty can be calculated for different SBR_{co}. This is done for a high power of +4.5dBm into the fibre and a lower power of -5.5dBm, to determine whether the influence of the stimulated Brillouin scattering is present at this input power. For the higher input power the coherence control of the laser is used to increase the linewidth of the optical signal from <0.2MHz to around 200MHz. For all the measurements the polarisation was optimised by the polarisation controllers. Equation 5.2 is used to calculate the SBR_{co} values.

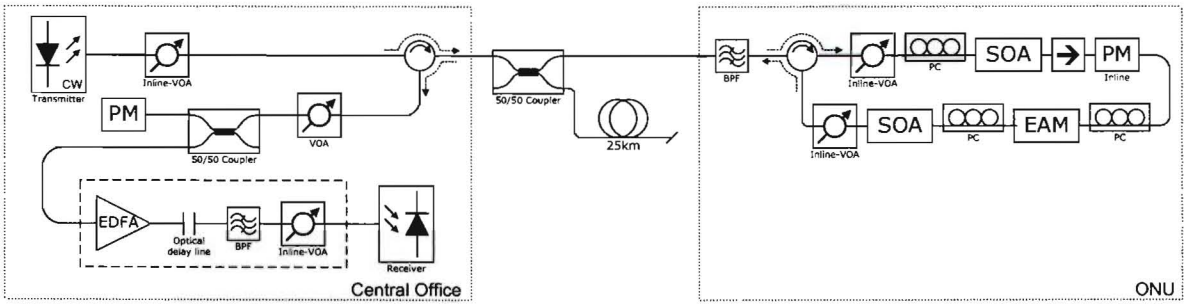

Figure 5.9.: Setup for the carrier-backscattering measurements

Results and Discussion

The results of the BER measurements are shown in Figure 5.10(a) and the eye diagrams are shown in Figure 5.10(b) to (e) and in Figure 5.11. From the spectra with and without coherence control for the high input power in Figure 5.12 can be seen that the Brillouin

backscattering peak is decreased. However, no difference in power penalty can be seen from the measured BER curves. From Section 4.6 was also known that the SBS is still lower than the RBS at +4.5dBm input power into the fibre. Because we use lower input powers into the fibre for the other measurements in this chapter, we set the coherence control of the laser off for the rest of the measurements.

The results for the lower input power into the fibre with the same SBR_{co} are almost equal to the results of the high power input measurement. Only a small power penalty difference is measured. For the low input power and an SBR_{co} of 18.5dB not enough power is received to reach a BER of 10^{-9}. The eye diagrams for the signals with a higher SBR_{co} do not show much degradation.

When the power penalties for both the high input power and the low input power are plotted against the SBR_{co} we get Figure 5.13. From this figure the trend can be seen that when the SBR_{co} decreases the power penalty increases slowly until a threshold value, after which the power penalty increases dramatically. The threshold where the power penalty is increased by 1dB is around an SBR_{co} of 24dB.

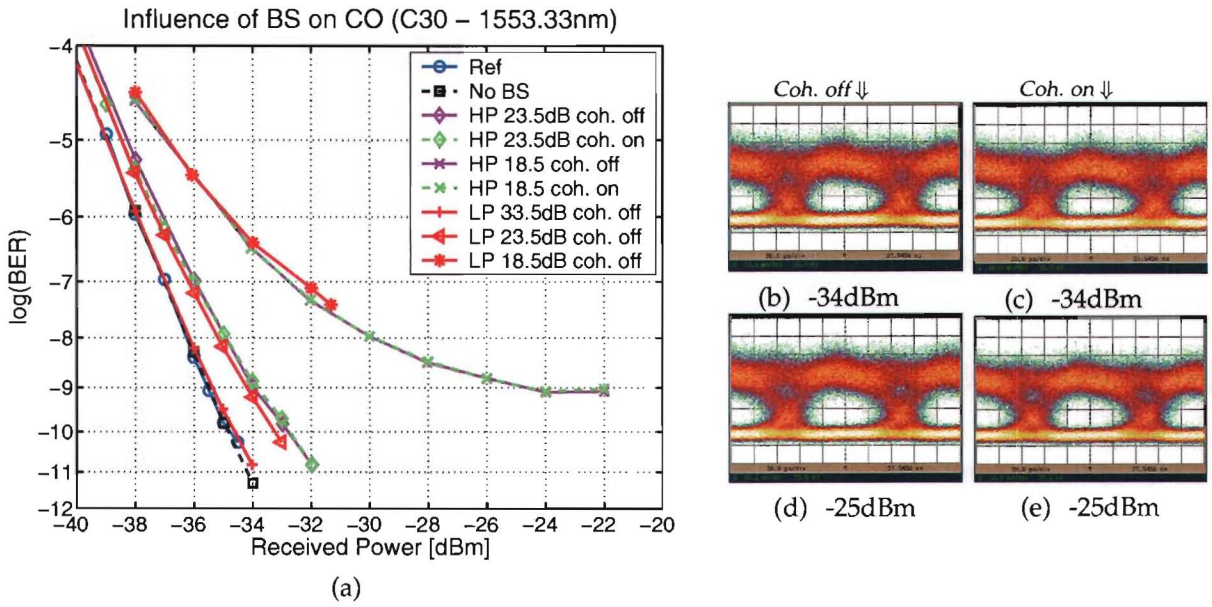

Figure 5.10.: BER results of the carrier-backscattering measurements with SBR_{co}s of 18.5, 23.5 and 33.5 dB(a) and the eye diagrams of: (b) HP input, SBR_{co} 23.5dB, coh. off; (c) HP input, SBR_{co} 23.5dB, coh. on; (d) HP input, SBR_{co} 18.5dB, coh. off; (e) HP input, SBR_{co} 18.5dB, coh. on

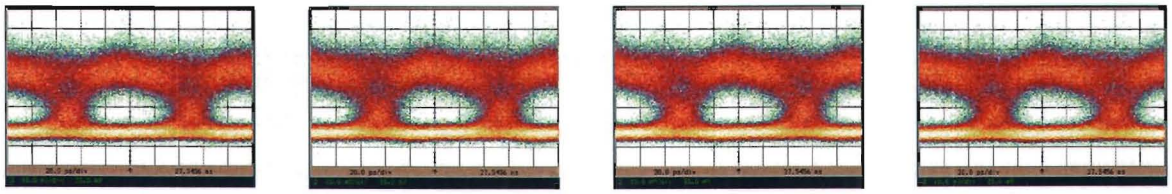

(a) *NO BS* -35.5dBm (b) -35.5dBm (c) -34.25dBm (d) -32dBm (10^{-7})

Figure 5.11.: Eye diagrams for: (a) HP input, no backscattering; (b) LP input, SBR 33.5dB; (c) LP input, SBR 23.5dB; (d) LP input, SBR 18.5dB

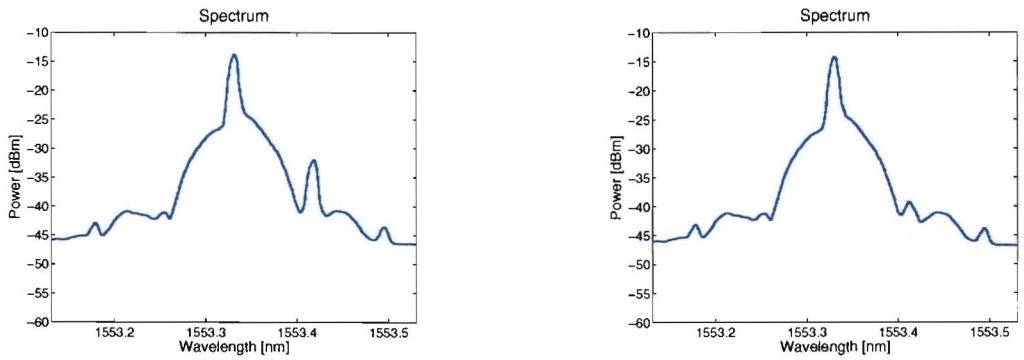

(a) (b)

Figure 5.12.: Spectrum with and without coherence control of the signal with HP input and SBR 18.5dB

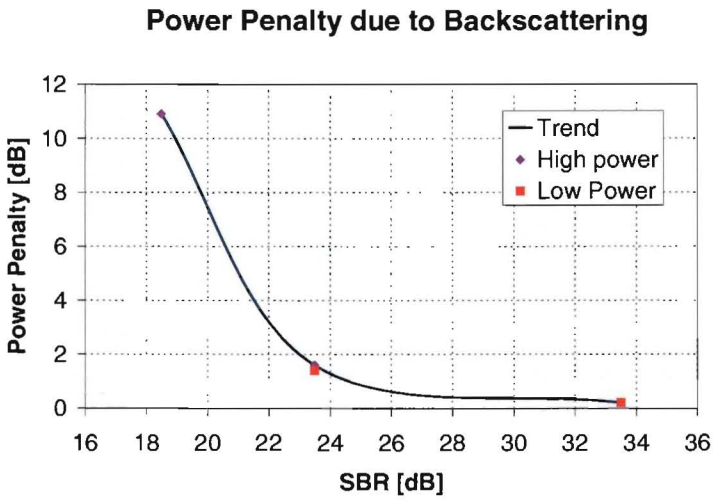

Figure 5.13.: Power Penalty at 10-9 for the HP- and LP input

5.2.2. Impairments of Signal Backscattering

In this section the measurements are described that were carried out to determine the impairments of the backscattering into the direction of the ONU, the signal-backscattering. The measurements were carried out in the same manner as the measurements in the previous section.

Measurement Setup

A similar setup as in the previous section is used, but the 25km of fibre is connected to the other output of the 50/50 coupler as is shown in Figure 5.15. To achieve a low SBR_{onu} the power into the ONU has to be low, and the power coming from the ONU has to be high. This is difficult however, since the gain of the ONU is limited. The input power into the pre-amplifier SOA was -20dBm for the measurements in this section and two driving currents for the booster SOA were used: 100mA and 350mA. Equation 5.3 is used to calculate the SBR_{onu} values. For all the measurements the polarisation was optimised by the polarisation controllers to the best BER. Because the polarisation before the second SOA is also change to the best bitrate we assume that there is be a trade-off between the gain of the second SOA and the polarisation of the backscattered signal which has the lowest power penalty.

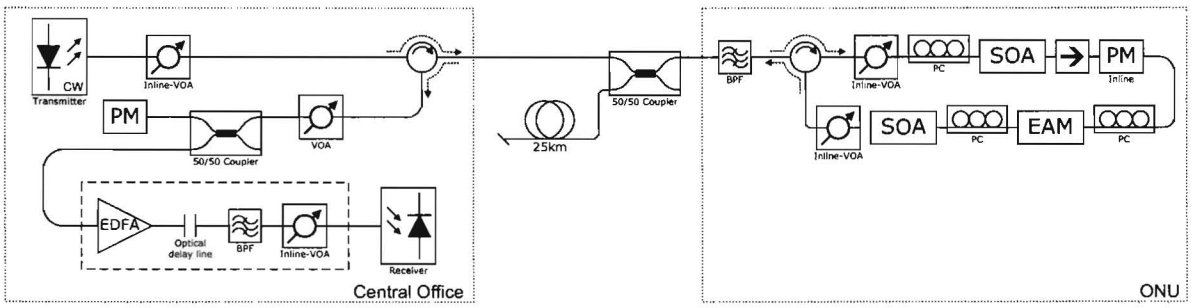

Figure 5.14.: Setup for the signal-backscattering measurements

Results and Discussion

The BER results and eye diagrams are shown in Figure 5.15. Not a large power penalty can be seen for the case when the second SOA is driven by a current of 100mA because the gain is too low what results in an SBR_{onu} that is too high. Therefore the gain of the ONU was increased by changing the driving current from 100mA to 350mA. To determine the influence of the higher ASE-noise and other power penalties a reference measurement was done without backscattering for the driving current of 350mA of the second SOA. The power penalty of the BER curve with the SBR_{onu} is a bit larger but is still not significant. With this setup it is not possible to achieve a lower SBR_{onu}, when another modulator is used in a setup like described in [68] it is possible to achieve a lower SBR_{onu}.

Some level difference is visible in the eyes diagrams which is larger for Figure 5.15(c) than

for (b), this might be because the SOA is working in the gain-saturation region. From the spectra measured at the receiver site, shown in Figure 5.16, can be seen that the spectrum is more asymmetrical in the case that the driving current of the second SOA is larger. The higher power level at the longer wavelength region of the peak is caused by the chirp of the second SOA.

Figure 5.17 compares the power penalty at 10^{-9} for the backscattering to the CO with the backscattering to the ONU. It shows that the results are equal for the measured values, but the SBR_{onu} is too high to conclude what the power penalty will be for lower SBR_{onu}.

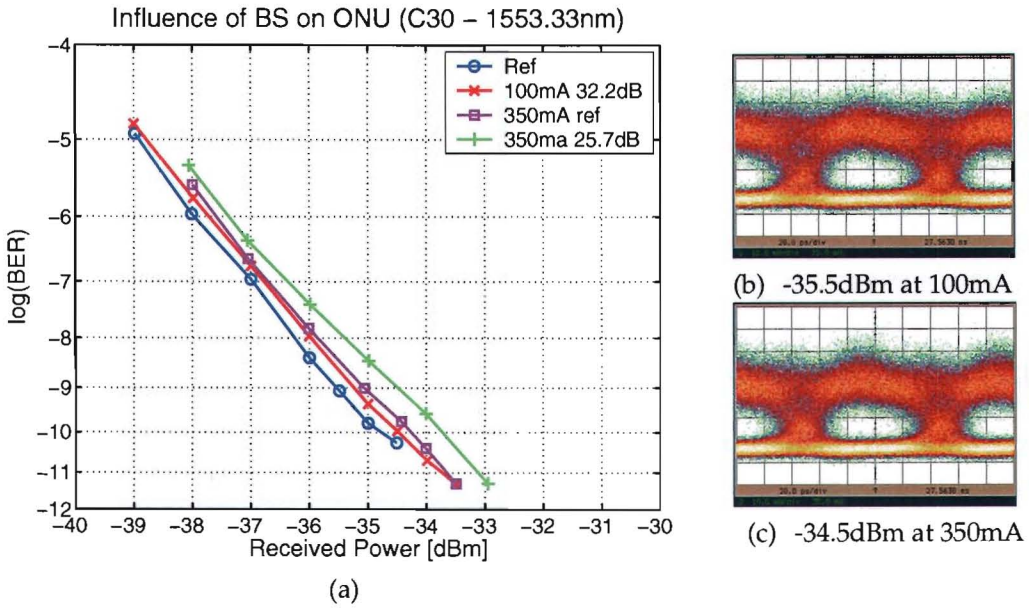

Figure 5.15.: BER backscattering to ONU for C30 with SBR_{onu}s of 25.7 and 32.2 dB (a) and eye diagrams for -10dBm (b) and for -20dBm (c)

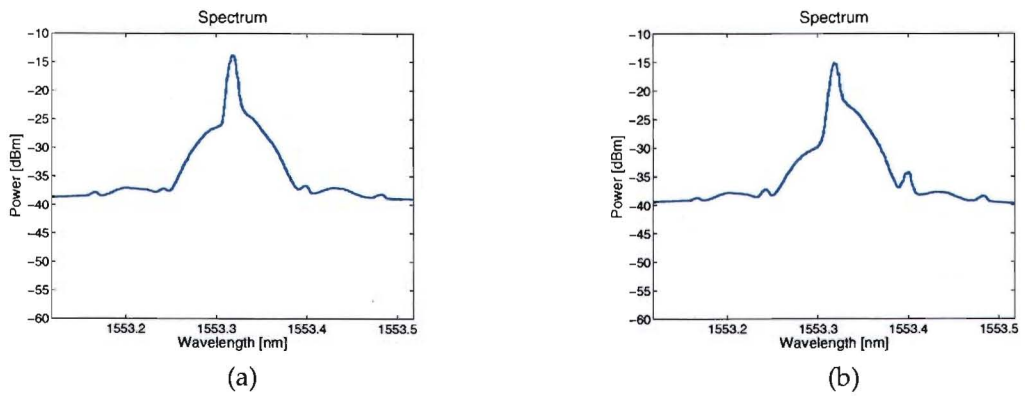

Figure 5.16.: Spectrum for the case that SOA2 is operated at 100mA (a) and 350mA (b)

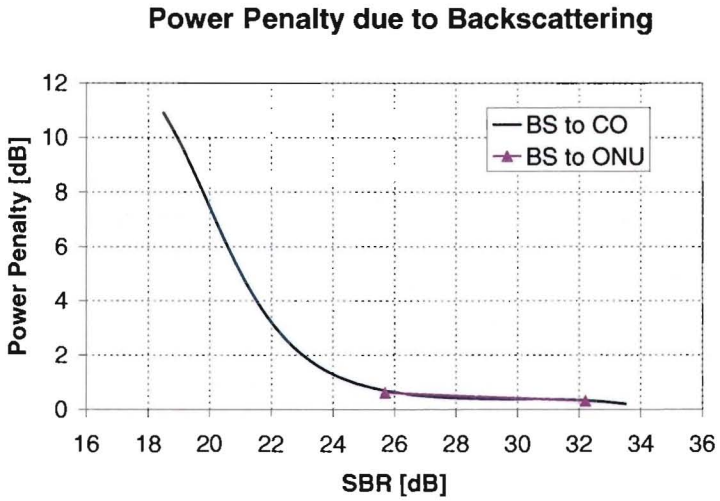

Figure 5.17.: Power Penalty at 10-9

5.3. Transmission Measurements

In this section the transmission measurements are described. In the transmission measurements all the factors will contribute to the final result. Both carrier- and signal-backscattering will deteriorate the performance of the system. All the transmissions were done over 25km of fibre because this distance is similar to the distance required by the project. Section 5.3.1 describes the measurements with the SOA-EAM combination, and Section 5.3.2 uses the SOA-EAM-SOA combination.

5.3.1. Transmission over 25km of Fibre using the SOA-EAM Combination

In this section we consider the transmission over 25km of fibre with the SOA-EAM combination. Because the gain of the ONU was low in this setup only measurements for one wavelength channel were carried out. Measurements with another SOA in the ONU are described in Section 5.3.2.

Measurement Setup

The setup shown in Figure 5.18 was used. The power into the pre-amplifier SOA of the ONU was adjusted by the inline attenuator/power meter at the central office. The measurements were done for an input power of -20 and -10dBm. The measurements were only done for channel C30.

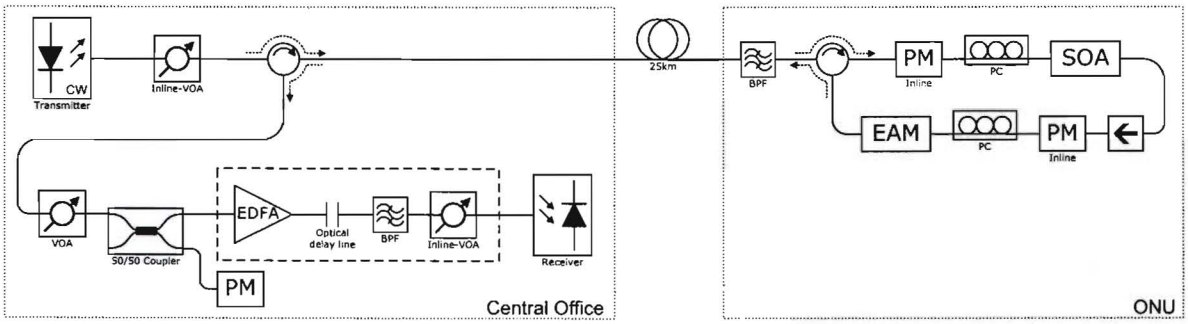

Figure 5.18.: Setup for the transmission measurement over 25km with the SOA-EAM combination

Results and Discussion

The results in Figure 5.19 show that for the higher input signal of -10dBm the performance is less with a power penalty of around 6.1dB at a BER of 10^{-9} than for the lower input signal of -20dBm, which has a power penalty of around 4.3dB. When we use the recorded power levels and the Equations 5.2 and 5.3 we can determine the SBR_{co} and the SBR_{onu}, see Table 5.2. P_{co} is considered to be the power from the central office into the fibre and P_{onu} is the power from the ONU into the fibre.

The gain is increased for the -20dBm input compared to the -10dBm input; this is because the SOA is in the saturation region for the -10dBm input. Because the gain is lower for the -10dBm input signal, also the SBR_{co} is lower than for the -20dBm input signal. According to the backscattering measurements of Section 5.2.1 and 5.2.2 we can see that the SBR_{onu} values are very high and do not contribute to the power penalty. The power penalty due to backscattering for the -20dBm input signal at the SBR_{co} of 24.4dB, as in Figure 5.13, is not as large as the measured power penalty. The larger power penalty is probably due to transmission impairments like dispersion along the 25km of fibre and the ASE-noise of the optical amplifiers. For the -10dBm signal, the power penalty due to backscattering for the -10dBm input signal at the SBR_{co} of 21dB, is also not as large as the measured power penalty, but this offset is lower than for the -20dBm input. This offset is also caused by the transmission impairments.

The eye diagram for the -10dBm input signal shows some more noise. The received optical spectrum measured after the optical pre-amplifier is shown in Figure 5.20. The spectrum is symmetrical for the powers at the shorter and longer wavelength side.

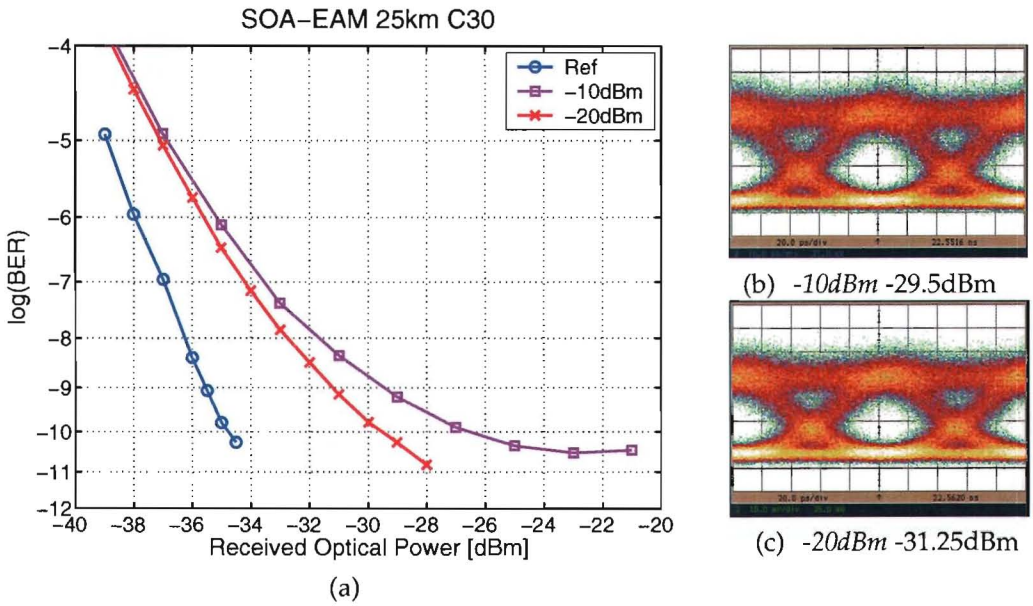

Figure 5.19.: BER (a) for C30 and eye diagrams for -10dBm (b) and for -20dBm (c)

Table 5.2.: power levels

P_{SOA1}	P_{co} [dBm]	P_{onu} [dBm]	Gain [dB]	SBR_{co} [dB]	SBR_{onu} [dB]
-10dBm	-0.4	-9.4	-4	21	39
-20dBm	-10.5	-16.3	-0.8	24.2	38.5

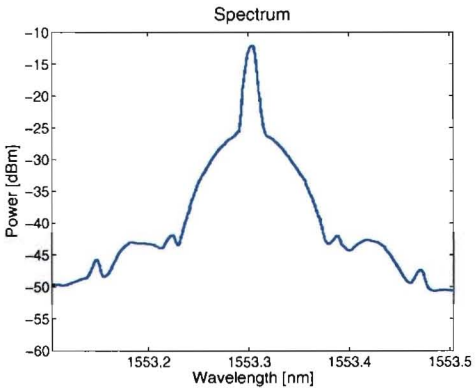

Figure 5.20.: Received spectrum

5.3.2. Transmission over 25km of Fibre using the SOA-EAM-SOA Combination

The transmission measurement over 25km of fibre using the ONU with the booster SOA are described in this section. The measurements were carried out for the four wavelength channels.

Measurement Setup

The same setup as for the previous section is used except for the fact that a booster SOA is added after the EAM to increase the gain of the ONU, as shown in Figure 5.21. The BER was measured for different input powers into the pre-amplifier SOA: -10, -20, and -25dBm, by changing the CW-power from the central office. The gain of the second ONU was adjusted by driving the booster SOA by three different currents: 100, 200 and 350mA. The inline power meters were used to record the power levels. The measurements were done for the channels C19, C30, C40, and C50. The polarisation was optimised to the best BER for all the measurements. For all the measurements the backscattering is assumed to be in the linear region (RBS higher than SBS) and Equations 5.2 and 5.3 are used to determine the SBRs.

To measure the pattern of the signal the setup was changed temporarily: a 90/10 coupler was added after the booster SOA to determine the pattern before transmission. The pattern after transmission was measured after the optical pre-amplifier. For the pattern measurements a PRBS of 2^7-1 was used.

Results and Discussion

Figures 5.22 to 5.25 show the results for C19, C30, C40, and C50. The power values, the gain of the ONU and the SBRs for the different curves are shown in Table 5.3. From the data in the table can be seen that for all the curves the SBR_{co} values are quite high and will thus not introduce any significant power penalty. The SBR_{onu} values, however, are low and will cause a power penalty.

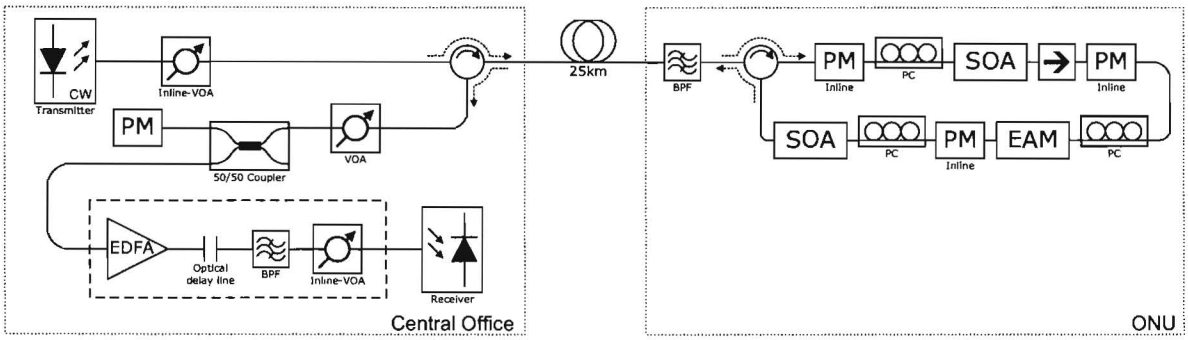

Figure 5.21.: Setup for the transmission measurement over 25km with the SOA-EAM-SOA combination

From the eye diagrams can be seen that noise increases for the shorter wavelengths. It can also be seen that there is some kind of overshoot present at the right side of the eye. To determine the origin of this peak, some pattern measurements were done. Figure 5.26(a) shows the pattern before transmission and (b) shows the pattern after transmission and after the optical pre-amplifier. The patterns were measured with an input power of -20dBm into the pre-amplifier SOA and a high drive current of 350mA of the booster SOA. Some pattern effects due to gain saturation of the SOA are visible. Furthermore can be seen that after transmission the shape of the pulses is changed, and a peak is present with a slower rising slope than the falling slope. This shape is caused by the dispersion of the highly chirped signal. It can be seen from the spectra in Figure 5.27 that the signal is highly chirped. Furthermore can be seen from the spectra that when the current is increased, the chirp is also increased; this corresponds to the larger peak visible at higher currents in the eye diagrams. The chirp is caused by the booster SOA, since no chirp was visible with the setup without the second SOA (Figure 5.20). The chirp of the SOA is larger when the device is working more in the gain-saturation region. This can also be seen from the fact that the peak is larger in the eye diagrams for the -10dBm signals than for the -20dBm signals.

Since the power was set by looking at the power into the pre-amplifier SOA, the SBRs for the different wavelengths channels are not equal. Therefore we have to consider each wavelength channel separately to understand what is happening. For each channel the power penalty increases when the input power decreases for the same drive current to the booster SOA. Furthermore can be seen that the larger drive current and thus the larger gain of the ONU result in a larger power penalty. As was mentioned before the system is limited by the signal-backscattering. According to Equation 5.3 the SBR_{onu} is lower for higher gain values, what will result in a higher power penalty. This corresponds to the behaviour of the BER curves we measured. The power penalties for the higher input power (-10dBm) are lower than for the lower input power. This is caused by two factors: 1) the pre-amplifier SOA is operated in the gain-saturation region what will reduce the gain of the ONU, and 2) the effects of the signal-backscattering are suppressed due to the pre-amplifier SOA in gain saturation.

Since we found that the power penalty is mainly caused by the low SBR_{onu} we can look at the differences between the different wavelength channels. We know from Section 4.1, 4.2 and 4.3 that the gain of the SOAs and the insertion loss of the EAM is wavelength dependent.

Also the insertion loss of the filter is different for each channel. If we consider these factors and and we look at the gain values of Table 5.3 we can see that for high drive currents of the booster SOA the gain of the whole ONU is the largest for channel C40, followed by C50, C19, and C30. If we consider this fact, than we can explain why the performance of the BER measurements is the best for channel C30, followed by C19, C50 and C40.

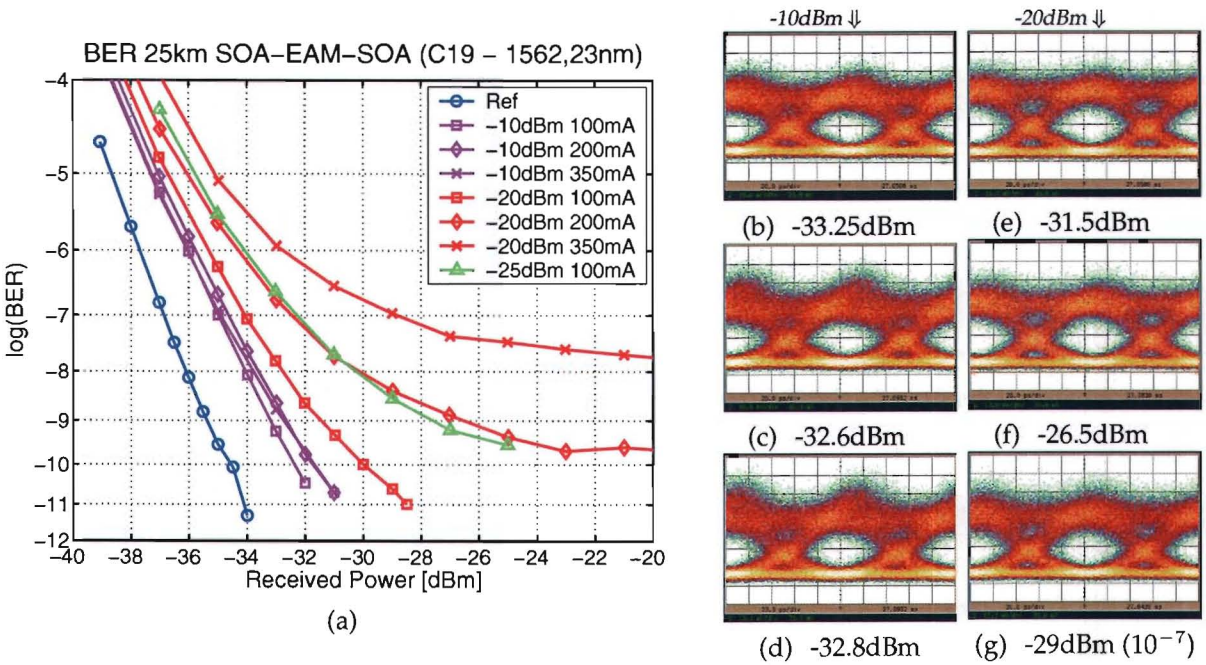

Figure 5.22.: BER for C19 (a) and the eye diagrams for an input power of -10dBm and a drive current of: (b) 100mA, (c) 200mA, (d) 350mA, and for an input power of -20dBm and a drive current of: (e) 100mA, (f) 200mA, and (g) and 350mA

If we plot the gain of the ONU versus the power penalty (compared to the reference line) we get Figure 5.28(a) for the -10dBm input signal and (b) for the -20dBm input signal. For some points an error floor was reached and thus the power penalty could not be determined. The power penalty is for the same gain within a range of 1dB difference. The difference is probably caused by ASE-noise, extinction ration difference or offset power penalty. It can be seen that the power penalties are lower for the higher input power (with the same gain values) what is probably caused because the pre-amplifier SOA is in the saturation region what reduces the signal-backscattering effects.

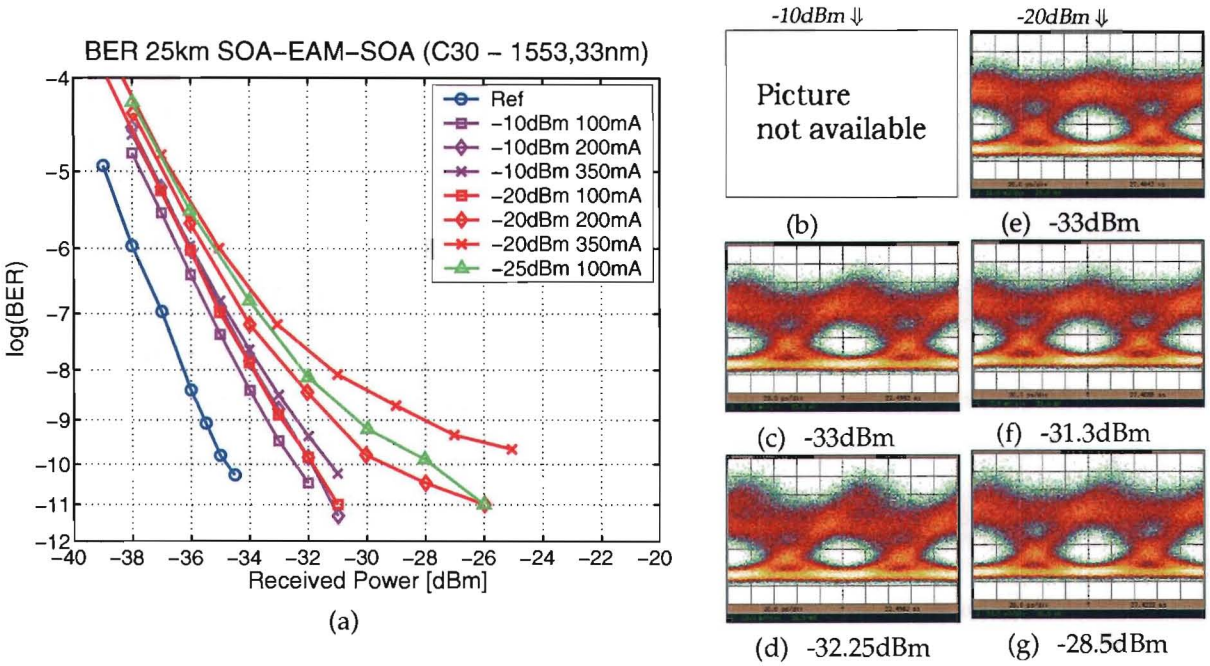

Figure 5.23.: BER for C30 (a) and the eye diagrams for an input power of -10dBm and a drive current of: (b) 100mA, (c) 200mA, (d) 350mA, and for an input power of -20dBm and a drive current of: (e) 100mA, (f) 200mA, and (g) and 350mA

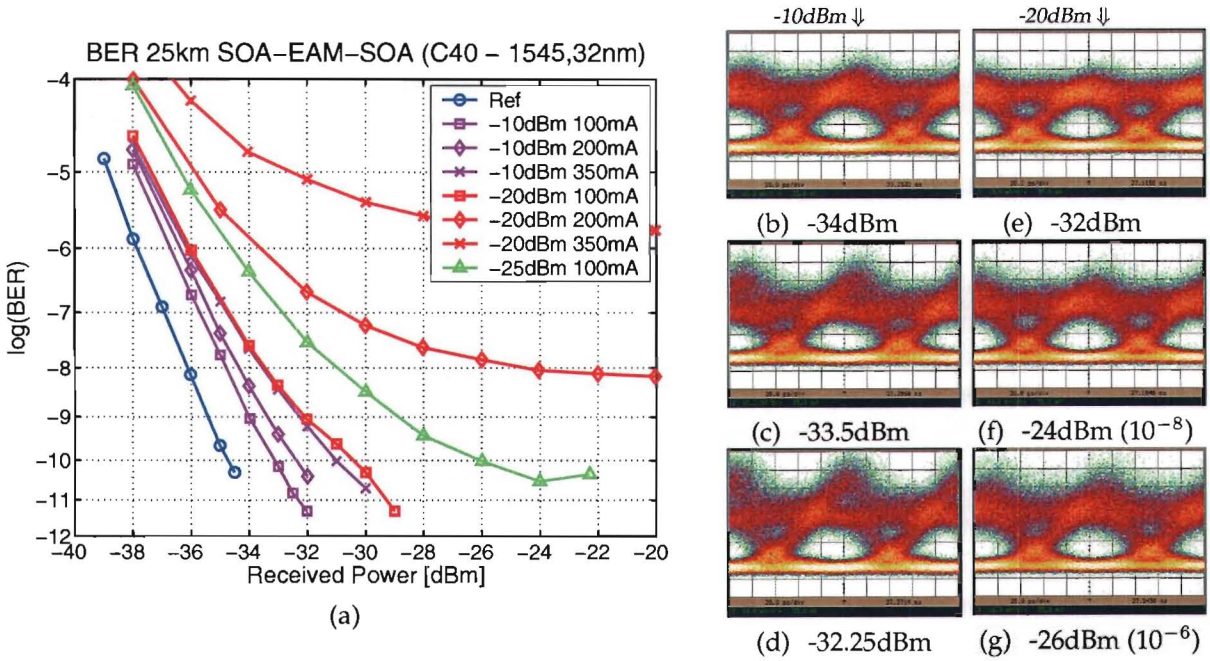

Figure 5.24.: BER for 40 (a) and the eye diagrams for an input power of -10dBm and a drive current of: (b) 100mA, (c) 200mA, (d) 350mA, and for an input power of -20dBm and a drive current of: (e) 100mA, (f) 200mA, and (g) and 350mA

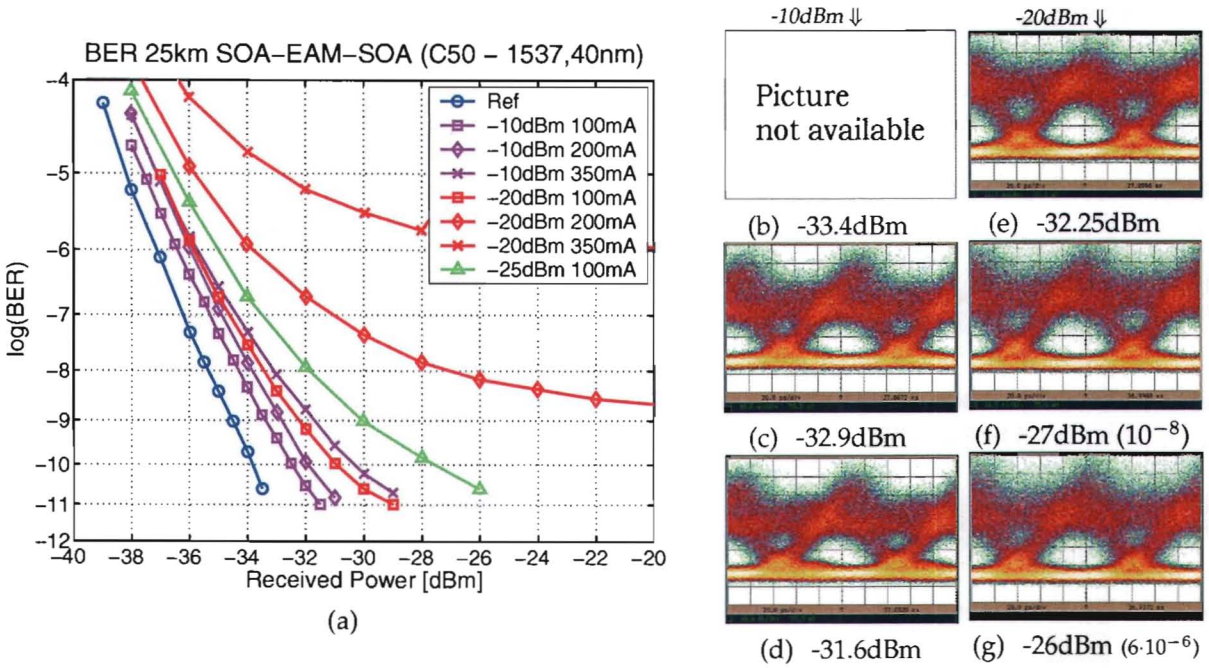

Figure 5.25.: BER for C50 (a) and the eye diagrams for an input power of -10dBm and a drive current of: (b) 100mA, (c) 200mA, (d) 350mA, and for an input power of -20dBm and a drive current of: (e) 100mA, (f) 200mA, and (g) and 350mA

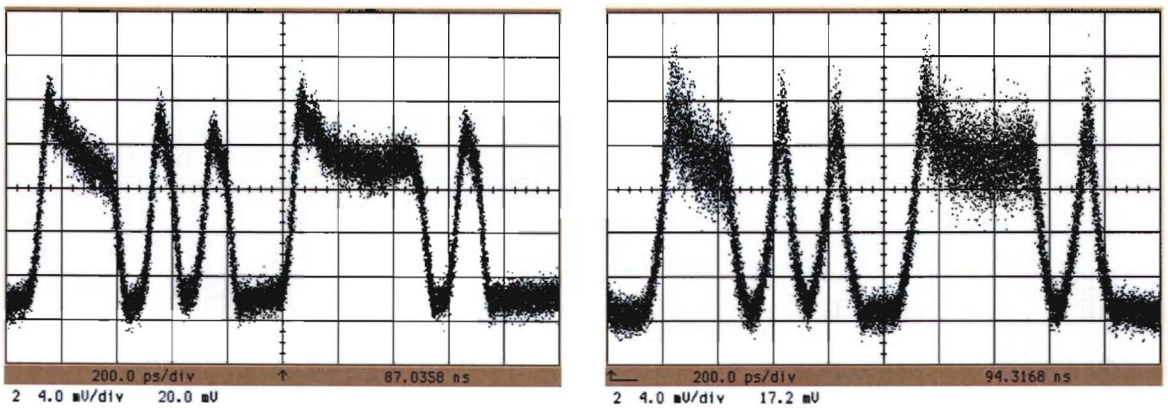

Figure 5.26.: Pattern before fibre (a) and after fibre (b) for channel C30, input power into the first SOA -20dBm, a current of 350mA to the second SOA, and a PRBS 2^7-1

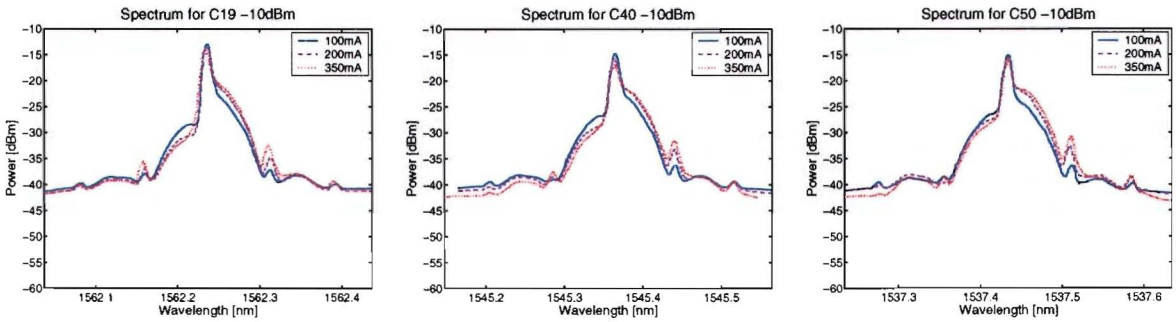

(a) C19 -10dBm (b) C40 -10dBm (c) C50 -10dBm

Figure 5.27.: Output spectra for 25km transmission experiment

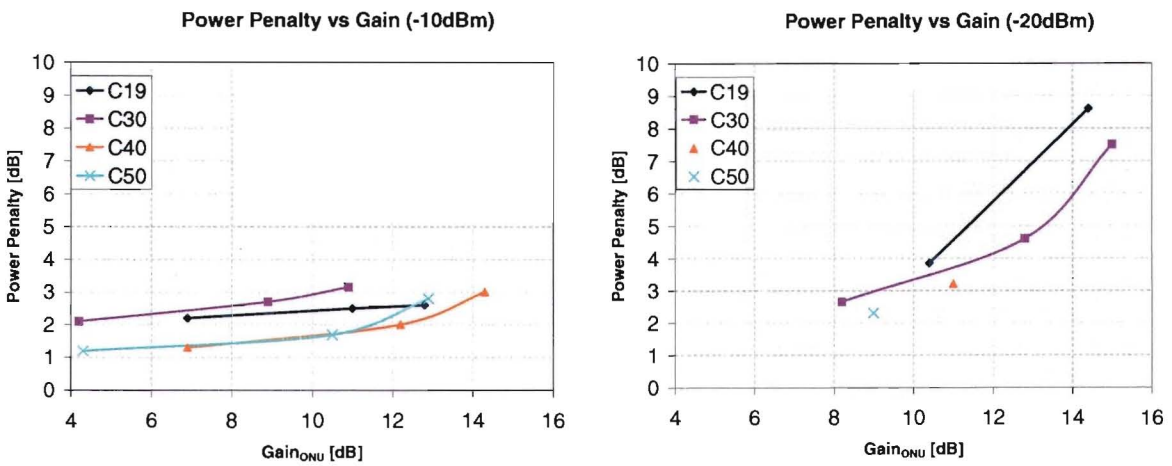

(a) (b)

Figure 5.28.: Power penalty for the signals with input power: (a) -10dBm and (b) -20dBm

Table 5.3.: The power levels, gain of the ONU and the SBRs for the measured BER curves

Channel	I_{SOA2} [mA]	P_{co} [dBm]	P_{onu} [dBm]	Gain [dB]	SBR_{co} [dB]	SBR_{onu} [dB]
C19 -10dBm	100	-1.8	+0.1	6.9	31.9	28.1
	200	-1.8	+4.2	11	36	24
	350	-1.8	+6.0	12.8	37.8	22.2
C19 -20dBm	100	-11.9	-6.5	10.4	35.4	24.6
	200	-12	-2.6	14.4	39.4	20.6
	350	-11.9	-0.8	16.1	41.1	18.9
C19 -25dBm	100	-16.9	-11.6	10.3	35.3	24.7
C30 -10dBm	100	-0.4	-1.2	4.2	29.2	30.8
	200	-0.4	+3.5	8.9	33.9	26.1
	350	-0.4	+5.5	10.9	35.9	24.1
C30 -20dBm	100	-10.6	-7.4	8.2	33.2	26.9
	200	-10.6	-2.8	12.8	37.8	22.2
	350	-10.6	-0.6	15	40	20
C30 -25dBm	100	-15.6	-12.2	8.4	33.4	26.6
C40 -10dBm	100	-2.4	-0.5	6.9	31.9	28.1
	200	-2.4	+4.8	12.2	37.2	22.8
	350	-2.5	+6.8	14.3	39.3	20.7
C40 -20dBm	100	-12.4	-6.4	11	36	24
	200	-12.4	-0.5	16.9	41.9	18.1
	350	-12.4	+1.7	19.1	44.1	15.9
C40 -25dBm	100	-17.6	-10.7	11.9	36.9	23.1
C50 -10dBm	100	-2.4	-3.1	4.3	29.3	30.7
	200	-2.3	+3.2	10.5	35.5	24.5
	350	-2.3	+5.6	12.9	37.9	22.1
C50 -20dBm	100	-12.5	-8.5	9	34	26
	200	-12.5	-1.7	15.8	40.8	19.2
	350	-12.5	+0.6	18.1	43.1	16.9
C50 -25dBm	100	-17.4	-12.9	9.5	34.5	25.5

5.4. Measurement Conclusions

If we consider the measurements carried out in this chapter we can conclude that for a low ONU gain the system is limited by carrier-backscattering and that for a high gain the system is limited by signal-backscattering. If we combine the results of the measurements with the SOA-EAM combination in Section 5.3.1 and the measurements with the SOA-EAM-SOA combination in Section 5.3.2 for channel C30 and add a trendline we can make Figure 5.29. There is some difference in additional power penalty for the second combination due to larger ASE-noise and pattern effect, but this power penalty is considered to be small compared to the backscatter penalties. From the trendlines in the figures can be seen that an optimum gain of the ONU can be achieved where the deterioration due to backscattering is limited.

For a lower SBR the power penalty due to signal-backscattering is larger than the power penalty due to carrier-backscattering [68], but for high SBRs the power penalty due to carrier- and signal-backscattering is almost similar as is shown in Figure 5.17. If you consider this and if you take the backscattering factor 35dB and the attenuation of the fibre 5dB, than the Equations 5.4 and 5.5, which were copied from Section 5.2, can be used to determine the optimum gain. With these assumptions the gain of the ONU, what will result in an equal SBR_{onu} and SBR_{co}, is 5dB. This value corresponds to the optimum gain of Figure 5.29.

$$SBR_{co} = Gain_{onu} + \text{BS-factor} - 2 \cdot att_{fibre} \tag{5.4}$$

$$SBR_{onu} = \text{BS-factor} - Gain_{onu} \tag{5.5}$$

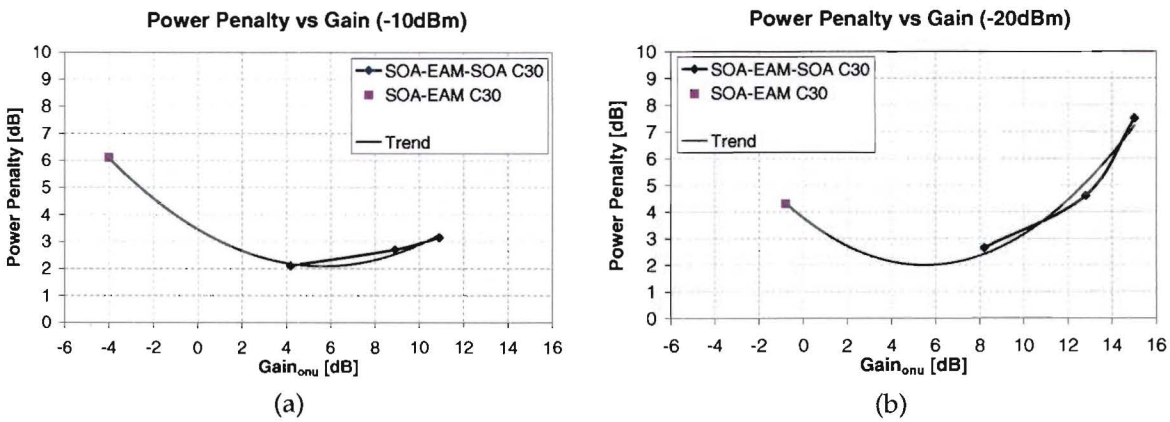

Figure 5.29.: Power penalties for: (a) -10dBm input power, and (b) -20dBm input power

The optimum gain is a bit higher for the -10dBm input signal, than for the -20dBm case; this is because the SBR_{onu} gives less power penalty than the SBR_{co} due to the power saturation condition of the pre-amplifier SOA, which reduces the backscatter power penalty.

All the transmission measurements were done with a fibre length of 25km. It is also interesting to consider what will happen if the fibre length is increased. According to Figure B.1 the Rayleigh backscattering is only increased slightly for longer distances. This means that the backscatter factor of Equations 5.4 and 5.5 is also changed slightly. However, the

attenuation of the fibre is changes significantly. A higher gain of the ONU is necessary to increase the SBR_{co}, but the higher gain will also decrease the SBR_{onu}. Thus, for different fibre lengths another optimum gain of the ONU must be found.

6. Conclusions and Recommendations

The conclusions of the report are given in this chapter. Furthermore some recommendations for future research are given.

6.1. Conclusions

In Chapter 2 an overview was given of the options for colourless reflective modulators that can be used in access networks. An electro-absorption modulator (EAM) was chosen to be used in the ONU because of its high electrical bandwidth and availability in the lab-environment. The EAM was combined with an SOA to overcome the high insertion loss.

Many combinations of modulation formats that enable bidirectional transmission on the same wavelengths are possible. An overview of the methods that were found was shown in Chapter 3. The combinations that limit the backscattering are very interesting for single-fibre architectures. For the transmission experiments a continuous-wave signal was used as a feeder signal for the ONU. The continuous-wave was chosen due to its simplicity and can be extended to one of the other formats.

Backscattering was found to be the limiting factor in the single-fibre architecture. For low input powers the Rayleigh backscattering is the main backscattering at around 35dB lower than the input power. The Brillouin scattering is shifted, related to the centre wavelength by, -10.9 and +10.9GHz for lower input powers. An asymmetry occurs for higher input powers, then the Brillouin process introduces gain at the 10.9GHz lower optical frequency, while the same process introduces depletion (attenuation) at the 10.9GHz higher optical frequency. The power where the Brillouin backscattering exceeds the Rayleigh backscattering was found to be around +6dBm for a laser with a narrow linewidth.

The impairments of both carrier- and signal-backscattering were measured. Transmission over 25km of fibre was experimentally demonstrated to be possible using an ONU with a combination of an SOA and EAM for the wavelength range of 1537.40 to 1562.23nm. A booster SOA was added after the EAM to increase the gain of the ONU. The booster SOA caused large chirp and some pattern effects. It was found that for large gain of the ONU the transmission is limited by signal-backscattering (backscattering of the modulated upstream signal towards the ONU) and for low gain is limited by carrier-backscattering (backscattering of the continuous-wave feeder signal towards the central office). The gain where both the carrier- and the signal-backscattering are minimum is around 5dB. For different fibre length the optimum gain is different. Furthermore was found that a gain-saturated SOA at the input of the ONU might reduce the signal-backscattering impairments.

6.2. Recommendation

More measurements with different gain of the ONU have to be carried out to determine the exact optimum gain of the ONU. Also more measurements have to be carried out to determine the precise power penalties for the carrier-backscattering and especially the signal-backscattering. A setup with a heavily gain-saturated SOA at the input of the ONU can be tested to determine the reduction of the signal-backscattering impairments.

For future research it is interesting to do measurements with an integrated reflective SOA-EAM structure or with a high-speed injection-locked FP-LD to determine the behaviour of these devices as reflective modulator.

It is also interesting to see how much the system improves if the backscattering is reduced by dithering the laser source or by using FSK- or PSK-modulation or SCM the downstream signal as is described in Chapter 3.

For the proposed reconfigurable access network proposed in the BB Photonics project, as is shown in Figure 1.1 it is interesting to consider the option of using a double fibre structure between the central office and the remote nodes and a single fibre structure between the remote node and the ONU. Because the proposed distance between the remote node and the ONU is 5km maximum, the backscattering impairments will not be the limiting factor. Furthermore, the number of optical connections are not increased dramatically, since only a few remote nodes are located in the network.

References

[1] H. de Waardt and A. Koonen, "BBPhotonics, dynamically reconfigurable broadband photonic access networks," October 2004. Restricted.

[2] X. Ling and X. Leijtens, "Broadband photonic access: D.2.3. design of photonic integrated transceiver," tech. rep., Technical University of Eindhoven, 28 November 2005.

[3] K. W. Goossen, J. A. Walker, and S. C. Arney, "Silicon modulator based on mechanically-active anti-reflection layer with 1 mbit/sec capability for fiber-in-the-loop applications," *IEEE Photonics Technology Letters*, vol. 6, no. 9, pp. 1119–1121, September 1994.

[4] C. Marxer, M. A. Gretillat, N. F. de, Rooij, R. Battig, O. Anthamatten, B. Valk, and P. Vogel, "Reflective duplexer based on silicon micromechanics for fiber-optic communication," *Journal of Lightwave Technology*, vol. 17, no. 1, pp. 115–122, January 1999.

[5] P. J. Duthie, M. J. Wale, I. Bennion, and J. Hankey, "Bidirectional fiber-optic link using reflective modulation," *Electronics Letters*, vol. 22, pp. 517–518, 8 May 1986.

[6] E. J. Murphy, J. Ocenasek, C. R. Sandahl, R. J. Lisco, and Y. C. Chen, "Simultaneous single-fiber transmission of video and bidirectionall voice data using LiNbO3 guided-wave devices," *Journal of Lightwave Technology*, vol. 6, no. 6, pp. 937–945, June 1988.

[7] T. Ishikawa, "Polarisation-independent LiNbO3 waveguide optical modulator for bidirectional transmission," *Electronics Letters*, vol. 28, no. 6, pp. 566–567, 12 March 1992.

[8] C. Gibassier, J. Abiven, C. Ramus, F. Huet, and J. Saulnier, "Simultaneous two-way light intensity modulation optical transmission at the same bit rate without a light source in the subscriber terminal," *Electronics Letters*, vol. 30, no. 14, pp. 1162–1163, 7 July 1994.

[9] U. Koren, B. I. Miller, M. G. Young, M. Chien, G. Raybon, T. Brenner, R. Ben-Michael, K. Dreyer, and R. J. Capik, "Polarisation insensitive semiconductor optical amplifier with integrated electroabsorption modulators," *Electronics Letters*, vol. 32, no. 2, pp. 111–112, 18 January 1996.

[10] G. Talli and P. D. Townsend, "Hybrid DWDM-TDM long-reach PON for next-generation optical access," *Journal of Lightwave Technology*, vol. 24, no. 7, pp. 2827–2834, July 2006.

[11] A. Garreau, J. Decobert, C. Kazmierski, M. C. Cuisin, J. G. Provost, H. Sillard, F. Blache, D. Carpentier, J. Landreau, and P. Chanclou, "10 Gbit/s amplified reflective electroabsorption modulator for colorless access networks," in *2006 International Conference on Indium Phosphide and Related Materials Conference Proceedings*, (Princeton, NJ, USA), pp. 168–170, IEEE, Piscataway, NJ, USA, 7-11 May 2006.

[12] I. Tafur-Monroy, F. Öhman, K. Yvind, L. Jin-Christiansen, J. Mørk, C. Peucheret, and P. Jeppesen, "Monolithically integrated reflective SOA-EA carrier re-modulator for broadband access nodes," *Optics Express*, vol. 14, no. 18, pp. 8060–8064, 4 September 2006.

[13] T. H. Wood, E. C. Carr, B. L. Kasper, R. A. Linke, and C. A. Burrus, "Bidirectional fibre-optical transmission using a multiple-quantum-well (MQW) modulator/detector," *Electronics Letters*, vol. 22, pp. 528– 529, 8 May 1986.

[14] C. J. G. Kirkby, R. M. Ash, A. J. Moseley, and A. C. Carter, "Simultaneous bidirectional signalling using multiquantum wellreflective modulator/detector," *Electronics Letters*, vol. 27, pp. 2373–2374, 5 December 1991.

[15] M. D. Feuer, J. M. Wiesenfeld, J. S. Perino, C. A. Burrus, G. Raybon, S. C. Shunk, and N. K. Dutta, "Single-port laser-amplifier modulators for local access," *IEEE Photonics Technology Letters*, vol. 8, no. 9, pp. 1175–1177, September 1996.

[16] N. Buldawoo, S. Mottet, F. Le-Gall, D. Sigogne, D. Meichenin, and S. Chelles, "A semiconductor laser amplifier-reflector for the future FTTH applications," in *11th International Conference on Integrated Optics and Optical Fibre Communications 23 European Conference on Optical Communications IOOC-ECOC97*, vol. 2, (Edinburgh, UK), pp. 196–199, IEE, London, UK, 22-25 September 1997.

[17] J. Prat, C. Arellano, V. Polo, and C. Bock, "Optical network unit based on a bidirectional reflective semiconductor optical amplifier for fiber-to-the-home networks," *IEEE Photonics Technology Letters*, vol. 17, no. 1, pp. 250–252, January 2005.

[18] N. Bouche, B. Corbett, R. Kuszelewicz, and R. Raj, "Vertical-cavity amplifying photonic switch at 1.5 μm," *IEEE Photonics Technology Letters*, vol. 8, no. 8, pp. 1035–1037, August 1996.

[19] E. S. Bjorlin, T. Kimura, and J. E. Bowers, "Carrier-confined vertical-cavity semiconductor optical amplifiers for higher gain and efficiency," *IEEE Journal of Selected Topics in Quantum Electronics*, vol. 9, no.5, pp. 1374–1385, Sept.-Oct. 2003.

[20] T. Kimura, S. Bjorlin, J. Piprek, and J. E. Bowers, "High-temperature characteristics and tunability of long-wavelength vertical-cavity semiconductor optical amplifiers," *IEEE Photonics Technology Letters*, vol. 15, no. 11, pp. 1501–1503, November 2003.

[21] G. D. Cole, E. S. Bjorlin, Q. Chen, C.-Y. Chan, S. Wu, C. S. Wang, N. C. MacDonald, and J. E. Bowers, "MEMS-tunable vertical-cavity SOAs," *IEEE Journal of Quantum Electronics*, vol. 41, no. 3, pp. 390–407, March 2005.

[22] S. Kobayashi and T. Mimura, "Injection locking in AlGaAs semiconductor laser," *IEEE Journal of Quantum Electronics*, vol. 17, no. 5, pp. 681–689, May 1981.

[23] K. Iwashita and K. Nakagawa, "Suppression of mode partition noise by laser diode light injection," *IEEE Transactions on Microwave Theory and Techniques*, vol. 30, no. 10, pp. 1657–1662, October 1982.

[24] H.-D. Kim, S.-G. Kang, and C.-H. Lee, "A low-cost WDM source with an ASE injected Fabry-Perot semiconductor laser," *IEEE Photonics Technology Letters*, vol. 12, no. 8, pp. 1067–1069, Augustus 2000.

[25] W. D. Lee, T. T. Shih, and T. F. Chen, "Novel 10 Gb/s Fabry-Perot Laser with Enhanced Confinement Layers," *Japanese Journal of Applied Physics*, vol. 46, no. 1, no. 1, p. 223, 2007.

[26] Y. J. Wen and C. J. Chae, "WDM-PON upstream transmission using Fabry-Perot laser diodes externally injected by polarization-insensitive spectrum-sliced supercontinuum pulses," *Optics Communications*, vol. 260, pp. 691–695, 2006.

[27] W. Hung, C.-K. Chan, L.-K. Chen, and F. Tong, "An optical network unit for WDM access networks with downstream DPSK and upstream remodulated OOK data using injection-locked FP laser," *IEEE Photonics Technology Letters*, vol. 15, no. 10, pp. 1476–1478, October 2003.

[28] S. S. Cheng, "Novel systems architecture for broad-band distributions in the local access and transport areas," in *Conference on Optical Fiber Communication. Digest of Technical Papers*, (San Diego, CA, USA), p. 8, Opt. Soc. America, Washington, DC, USA, 11-13 February 1985.

[29] H. Kobrinski and S. S. Cheng, "Laser power sharing in the subscriber loop," *Electronics Letters*, vol. 23, no. 18, pp. 943–944, 27 August 1987.

[30] E. K. MacHale, G. Talli, and P. D. Townsend, "10 Gb/s Hybrid DWDM-TDM PON for Long-Reach Optical Access," in *The 2nd Institution of Engineering and Technology International Conference on Access Technologies*, (Cambridge, UK), pp. 37–40, 21-22 June 2006.

[31] I. Tafur-Monroy, F. Öhman, K. Yvind, R. Kjaer, C. Peucheret, A. Koonen, and P. Jeppesen, "85 km long reach PON system using a reflective SOA-EA modulator and distributed Raman fiber amplification.," in *Proceedings of the IEEE/LEOS Annual Meeting 06, WEE4*, (Montreal, Canada), pp. pp. 705–706., 29 October - 2 November 2006.

[32] N. Buldawoo, S. Mottet, H. Dupont, D. Sigogne, and D. Meichenin, "Transmission experiment using a laser amplifier-reflector for DWDM access network," in *24th European Conference on Optical Communication*, vol. 1, (Madrid, Spain), pp. 273–274, Telefonica, Madrid, Spain, 20-24 September 1998.

[33] P. Healey, P. Townsend, C. Ford, L. Johnston, P. Townley, I. Lealman, L. Rivers, S. Perrin, and R. Moore, "Spectral slicing WDM-PON using wavelength-seeded reflective SOAs," *Electronics Letters*, vol. 37, no. 19, pp. 1181–1182, 13 September 2001.

[34] D. J. Shin, D. K. Jung, H. S. Shin, J. W. Kwon, S. Hwang, Y. Oh, and C. Shim, "Hybrid WDM/TDM-PON With Wavelength-Selection-Free Transmitters," *Journal of Lightwave Technology*, vol. 23, no. 1, pp. 187–195, January 2005.

[35] H. C. Kwon, W. S. Jang, and S. K. Han, "Optimisation of remote seeding optical source in wavelength-locked FP-LD bidirectional WDM access optical link," *Optoelectronics, IEE Proceedings-*, vol. 152, no. 5, pp. 247–249, October 2005.

[36] N. J. Frigo, P. P. Iannone, P. D. Magill, T. E. Darcie, M. M. Downs, B. N. Desai, U. Koren, T. L. Koch, C. Dragone, H. M. Presby, and G. E. Bodeep, "A wavelength-division multiplexed passive optical network with cost-shared components," *IEEE Photonics Technology Letters*, vol. 6, no. 11, pp. 1365–1367, November 1994.

[37] G.-W. Lu, N. Deng, C.-K. Chan, and L.-K. Chen, "Use of downstream inverse-RZ signal for upstream data re-modulation in a WDM passive optical network," in *2005 Optical Fiber Communications Conference Technical Digest*, vol. 6, (Anaheim, CA, USA), p. 3, IEEE, Piscataway, NJ, USA, 6-11 March 2005.

[38] J. K. Wheeler, J. Ocenasek, and P. Bohn, "Two-way transmission using electro-optical modulator," *Electronics letters*, vol. 22, no. 9, pp. 479–481, 24 April 1986.

[39] B. K. Kim, H. Park, S. Park, and K. Kim, "Optical access network scheme with downstream Manchester coding and upstream NRZ remodulation," *Electronics Letters*, vol. 42, no. 8, pp. 484–485, 13 April 2006.

[40] F. Payoux, P. Chanclou, T. Soret, N. Genay, and R. Brenot, "Demonstration of a RSOA-based wavelength remodulation scheme in 1.25 Gbit/s bidirectional hybrid WDM-TDM PON," in *Optical Fiber Communication Conference, 2006 and the 2006 National Fiber Optic Engineers Conference*, (Anaheim, CA, USA), p. 3, 5-10 March 2006.

[41] J. J. Koponen and M. J. Soderlund, "A duplex WDM passive optical network with 1:16 power split using reflective SOA remodulator at ONU," in *Optical Fiber Communication Conference*, (Los Angeles, CA, USA), pp. 3–6, Opt. Soc. America, Washington, DC, USA, 23-27 February 2004.

[42] K. C. Reichmann, N. J. Frigo, and P. P. Iannone, "Wavelength registration in WDM ring networks by reconstitution of dropped optical carriers," in *Proceedings of ECOC'99. 25th European Conference on Optical Communication*, vol. 1, (Nice, France), pp. 136–137, Soc. Electr. Electron, Paris, France, 26-30 September 1999.

[43] E. Conforti, A. C. Bordonalli, S. Ho, and S. M. Kang, "Optical 2R remodulator using feedforward control of semiconductor optical amplifier gain," *Microwave and Optical Technology Letters*, vol. 21, no. 1, pp. 39–42, 5 April 1999.

[44] E. Conforti, C. M. Gallep, S. H. Ho, A. C. Bordonalli, and S.-M. Kang, "Carrier reuse with gain compression and feed-forward semiconductor optical amplifiers," *IEEE Transactions on Microwave Theory and Techniques*, vol. 50, no. 1, pp. 77–87, January 2002.

[45] H. Takesue and T. Sugie, "Wavelength channel data rewrite using saturated SOA modulator for WDM networks with centralized light sources," *Journal of Lightwave Technology*, vol. 21, no. 11, pp. 2546–2556, November 2003.

[46] H. Takesue, N. Yoshimoto, Y. Shibata, T. Ito, Y. Tohmori, and T. Sugie, "Wavelength channel data rewriter using semiconductor optical saturator/modulator," *Journal of Lightwave Technology*, vol. 24, no. 6, pp. 2347–2354, June 2006.

[47] W. Lee, M.-Y. Park, S.-H. Cho, J. Lee, C. Kim, G. Jeong, and B.-W. Kim, "Bidirectional wdm-pon based on gain-saturated reflective semiconductor optical amplifiers," *IEEE Photonics Technology Letters*, vol. 17, no. 11, pp. 2460–2462, November 2005.

[48] A. C. Bordonalli, J. A. Guimaraes, J. L. Benitez, E. Conforti, and C. M. Gallep, "Remodulation and filtering of WDM channels using the optical injection locking technique," in *Microwave and Optoelectronics Conference, 2001. Proceedings of the 2001 SBMO/IEEE MTT-S International*, vol. 1, (Belem, Brazil), pp. 541–544, IEEE, Piscataway, NJ, USA, 6-10 August 2001.

[49] L. Y. Chan, C. K. Chan, T. K. Tong, S. Y. Cheung, F. Tong, and L. K. Chen, "Demonstration of data remodulation for upstream traffic in wdm access networks using injection-locked fp laser as modulator," in *Optical Fiber Communication Conference and Exhibition. Technical Digest.*, vol. 3, (Anaheim, CA, USA), Opt. Soc. America, Washington, DC, USA, 17-22 March 2001.

[50] L. Y. Chan, C. K. Chan, D. T. K. Tong, F. Tong, and L. K. Chen, "Upstream traffic transmitter using injection-locked Fabry-Perot laser diode as modulator for WDM access networks," *Electronics Letters*, vol. 38, no. 1, pp. 43–45, 3 January 2002.

[51] L. Altwegg, A. Azizi, P. Vogel, Y. Wang, and F. Wyler, "LOCNET: a fiber in the loop system with no light source at thesubscriber end," *Journal of Lightwave Technology*, vol. 12, no. 3, pp. 535–540, March 1994.

[52] J. Zhang, N. Chi, P. Holm-Nielsen, C. Peucheret, and P. Jeppesen, "A novel optical labeling scheme using a FSK modulated DFB laser integrated with an EA modulator," *Optical Fiber Communications Conference, 2003. OFC 2003*, vol. 1, pp. 279–280, 2003.

[53] N. Deng, C. K. Chan, L. K. Chen, and F. Tong, "Experimental investigation of remodulating upstream OOK data on downstream OFSK signal in a two-way WDM access network," *Lasers and Electro-Optics, 2003. The 5th Pacific Rim Conference on*, vol. 1, 2003.

[54] N. Deng, C.-K. Chan, L.-K. Chen, and F. Tong, "Data remodulation on downstream OFSK signal for upstream transmission in WDM passive optical network," *Electronics Letters*, vol. 39, no. 24, pp. 1741–1743, 27 November 2003.

[55] C. Arellano, V. Polo, C. Bock, and J. Prat, "Bidirectional single fiber transmission based on a RSOA ONU for FTTH using FSK-IM modulation formats," in *Optical Fiber Communication Conference, 2005. Technical Digest. OFC/NFOEC*, vol. 3, (Anaheim, CA, USA), p. 3, 6-11 March 2005.

[56] S. Y. Cheung, L. Y. Chan, C. K. Chan, D. T. K. Tong, F. Tong, and L. K. Chen, "Demonstration of an ONU for WDM access network with downstream BPSK and upstream remodulated OOK data using injection-locked FP laser," in *Proceedings 27th European Conference on Optical Communication*, vol. 3, (Amsterdam, Netherlands), pp. 358–359, IEEE, Piscataway, NJ, USA, 30 September - 4 October 2001.

[57] W. Hung, C. K. Chan, L. K. Chen, and F. Tong, "An optical network unit for WDM access networks with downstream DPSK and upstream re-modulated OOK data using injection-locked FP laser," in *Optical Fiber Communication Conference and Exhibition*, vol. 1, (Atlanta, GA, USA), pp. 281–282, Opt. Soc. America, Washington, DC, USA, 23-28 March 2003.

[58] M. Attygalle, N. Nadarajah, and A. Nirmalathas, "Wavelength reused upstream transmission scheme for WDM passive optical networks," *Electronics Letters*, vol. 41, no. 18, pp. 1025–1027, 1 September 2005.

[59] M. Attygalle, T. Anderson, D. Hewitt, and A. Nirmalathas, "WDM passive optical network with subcarrier transmission and baseband detection scheme for laser-free optical network units," *IEEE Photonics Technology Letters June 2006; 18(11): 1279-81*, vol. 18, no. 11, pp. 1279–1281, June 2006.

[60] J.-M. Kang and S.-K. Han, "A novel hybrid WDM/SCM-PON sharing wavelength for up- and down-link using reflective semiconductor optical amplifier," *IEEE Photonics Technology Letters*, vol. 18, no. 3, pp. 502–504, 1 February 2006.

[61] C. Bock, M. P. Thakur, C. Arellano, J. J. Lepley, I. Tsalamanis, S. D. Walker, and J. Prat, "Wavelength independent RSOA-based ONU for FTTH PON implementation of switched Ethernet services," in *Optical Communication, 2005. ECOC 2005. 31st European Conference on*, vol. 1, (Glasgow, Scotland), pp. 85–86, 25-29 September 2005.

[62] H.-D. Jung, A. M. J. Koonen, S.-K. Han, and J. Kim, "EAM cascaded a SOA with Ring Configuration for a base station in a bi-directional RoF link," in *2007 Asia-Pacific Microwave Photonics Conference*, (Jeju Island, Korea), 25-27 April 2007.

[63] J. P. Goedgebuer, A. Hamel, and H. Porte, "Full bidirectional fiber transmission using coherence-modulated lightwaves," *IEEE Journal of Quantum Electronics*, vol. 28, vol. 12, pp. 2685–2691, December 1992.

[64] J. Hauden, H. Porte, and J. P. Goedgebuer, "Demonstration of a single source bidirectional fibre link using polarisation insensitive LiNbO3 integrated coherence modulators," *Electronics Letters*, vol. 32, no. 8, pp. 751–750, 11 April 1996.

[65] J. Hauden, H. Porte, J. P. Goedgebuer, J. Abiven, C. Gibassier, and C. Gutierrez-Martinez, "Polarization independent bidirectional fiber link using coherence-multi/demultiplexing LiNbO 3 integrated electroopticalcircuits," *Journal of Lightwave Technology*, vol. 14, no. 7, pp. 1630–1638, July 1996.

[66] T. H. Wood, "Direct measurement of the electric-field-dependent absorption coefficient in GaAs/AlGaAs multiple quantum wells," *Applied Physics Letters*, vol. 48, no. 21, p. 1413, 26 May 1986.

[67] M. O. van Deventer, J. van der Tol, and A. J. Boot, "Power penalties due to Brillouin and Rayleigh scattering in abidirectional coherent transmission system," *Photonics Technology Letters, IEEE*, vol. 6, no. 2, pp. 291–294, February 1994.

[68] G. Talli, D. Cotter, and P. D. Townsend, "Rayleigh backscattering impairments in access networks with centralised light source," *Electronics Letters*, vol. 42, no. 15, pp. 877–878, 20 July 2006.

[69] Z. Li, Y. Dong, Y. Wang, and C. Lu, "A novel psk-manchester modulation format in 10-gb/s passive optical network system with high tolerance to beat interference noise," *IEEE Photonics Technology Letters*, vol. 17, no. 5, pp. 1118–1120, May 2005.

[70] T. Yoshida, S. Kimura, H. Kimura, K. Kumozaki, and T. Imai, "A new single-fiber 10-Gb/s optical loopback method using phase modulation for WDM optical access networks," *Journal of Lightwave Technoly*, vol. 24, no. 2, pp. 786–796, February 2006.

[71] C. W. Chow, G. Talli, and P. D. Townsend, "Rayleigh Noise Reduction in 10-Gb/s DWDM-PONs by Wavelength Detuning and Phase-Modulation-Induced Spectral Broadening," *IEEE Photonics Technology Letters*, vol. 19, no. 6, pp. 423–425, 15 March 2007.

Appendix A.

ONU Wavelength Splitter Alternatives

This appendix describes some alternative designs that can be used as wavelength splitters in the ONU.

The first architecture uses a combination of a passive power splitter and wavelength filters to separate the wavelengths. The incoming signal is split into two arms, the upper arm contains a filter to filter out the upstream wavelengths before it is detected. The filter in the lower arm filters out the downstream wavelengths before it is modulated by the reflective modulator. The device can be integrated and doesn't require active control. The disadvantage is the power loss caused by the splitter, the downstream signal will have a loss of 3dB. The upstream channel passes the splitter twice, which will result in a power loss of 6dB.

A novel method to split the upstream and the downstream wavelengths is proposed in the second architecture. An AWG is used to separate all the wavelength channels used in the network. A second AWG combines only the downstream signals before it arrives at the detector. A third AWG is used to combine the upstream wavelengths. The advantages of this method is that no active control is required. Furthermore the ASE-noise is filtered out by the AWG, this can be very useful if an RSOA is used as a reflective modulator. The disadvantage is that the device is not suitable for upgrade of the network. Furthermore, crosstalk will be added to the downstream and upstream signals by the first AWG.

The third architecture uses a circulator and an FBG to separate the downstream and upstream band. The FBG reflects the upstream channels and passes the downstream channels to the detector. The circulator cannot be integrated, but can easily be added to the input of the ONU.

The fourth method is to use a red/blue filter. The device has three ports, the signal from port 1 reflects the downstream band to port 2 (detector) and passes the upstream band to port 3 (reflective modulator). The device cannot be integrated easily which makes it unsuitable for commercial purposes but it is commercially available as a building block and therefore can be used for experimental purposes.

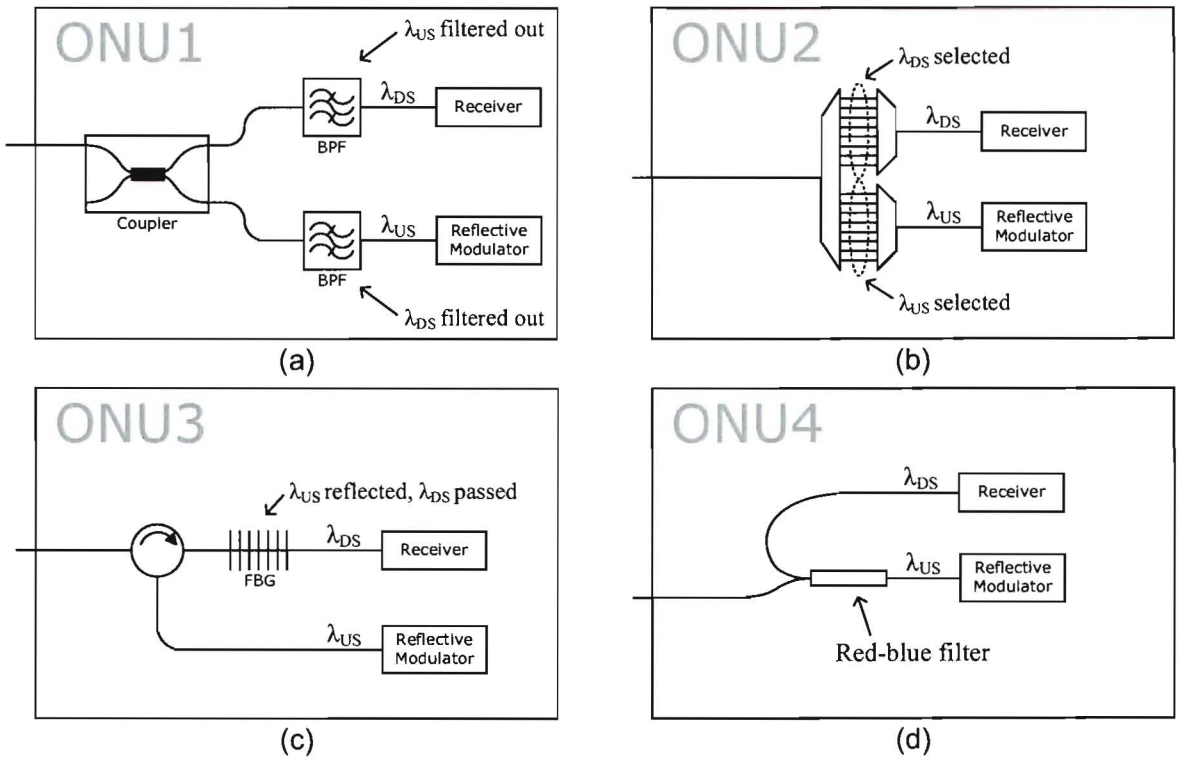

Figure A.1.: Alternative ONU designs using: (a) a coupler and coarse filters, (b) a novel AWG configuration, (c) a circulator and an FGB, and (d) a red-blue filter

Appendix B.

Rayleigh Backscattering

Rayleigh scattering in the fibre is caused by material density imperfections occurring during fibre manufacture. The backscattering intensity increases with the length of the fibre until it converges after about 20km, achieving around -35dBm, as is shown in FigureB.1.

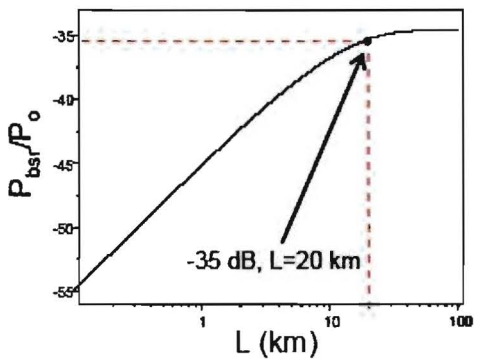

Figure B.1.: Rayleigh backscattering

B.1. Methods to Reduce Rayleigh Backscattering

To date various methods have been developed and introduced to reduce the Rayleigh Backscattering, some of the methods are discussed in this Appendix.

The most simple way to overcome the backscattering issue is to use two separate fibres in stead of a bidirectional fibre. This however, increases the total fibre length and the number of connectors.

The mostly used method to reduce the backscattering is to increase the optical linewidth. Increasing the linewidth by dithering the signal to reduce Rayleigh noise was already suggested by [13] in 1986. Another optical is to use a source with a broader linewidth. Phase scrambling and frequency scrambling also increase the linewidth of the optical signal. Another option is to modulate the downstream signal as phase or frequency shift keying [55]. This will reduce the backscattering, since a broader linewidth is achieved and the signal has a constant intensity, so it can be used in the ONU to modulate the upstream data upon.

A different technique sends a narrow-linewidth optical carrier to the ONU. At the ONU the signal is intensity modulated with the upstream data and then phase modulated. Due to the phase modulation the centre wavelength is suppressed and multiple side-modes are generated. A narrowband optical filter at the central office filters out the backscattering and the carrier frequency, but transmits the phase modulated signal and thus the backscattering is reduced [69, 70, 71].

Appendix C.

Measurement Equipment

The following devices were used in the measurements:

- **Laser:** The laser used was an external cavity tunable multi-channel LD light source from Santec with model number ECL-210. The wavelength can be tuned from 1530 to 1630nm with a resolution of <0.001nm. Coherence control is achieved by frequency modulation against the external cavity module. The spectrum linewidth can be set with a coherence control to OFF, which corresponds to a linewidth <0.2 MHz, and to ON, in which levels can be set to change the linewidth between 0.2 and 200MHz. The minimum sideband suppression ratio (SSR) is 50dB.
- **Power Meter:** The fixed power meter used was a Newport Dual Power Meter with model number 2832-C and detector with model number 818-IS-1. The device has an applicable wavelength range from 400 to 1650nm, a power range from -70 to +23dBm and an accuracy of $\pm 2.5\%$
- **Attenuator:** The attenuator was an HP 8157A. The device has a wavelength range from 1200 to 1650nm, a resolution of 0.01dB, an insertion loss of 2dB, an attenuation range of 60dB and a return loss of 45dB
- **In-line Attenuatior/power meter:** The in-line power meter / attenuators used are the Power Monitor 410 models from Eigenlight. It has an attenuator range of 40dB with a resolution of 0.1dB. The power range is from -50 to +16dBm and it has a return loss > 40dB and an insertion loss < 1dB
- **Optical Spectrum Analyser (OSA):** The OSA was an Adventest Q8384A. It has a wavelength range from 600 to 1700nm and a sensitivity of -87dBm. It has a 10pm resolution bandwidth, a 20pm wavelength accuracy and a wide dynamic range: 50dB ($\pm$ 0.1nm), 60dB ($\pm$ 0.2nm). All the measurements were done with the lowest resolution of 0.01nm, and the accuracy of the resolution bandwidth is $\pm 2\%$.
- **Lightwave Converter:** The HP 11982A lightwave converter used covers the wavelengths from 1200 to 1600nm and bandwidths from dc to 15GHz. It has a 300volts/watt conversion gain an input return loss of > 23dB.
- **10-Gbit/s Lightwave Receiver:** As lightwave receiver the HP 83434A was used. This PIN diode based receiver was used with clock recovery at 9953.28 MHz and has a -16dBm sensitivity (BER of 1×10^{-10} for 2^{31-1} PRBS)
- **Pattern Generator:** The Anritsu MP1701A that was used as pattern generator operates at clock frequencies from 50 MHz to 10 GHz. For the output interface, the offset can be set in 5mV steps, the amplitude can be set in 10mV steps and the delay between output data signal and clock signal can be set in 1 ps steps.

- **Error Detector:** ED Anritsu MP1764C. The eror detector operates over the 50MHz to 12.5Ghz frequency range. The input threshold voltage (-3V to +1.875 V) can be set in 1mV steps and the clock pahse (-500 to +500ps) in 1ps steps.
- **Oscilloscope:** The HP 83480A Digital Communications Analyser was used as an oscilloscope. The electrical channels have up to 50GHz bandwidths.

Table C.1.: Active Devices

Device	**Manufacturer**	**Model**	**Serial Number**
SOA (Pre-amplifier)	JDS/Uniphase	CQF 872/108-C	917
SOA (Booster)	JDS/Uniphase	CQF 872/0	578
EAM	OKI	OM 5754C-30B	347-6
EDFA	JDS/Uniphase	OA 400	